

# Modeling Magnetic Core Loss for Sinusoidal Waveforms

By

**Colin J. Dunlop**

B.S., Electrical Engineering

United States Naval Academy, 2002

Submitted to the Department of Mechanical Engineering and the  
Department of Electrical Engineering and Computer Science in Partial  
Fulfillment of the Requirements for the Degrees of

Naval Engineer

and

Master of Science in Electrical Engineering

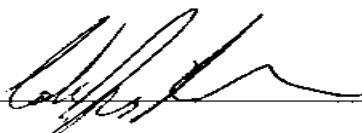
at the

Massachusetts Institute of Technology

June 2008

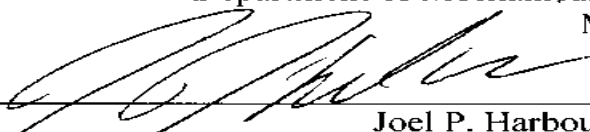
© 2008 Massachusetts Institute of Technology. All rights reserved.  
MIT hereby grants to the US Government permission to reproduce and  
to distribute publicly paper and electronic copies of this thesis  
document in whole or in part.

Signature of  
Author



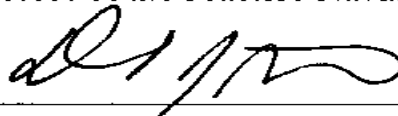
Department of Mechanical Engineering  
May 09, 2008

Certified by



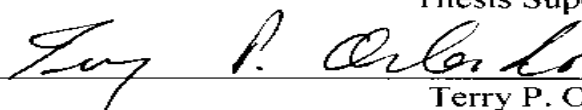
Joel P. Harbour CDR, USN  
Associate Professor of the Practice Naval Construction and Engineering  
Thesis Supervisor

Certified by



David J. Perreault  
Associate Professor of Electrical Engineering  
Thesis Supervisor

Accepted by



Terry P. Orlando  
Chairman, Committee on Graduate Students  
Department of Electrical Engineering and Computer Science

Accepted by



Lallit Anand  
Chairman, Committee on Graduate Students  
Department of Mechanical Engineering

<b>REPORT DOCUMENTATION PAGE</b>					<i>Form Approved OMB No. 0704-0188</i>	
<small>The public reporting burden for this collection of information is estimated to average 1 hour per response, including the time for reviewing instructions, searching existing data sources, gathering and maintaining the data needed, and completing and reviewing the collection of information. Send comments regarding this burden estimate or any other aspect of this collection of information, including suggestions for reducing the burden, to Department of Defense, Washington Headquarters Services, Directorate for Information Operations and Reports (0704-0188), 1215 Jefferson Davis Highway, Suite 1204, Arlington, VA 22202-4302. Respondents should be aware that notwithstanding any other provision of law, no person shall be subject to any penalty for failing to comply with a collection of information if it does not display a currently valid OMB control number.</small>						
<b>PLEASE DO NOT RETURN YOUR FORM TO THE ABOVE ADDRESS.</b>						
<b>1. REPORT DATE (DD-MM-YYYY)</b>		<b>2. REPORT TYPE</b>			<b>3. DATES COVERED (From - To)</b>	
<b>4. TITLE AND SUBTITLE</b>				<b>5a. CONTRACT NUMBER</b>		
				<b>5b. GRANT NUMBER</b>		
				<b>5c. PROGRAM ELEMENT NUMBER</b>		
<b>6. AUTHOR(S)</b>				<b>5d. PROJECT NUMBER</b>		
				<b>5e. TASK NUMBER</b>		
				<b>5f. WORK UNIT NUMBER</b>		
<b>7. PERFORMING ORGANIZATION NAME(S) AND ADDRESS(ES)</b>					<b>8. PERFORMING ORGANIZATION REPORT NUMBER</b>	
<b>9. SPONSORING/MONITORING AGENCY NAME(S) AND ADDRESS(ES)</b>					<b>10. SPONSOR/MONITOR'S ACRONYM(S)</b>	
					<b>11. SPONSOR/MONITOR'S REPORT NUMBER(S)</b>	
<b>12. DISTRIBUTION/AVAILABILITY STATEMENT</b>						
<b>13. SUPPLEMENTARY NOTES</b>						
<b>14. ABSTRACT</b>						
<b>15. SUBJECT TERMS</b>						
<b>16. SECURITY CLASSIFICATION OF:</b>			<b>17. LIMITATION OF ABSTRACT</b>	<b>18. NUMBER OF PAGES</b>	<b>19a. NAME OF RESPONSIBLE PERSON</b>	
a. REPORT	b. ABSTRACT	c. THIS PAGE			<b>19b. TELEPHONE NUMBER (Include area code)</b>	

## INSTRUCTIONS FOR COMPLETING SF 298

**1. REPORT DATE.** Full publication date, including day, month, if available. Must cite at least the year and be Year 2000 compliant, e.g. 30-06-1998; xx-06-1998; xx-xx-1998.

**2. REPORT TYPE.** State the type of report, such as final, technical, interim, memorandum, master's thesis, progress, quarterly, research, special, group study, etc.

**3. DATES COVERED.** Indicate the time during which the work was performed and the report was written, e.g., Jun 1997 - Jun 1998; 1-10 Jun 1996; May - Nov 1998; Nov 1998.

**4. TITLE.** Enter title and subtitle with volume number and part number, if applicable. On classified documents, enter the title classification in parentheses.

**5a. CONTRACT NUMBER.** Enter all contract numbers as they appear in the report, e.g. F33615-86-C-5169.

**5b. GRANT NUMBER.** Enter all grant numbers as they appear in the report, e.g. AFOSR-82-1234.

**5c. PROGRAM ELEMENT NUMBER.** Enter all program element numbers as they appear in the report, e.g. 61101A.

**5d. PROJECT NUMBER.** Enter all project numbers as they appear in the report, e.g. 1F665702D1257; ILIR.

**5e. TASK NUMBER.** Enter all task numbers as they appear in the report, e.g. 05; RF0330201; T4112.

**5f. WORK UNIT NUMBER.** Enter all work unit numbers as they appear in the report, e.g. 001; AFAPL30480105.

**6. AUTHOR(S).** Enter name(s) of person(s) responsible for writing the report, performing the research, or credited with the content of the report. The form of entry is the last name, first name, middle initial, and additional qualifiers separated by commas, e.g. Smith, Richard, J, Jr.

**7. PERFORMING ORGANIZATION NAME(S) AND ADDRESS(ES).** Self-explanatory.

**8. PERFORMING ORGANIZATION REPORT NUMBER.** Enter all unique alphanumeric report numbers assigned by the performing organization, e.g. BRL-1234; AFWL-TR-85-4017-Vol-21-PT-2.

**9. SPONSORING/MONITORING AGENCY NAME(S) AND ADDRESS(ES).** Enter the name and address of the organization(s) financially responsible for and monitoring the work.

**10. SPONSOR/MONITOR'S ACRONYM(S).** Enter, if available, e.g. BRL, ARDEC, NADC.

**11. SPONSOR/MONITOR'S REPORT NUMBER(S).** Enter report number as assigned by the sponsoring/monitoring agency, if available, e.g. BRL-TR-829; -215.

**12. DISTRIBUTION/AVAILABILITY STATEMENT.** Use agency-mandated availability statements to indicate the public availability or distribution limitations of the report. If additional limitations/ restrictions or special markings are indicated, follow agency authorization procedures, e.g. RD/FRD, PROPIN, ITAR, etc. Include copyright information.

**13. SUPPLEMENTARY NOTES.** Enter information not included elsewhere such as: prepared in cooperation with; translation of; report supersedes; old edition number, etc.

**14. ABSTRACT.** A brief (approximately 200 words) factual summary of the most significant information.

**15. SUBJECT TERMS.** Key words or phrases identifying major concepts in the report.

**16. SECURITY CLASSIFICATION.** Enter security classification in accordance with security classification regulations, e.g. U, C, S, etc. If this form contains classified information, stamp classification level on the top and bottom of this page.

**17. LIMITATION OF ABSTRACT.** This block must be completed to assign a distribution limitation to the abstract. Enter UU (Unclassified Unlimited) or SAR (Same as Report). An entry in this block is necessary if the abstract is to be limited.

# **Modeling Magnetic Core Loss for Sinusoidal Waveforms**

by

**Colin J. Dunlop**

Submitted to the Department of Ocean Engineering and the Department of Electrical Engineering and Computer Science in Partial Fulfillment of the Requirements for the

Degrees of

Naval Engineer

and

Master of Science in Electrical Engineering

## **ABSTRACT**

Among the challenging unsolved technical problems that have plagued the minds of scientist and engineers throughout the 20<sup>th</sup> and 21<sup>st</sup> century is the development of a quantifiable model to accurately estimate or explain Core Power Losses (CPL). Theoretical advances in magnets led to many model proposals, but as these models were experimentally examined, they quickly lost their validation. Many of the current models use manufacturer's material estimates to form limited curve fitted equations. These equations are only valid for a specific waveform over a specified range. Unless the designers use the same conditions used to determine the manufacturer's fitted equations, the models quickly lose their precision. The scope of this thesis is to explain and compare several of the current models and evaluate them using experiment data. The validity of some of the term component used in many of these models will also be investigated.

Thesis Supervisor: David J. Perreault

Title: Associate Professor of Electrical Engineering, MIT

Thesis Reader: Charles R. Sullivan

Title: Professor of Electrical Engineering, Dartmouth University

## Table of Contents

Section 1 Introduction.....	6
1.1 Purpose/Problem.....	6
1.2 Significance.....	6
1.3 Thesis Overview .....	6
1.4 Background .....	7
1.5 Hysteresis Loss .....	7
1.6 Empirical Equations.....	9
1.7 Separation of Total Power Losses.....	12
1.7.1 Hysteresis Loss.....	13
1.7.2 Classical Eddy Current Loss .....	13
1.7.3 Excess Eddy Current Loss.....	17
Section 2 Experimental Data Collection Method and Design .....	19
2.0 Required Experiments to achieve thesis goals .....	19
2.1 Digitizing Method for Core Power Losses Calculations .....	20
2.2 Preconditioning Circuit.....	22
2.3 Overall Circuit Design: Digitizing CPL and Preconditioning Circuit.....	25
2.4 Conductibility Apparatus and Measurement Procedure .....	26
2.4 Capacitance and Conductivity vs Frequency using an Impedance Analyzer .....	31
2.5 Repetitive Digitizing Method for Primary Circuit Accuracy .....	31
2.6 CPL Code Validation.....	34
2.7 Accuracy of Matrix and MATLAB Best Fit Method .....	35
Section 3 Core Power Loss Equation Evaluation .....	39
3.0 Results of Empirical Equation Component Verification .....	39
3.1 The Validity of the Hysteresis Loss Equation for Low Frequencies .....	39
3.2 Conductivity in an Electrical Field .....	45
3.3 Core Area as a factor in CPL per volume Equations .....	51
Section 4 CPL Data Fitting and Statistics Analysis.....	61
4.1 Steinmetz Equation .....	61
4.2 Power Law Equation (PLE) .....	64
4.3 Hysteresis Loss Equation.....	71
4.4 Classical Eddy Current Equation (CECE).....	76
4.5 Separation of Total Power Losses Models .....	78
4.5.1 Bertotti's Model.....	78
4.5.2 Hysteresis Loss Equation and Classical Eddy Current Equation .....	84
4.5.3 Hysteresis Loss Equation and the PLE Equation Model.....	85
Section 5 Conclusions.....	88
5.0 Results.....	88
List of References .....	90
Appendix A: MATLAB CODE.....	92
Appendix B: CPL Collected Data.....	105

## **List of Figures**

Figure 1: Domain Wall Theory, adapted from figures in Reference [1] and [2] .....	8
Figure 2: Hysteresis Loop at 100kHz and @ 273mT .....	9
Figure 3: 3D Cylinder for Pc derivation .....	14
Figure 4: Rectangular toroidal Core Figure [40] .....	16
Figure 5: CPL Circuit Design .....	20
Figure 6: Ring Toroid .....	21
Figure 7: Preconditioning Circuit .....	23
Figure 9: FFT of Current in Preconditioning Circuit.....	24
Figure 8: Preconditioning Circuit values .....	24
Figure 10: Current Decay of Preconditioning Circuit.....	25
Figure 11: Overall Circuit Design: Digitizing CPL and Preconditioning Circuit .....	26
Figure 12: Conductivity Apparatus.....	28
Figure 13: Current and Voltage of Conductivity of the plate .....	29
Figure 14: Impedance Analyzer Setup.....	31
Figure 15: 3 Data Sets of 100 kHz Sinusoidal Signals for TN23/14/7 core .....	32
Figure 16: Region 1 of 3 Data Sets of 100 kHz Sinusoidal Signals for TN23/14/7 core .	33
Figure 17: Region 2 of 3 Data Sets of 100 kHz Sinusoidal Signals for TN23/14/7 core .	34
Figure 18: Validation of MATLAB Code Picture .....	35
Figure 19: Core Power Loss Test Fixture used in Hysteresis Loss Equation .....	40
Figure 20: Hysteresis Loss at 70 Hertz .....	41
Figure 21: 70 & 140 Hertz graph using 70 Hertz Best Fit Coefficients .....	42
Figure 22: PLE for 70 and 140 Hertz with $\alpha$ constrained to 1 .....	43
Figure 23: PLE for 70 and 140 Hertz with $\alpha$ unconstrained.....	44
Figure 24: Conductivity Apparatus.....	45
Figure 25: AC Conductivity vs varying AC Electric Field.....	47
Figure 26: DC Conductivity vs Electric Field .....	47
Figure 27: Voltage and Current of the 3F3 PLT 48/38/4 $\sigma$ measurements .....	49
Figure 28: 3F3 Plate Capacitance vs Freq .....	50
Figure 29: Phase Angle vs Freq .....	51
Figure 30: Resistance vs Freq for 3F3 Plate Measurement .....	51
Figure 31: Rectangular Toroid Figure .....	52
Figure 32: Core size visual difference .....	52
Figure 33: 3F3 TN 23/14/7 same size core lot Variability .....	54
Figure 34: Core Area effects on Core Loss .....	55
Figure 35: Core Area CPL Losses for 100 khz.....	56
Figure 36: Core Area CPL Losses for 500 khz.....	57
Figure 37: Hysteresis Loss Equation for 70 Hertz.....	62
Figure 38: Low Frequency Core Power Loss for TN 23/14/7 .....	62
Figure 39: High Freq (100-500kHz) Steinmetz Equation.....	63
Figure 40: CPL graph using MATLAB Method.....	65
Figure 41: PLE LSBF for the 100-300 (kHz) data .....	66
Figure 42: PLE LSBF for the 300-500 (kHz) data .....	67
Figure 43: PLE 100-300 kHz Data for Ferroxcube Estimates and Best Fit Estimates .....	68
Figure 44: PLE 300-500 kHz Data for Ferroxcube Estimates and Best Fit Estimates .....	69
Figure 45: 100-300 and 300-500 kHz 3F3 Ferroxcube equations vs 300 kHz data .....	70

Figure 46: 100-500 BFLS for Hysteresis Loss Equation.....	71
Figure 47: 100-500 kHz Using the HLE Coefficients from 70 & 140 Hz data.....	73
Figure 48: 100-300 kHz using the HLE Coefficients from 70 & 140 Hz data.....	74
Figure 49: 300-500 kHz using the HLE Coefficients from 70 & 140 Hz data.....	75
Figure 50: CECE for 100-500 kHz Data.....	77
Figure 51: Bertotti's STPL Model Using 100 kHz Data .....	79
Figure 52: Bertotti's STPL Model Using 500 kHz Data .....	80
Figure 53: Pex using Bertotti's STPL Model for 100-500 kHz data .....	81
Figure 54: Bertotti's Excess Eddy Loss LSBF Vo term using 100 kHz data .....	82
Figure 55: Bertotti's Model vs Actual data for 100-500 kHz .....	83
Figure 56: Plot of Bertotti's Model minus the Excess Loss Term .....	85
Figure 57: HLE & PLE Model Plot .....	86

### **List of Tables**

Table 1: Ferroxcube 3F3 Constants [12] .....	10
Table 2: List of MnZn Ferroxcube Power Loss Equation Coefficients [12] .....	13
Table 3: Matrix and MATLAB Validation Table.....	36
Table 4: Results of the MATLAB and Matrix Method .....	37
Table 5: Residuals of Hysteresis Equation at 70 Hertz.....	41
Table 6: Using the BFLS 70 hertz coefficients for 140 hertz estimates .....	42
Table 7: BFSL 70 and 140 Hertz data for Hysteresis Loss Equation ( $\alpha=1$ ) .....	43
Table 8: BFSL 70 and 140 Hertz data for Hysteresis Loss Equation ( $\alpha$ unconstrained) ..	44
Table 9: Effective Core Area of Cores used .....	53
Table 10: Error for same lot same size cores.....	54
Table 11: 100 kHz Region 1 Core Loss Core Comparison .....	56
Table 12: 100 kHz Region 2 Core Loss Core Comparison .....	57
Table 13: 500 kHz Region 1 Core Loss Core Comparison .....	59
Table 14: 500 kHz Region 2 Core Loss Core Comparison .....	59
Table 15: 500 kHz Region 3 Core Loss Core Comparison .....	59
Table 16: Core Resistivity and Permeability values .....	60
Table 17: Steinmetz Equation.....	61
Table 18: $R^2$ and LSBF Steinmetz Equation coefficients at High Freq.....	63
Table 19: Residuals for High Freq using the Power Law Equation .....	65
Table 20: Residual data for 100-300 (kHz) PLE .....	66
Table 21: Residual data for 300-500 (kHz) PLE .....	67
Table 22: Residuals of PLE for both Manufacturer Data and Estimated .....	68
Table 23: The Hysteresis Loss Equation LSBF for 100-300 kHz and 300-500 kHz .....	72
Table 24: LSBF of Low Freq Coefficients at 100-500 kHz .....	75
Table 25: Residuals for Classical Eddy Current Equation.....	77
Table 26: EECL LSBF Residuals in finding $V_o$ by using 100 kHz data at 100 kHz $P_{ex}$ ..	82
Table 27: $R^2$ for Bertotti's Model minus the Excess Loss Term .....	84
Table 28: HLE & PLE Model LSBF Results.....	86
Table 29: LSBF $R^2$ for all Models using only 100-300 kHz 3F3 TN23/17/4 data .....	88
Table 30: LSBF $R^2$ for all Models using only 300-500 kHz 3F3 TN23/17/4 data .....	89
Table 31: TN23/14/7 Data 70 Hz, 140 Hz and 100 kHz data.....	105
Table 32: TN23/14/7 Data 200 - 500 kHz data.....	106

Table 33: Conductivity AC data for 3F3 Plata .....	107
Table 34: DC Conductivity for 3F3 Plate .....	107
Table 35: Data using Impedance Analyzer .....	108
Table 36: 6 Varying Core Sizes CPL Data 100 kHz .....	108
Table 37: 6 Varying Core Sizes CPL Data 500 kHz .....	109



## Section 1 Introduction

### 1.1 Purpose/Problem

---

Methods to accurately predict power losses in magnetic materials have occupied the minds of engineers and scientists since Charles Steinmetz first published the "*Theory and calculation of alternating current phenomena*" in 1897. Steinmetz is credited with being the one to first describe hysteresis loss, a power loss mechanism. Since the beginning of this century many models have been developed and used in this estimation. Unfortunately, there is not a completely accurate model that can be used for all given inputs, materials and waveforms.

Even a hundred years after Steinmetz wrote his paper, authors are still in disagreement about what are the complete mechanisms that cause Core Power Losses (CPL). Many equations have been proposed to estimate CPL, but very little work has been reported that compares these models to actual Power Ferrite data. In addition, three components used in several of CPL empirical equations have been thoroughly investigated for many materials, but there seems to be a lack of literature in the realm of power ferrites. So, the three goals of this thesis are:

1. to verify the accuracy of the low frequency use of the Hysteresis Loss Equation,
2. to substantiate the validity of the use of two independent variables, core area and conductivity, commonly found in many CPL empirical equations,
3. and to explain and compare several empirical CPL equations against actual CPL experiment data in Ferrites,

### 1.2 Significance

---

CPL is the input power that is consumed by the magnetic material used in a magnetic circuit. These losses reduce the end users usable power and must be accounted for in system design. To compensate for these losses, large safety factors must be incorporated which result in over-designed systems (motors, generators). If the losses can be accurately modeled, the safety factors can be reduced. This results in smaller components, lighter displacement, and overall lower cost.

An example of a potential user of an accurate CPL model is the designers of the complex power systems that operate on United States Navy warships. Space and weight are two major constraints in ship design. Almost every electrical component used to power naval vessels, including the large and particularly heavy electrical engines, are over-designed due to inaccurate CPL estimates. This increases the weight of the ship and reduces available internal volume. Using a validated accurate core power loss model, engineers could effectively and efficiently design products based on size and weight using core power losses as a parameter.

### 1.3 Thesis Overview

---

This thesis is broken into 5 major chapters. Chapter 1 includes theory background behind Core Power Losses (CPL), descriptions of several CPL models, and the goals of the thesis. Chapter 2 describes the experiments required to accomplish these goals and the accuracy of those

experiments. Chapter 3 provides experimental results of using the Hysteresis Loss equation for low frequency applications. Chapter 3 also provides experimental data used to validate the use of core area and conductivity as independent terms in CPL empirical equations for 3F3 Power Ferrite cores. Chapter 4 presents the residuals of the Least Square Best Fit to several empirical models when compared to actual CPL measured data. The conclusion of this thesis can be found in Chapter 5.

---

## 1.4 Background

---

A robust history of the progression of the traditional models and methods used to calculate Core Power Losses from Steinmetz's Hysteresis paper of 1897 to Bertotti's 1981, "A new approach to the study of loss anomaly in SiFe" can be found in reference [1]. This paper provides an excellent reference for the interested reader in the scientific advances in the determinations of the causes of magnetic Core Power Losses.

To understand Core Power Losses, one must first understand the general theory behind the losses. As the author of [1] explains, a magnetic core sample with a changing magnetic field through the core produces closed path voltages in the core. Those closed path voltages induce resistive eddy currents which oppose the changing magnetic field. The total mechanism gives off energy in the form of heat. This heat is in the form of irreversible power, i.e. energy is consumed by the material itself.

Typically in literature, this energy loss, Core Power Losses (CPL), is grouped into two loss categories: Hysteresis Losses and Eddy Current Losses; and Eddy Current Losses are further subdivided into Classical Eddy Current Loss and Excess Current Losses. The only difference between these three losses is the method or equation that was used to calculate them [1]. As the authors of [1] and [2] explain, there is no distinction between them: the losses arise from the same mechanism. There is even a debate of which of the losses are the most dominant. Reference [3] states that Classical Eddy Current Loss is relatively small compared to the other three Losses in power ferrites. This is in contrast to [4] who explains that Excess Current Loss is the smallest CPL loss.

Two methods are used to estimate these Core Power Losses: Hysteresis models and empirical equations [2]. A material's CPL can be measured by calculating the area inside a material's hysteresis loop. Hysteresis models use hysteresis shaping algorithms to estimate this area and several of the commonly used models can be found in references [5] and [6]. Empirical Equations use previously-determined CPL data fit equations to estimate CPL. References [3], [7],[8],[9] and [10] provide many currently used CPL Empirical equations. An example of one the most widely used CPL empirical equations is the Separation of total power losses (STPL) equation. The STPL equation combines three empirical equations, one for each loss group, to give a total CPL equation. Reference [9] provides a good example of this STPL equation and how it is used. Both of these methods are discussed in the next several sections.

---

## 1.5 Hysteresis Loss

---

Hysteresis loss is the energy lost in a material during a non reversible energy cycle. A reversible cycle is a system that can start and end a process at the same point without the

accumulation of additional energy. An interesting discussion of this topic was conducted by Dr. Steinmetz in 1892. It is included in this paper due the relevance of the topic even today.

“If the complete conversion of one form of energy into another is possible, the opposite conversion is not completely possible. Or if we convert a certain amount of one form of energy into another form of energy, and this back again into the first form of energy, which we call a cyclic conversion of energy- we do not get back the original amount of energy, but less, and a part of the energy has been lost; that means, converted into and dissipated as heat. Therefore no complete cyclic conversion of energy exists, but by any such cycle the amount of available energy has decreased by the fraction that was converted into heat. ... Now, as long as the magnetism increases, electric energy is transferred from the electric current and converted into potential magnetic energy. While the magnetism decreases, potential magnetic energy is reconverted into electric energy, and appears in electric circuit as E.M.F. But the full amount is not given back to the electric circuit, but less. Less by that amount that has been converted into heat by hysteresis.” [7]

The general literature description of Hysteresis Loss is the loss of energy accrued during the domain direction shifts of magnetic materials. Magnetic domains are the portions of a material that are magnetized in the same direction. The author of [1] explains that most materials do not have uniform magnetic domains, i.e. the magnetization direction is not constant throughout the material. The material is broken up into same direction domains separated by a wall of adjacent and opposite direction domains. To get an overall increase in magnetic field, the area of the domains in that magnetic direction must increase with a corresponding decrease to the domains in the opposite direction. These domain area shifts result in the domain boundary walls shifting. These wall shifts produce local eddy currents which, in turn, give off unrecoverable energy in the form of heat. The following figure helps to explain this theory.

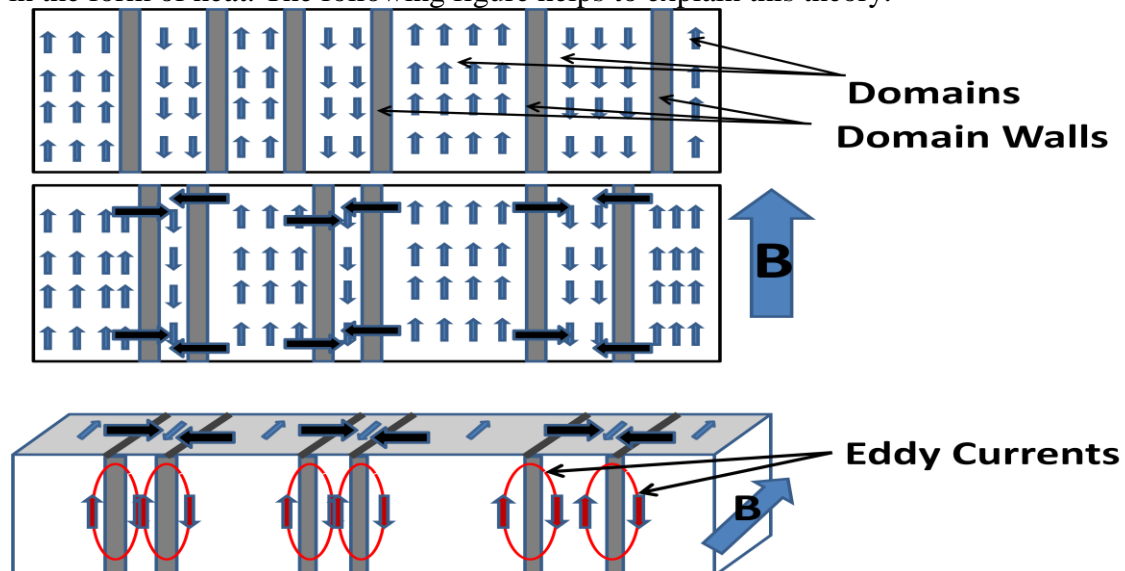


Figure 1: Domain Wall Theory, adapted from figures in Reference [1] and [2]

This process is pertinent to almost all magnet materials under a changing magnetic field. For materials acting under an Alternating Current (AC) signal, the domain walls shift direction

every half cycle. Since the same amount of energy is lost every cycle, once the energy losses are calculated for one cycle, the loss can be multiplied by the frequency of the cycle to get the a total loss. This loss mechanism is called Hysteresis Loss. For Power Ferrites, the Hysteresis loss curve has a double sigmoidal shape. The figure below is an example of this Hysteresis Loss curve. The energy lost, or CPL, in the cycle is the area enclosed in the curve.

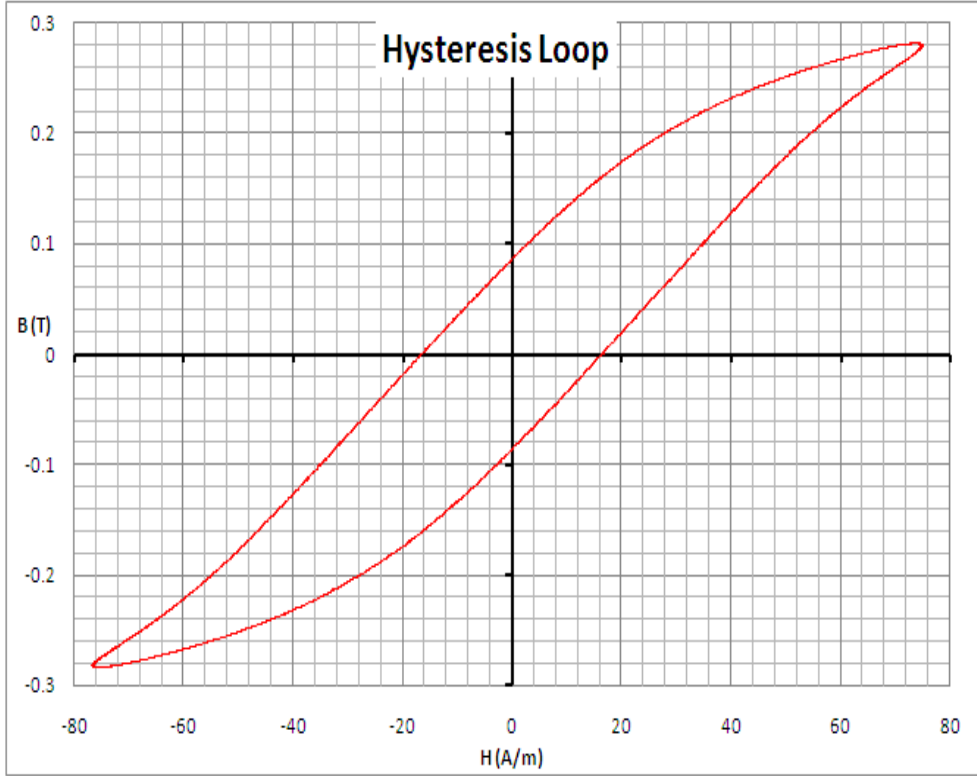


Figure 2: Hysteresis Loop at 100kHz and @ 273mT

Hysteresis loss can be mathematically estimated using algorithm methods such as Rayleigh, Peterson, Stoner-Wolhfarth, Jiles-Atherton, Globus, and Preisach [5], [6]. These methods use experimentally determined coefficients in algorithms to approximate the sigmoidal shape at varying points during the saturation curve. As explained above, the area bounded in the sigmoid is the CPL. One of the benefits of using algorithm models versus any other CPL calculation method is their adaptability for use in a variety of materials.

## 1.6 Empirical Equations

For a century, CPL empirical equations have been used as a method to model CPL. CPL empirical equations are equations that are statistically fit to actual CPL data to provide an estimate of what CPL could potentially be. Equation 1 is an example of one that was first proposed in 1892 by Steinmetz [7].

$$\bar{P}_v(t) = k\hat{B}^\beta \quad \text{Eqn 1}$$

$\hat{P}_v$  is the power loss per unit volume,  $\hat{B}$  is the maximum peak flux amplitude,  $\beta$  and  $k$  are curve fitted coefficients of actual experimental data. One limitation to using empirically fit equation is their accuracy. The amount of data, the range of data, the type of data and the equation used in the fit all vary CPL estimation accuracy. For instance, this model assumes that that core loss per unit volume is independent of core geometry, for a given flux level. Moreover, the above equation does not include frequency as an equation variable. As it will be later discussed, CPL is frequency dependent and can vary CPL estimation accuracy tremendously. To increase CPL estimation accuracies for broader ranges more terms are incorporated in the data fitting. Equation 2 is an example of this.

$$\bar{P}_v(t) = kf^\alpha \hat{B}^\beta \quad \text{Eqn 2}$$

$\hat{P}_v$  is the power loss per unit volume,  $\hat{B}$  is the maximum peak flux amplitude,  $\alpha$ ,  $\beta$  and  $k$  are curve fitted coefficients to actual experimental data. Equation 2 is what some authors refer to as the Steinmetz equation [11] but what the authors of [3] emphasize is actually the Power Law Equation (PLE). The PLE is a CPL empirical equation used by most manufacturers and engineers.

Gathering the required data to fit a CPL empirical equation is one shortcoming to using CPL empirical equation models. CPL data is either collected by the material manufacturer and equations are fit to it or data is gathered by intended material user. Data collection presents three obstacles: finding a standard procedure to take CPL data, obtaining equipment required by the procedure, and then having the time required to take the measurements. Typically, many scientists and engineers use already-fit manufacturer-provided CPL equations in lieu of actual data collection.

Table 1 is an example of a manufacturer's PLE coefficients used in CPL estimation. The validity of CPL attained by these equation coefficients is only as accurate as the method used to obtain them. Several factors that can vary CPL accuracy are the type of waveforms used, actual characteristics of the core, i.e. size, shape and material, and the ranges of the inputs. Thus, unless the engineer or scientist uses the same parameters as the manufacture, CPL accuracy may vary.

Table 1: Ferroxcube 3F3 Constants [12]

Freq (f)	k	$\alpha$	$\beta$
100-300	2.50E-04	1.63	2.45
300-500	2.10E-05	1.8	2.5
500-1000	3.60E-09	2.4	2.25

Phillips, a commercial magnetic core producer, states its empirical CPL fit formula has a standard deviation of 5 to 17 percent with an estimated CPL accuracy to within 25% [13]. This demonstrates that manufacture provided CPL best fit equations is only a rough estimate. This CPL estimation accuracy can be reduced through actual experimental data collection as long as care is taken to ensure comparable condition exists between the data set and the application of interest.

As stated in the previous section, there are many methods that can be used to estimate Core Power Losses (CPL), be it Hysteresis Loss models or empirical equations. However, very

little work has been reported that compares these models to actual Power Ferrite CPL data. The goal of this thesis was to evaluate several models and provide a brief comparison between them.

Unfortunately, due to time constraints, only methods that involve empirical equation estimations were used in this evaluation. This was done to limit the expanse of this thesis. A more robust CPL model comparison could be conducted which should also included all the Hysteresis Loss algorithm models.

A list of the predominant equations for calculating loss under sine wave excitation are included below.

1. Steinmetz Equation [7]

$$P_v = k_h \hat{B}^\beta \quad \text{Eqn 3}$$

2. Power Law Equation [3]

$$P_v = k_h f^\alpha \hat{B}^\beta \quad \text{Eqn 4}$$

3. Hysteresis Loss Equation [8],[9],[13]

$$P_h = k_h f \hat{B}^\beta \quad \text{Eqn 5}$$

4. Classical Eddy Current Loss [9],[10]

$$P_{cl} = k_c \sigma f^2 \hat{B}^2 \quad \text{Eqn 6}$$

where

$$k_c = \frac{\pi^2 d^2}{\beta} \quad \text{Eqn 7}$$

$\beta = 6$  for laminated thickness  $d$  (m) (laminated cores)  
 $\beta = 16$  for cylinders of diameter  $d$  (m) (cylindrical cores)  
 $\beta = 20$  for sphere of diameter  $d$  (m) (spherical cores)

and for square toroidal cores with  $d/2 \ll R_0$  using Section 1.7.2 Classical Eddy Current equation, Equation 8 gives  $k_c$  as

$$k_c = \frac{le\pi d^2 \log(\frac{R_2}{R_1})}{12(R_2 - R_1)} \quad \text{Eqn 8}$$

Both the Hysteresis Loss equation and the Classical Eddy Current Equation will be used in Equation 9 and 10 as the first and second term in the STPL equation (see Sect. 1.7).

5. Bertotti's Model [9]

$$P_v = k_h f \hat{B}^\beta + k_c \sigma f^2 \hat{B}^2 + 8\sqrt{(\sigma G S V_o)} f^{1.5} \hat{B}^{1.5} \quad \text{Eqn 9}$$

6. Hysteresis Loss Equation and Classical Eddy Current Equation Model<sup>1</sup>

$$P_v = k_h f \hat{B}^\beta + k_c \sigma f^2 \hat{B}^2 \quad \text{Eqn 10}$$

7. Hysteresis Loss Equation and PLE Equation Model<sup>1</sup>

$$P_v = k_h f \hat{B}^{\beta_1} + k_{ex} f^\alpha \hat{B}^{\beta_2} \quad \text{Eqn 11}$$

See Sections 1.7.1, 1.7.2, and 1.7.3 for a description of the terms in the above equations.

## 1.7 Separation of Total Power Losses

---

Separation of Total Power Losses (STPL) is a widely used method for Core Power Losses (CPL) calculation. STPL divides total Core Power Losses into three separate subdivisions; Hysteresis Loss ( $P_h$ ), Classical Eddy Current Loss ( $P_{cl}$ ), and Excess Eddy Current Loss ( $P_{ex}$ ). The following equation is how these three subdivisions are combined to provide a total CPL equation. An explanation of the terms used in (Eqn 12), a STPL model, will be presented in the following sections.

$$P_{tot} = P_h + P_{cl} + P_{ex} \quad \text{Eqn 12}$$

Hysteresis loss is defined as the loss equal to the area of the static magnetization loop times the cycle rate [13]. Classical Eddy Current loss is based on Maxwell's equations, but does not including domain wall theory [14]. Excess Loss is the loss not included in the two previous loss mechanisms.

(Eqn 9) is an example of a commonly used STPL model which all three CPL components are present; Hysteresis Loss, Classical Eddy Current Loss, along with an additional term he introduces as Excess Eddy Current Loss. This model was derived by Bertotti [9] and will be discussed in greater detail discussed later in the thesis.

$$P_{tot} = P_h + P_{cl} + P_{ex}$$

$$P_{tot} = k_h \hat{B}^\beta f + k_c \sigma \hat{B}^2 f^2 + 8\sqrt{(\sigma G S V_o)} \hat{B}^{1.5} f^{1.5}$$

$P_{tot}$  is the power loss per unit volume,  $\hat{B}$  is the maximum peak flux amplitude,  $f$  is frequency,  $\beta$ ,  $k_h$ ,  $k_c$  and  $V_o$  are curve fitted coefficients determined through actual experimental data.  $S$  is the cross-sectional area of the core,  $\sigma$  is the conductivity of the material and  $G$  is a unitless constant with value of .1356.

One argument used to justify STPL method in power ferrite applications is that when loss data from Manganese Zinc (MnZn) Power Ferrites between 100 kHz to 500 kHz CPL data is empirically fit to the PLE given in Equation 3, the values of the curve-fitted coefficients are consistent with several STPL terms. The first STPL term, Hysteresis Loss, will be experimentally justified in Section 3.1 and will not be discussed in this section, but justification of the other two can be deduced based on the range of the curve fitted coefficients. As the references [3],[5],and [12] state, the curve-fitted coefficients,  $\alpha$  and  $\beta$ , range between 1.4 and 2.8 and 2.4 and 3 respectively. As [5] points out, since  $\alpha$  is not 1, there must be an additional Power Loss term other than Hysteresis Loss implicitly (assuming that a linear sum of different terms is

an appropriate formation.) Reference [3] states that since Static Hysteresis is proportional to frequency, and  $\beta$  is about 1.5 to 2, the bulk of the Power Loss must come from an Excess Loss term.

An example of manufacturer curve fitted coefficients commonly used in Power Ferrite application can be found in Table 2.

Table 2: List of MnZn Ferroxcube Power Loss Equation Coefficients [12]

	Freq (khz)	C	$\alpha$	$\beta$
<b>3F3</b>	100-300	2.50E-04	1.63	2.45
	300-500	2.10E-05	1.8	2.5
	500-1000	3.60E-09	2.4	2.25
<b>3F4</b>	500-1000	1.20E-03	1.75	2.9
	1000-3000	1.10E-11	2.8	2.4
<b>3C30</b>	20-100	7.13E-03	1.42	3.02
	100-200	7.13E-03	1.42	3.02
<b>3C90</b>	20-200	3.20E-03	1.46	2.75
<b>3C94</b>	20-200	2.37E-03	1.46	2.75
	200-400	2.10-e9	2.6	2.75

As Table 2 indicates, the curve fitted coefficient's values are frequency dependent and change from one material to another. The next three sections will discuss the theory behind the three components of STPL equation in greater detail.

### 1.7.1 Hysteresis Loss

---

Hysteresis Loss is the first component of the traditional Separation of Total Power Losses equations. Several of the Hysteresis Loss methods discussed above can be used for this determination. For this thesis, an experimental determined method outlined in several papers was used. This method uses low frequency magnetic core experimentation to collect low frequency CPL data. This data is then curve fitted to provide a Hysteresis Loss equation to be used for the higher frequency applications of STPL.

Reference [13] says that the area of the Hysteresis loop times the frequency at very low frequencies is an accurate estimate of CPL. He explains that at low frequencies, the power loss due to the Classical Eddy Current Loss and Excess Eddy Current Loss is very small when compared to the Hysteresis Loss. Reference [9] also explains that for low frequencies, Hysteresis losses are the dominant loss mechanism [9]. The Hysteresis Loss equation, (Eqn 4), has the form

$$P_h = k_h f \hat{B}^\beta$$

The Power Loss due to Hysteresis,  $P_h$ , was found at low frequencies as suggested by reference [13]. Curve fitting coefficients  $k_h$  and  $\beta$  were determined using Core Power Loss data taken at 70 and 140 Hz. Section 3.1 provides the result of experimentation used to measure actual Hysteresis Loss curve fitted coefficients in (Eqn 4) for 3F3 power ferrite material.

### 1.7.2 Classical Eddy Current Loss

---



Classical Eddy Current Loss is usually described in terms of core sample in a changing magnetic field. The changing field creates closed path voltages in the sample, which then produces resistive eddy currents that oppose the changing magnetic field. The resultant eddy currents produce material power losses. Classical Eddy Current Loss, (Eqn 6), is a physics-based equation mathematically derived to describe power loss based on ohmic conduction. A form of this equation is included in Steinmetz's Iron Power Loss estimates presented in 1892 and as [1] explains, "it might have first been deduced by Steinmetz, himself [7]." The Classical Eddy Current Loss equation, has the form

$$P_{cl} = k_{cl} f^2 \hat{B}_{pk}^2$$

Where  $P_c$  is the classical eddy current power loss,  $f$  is frequency,  $\hat{B}$  is the maximum peak flux amplitude,  $k_{cl} = A_c \sigma \pi / 4$  for a cylindrical core, and  $\sigma$  is the conductivity.  $A_c$  is the cross-sectional area of the core.  $k_{cl}$  is the coefficient that accounts for geometry and conductivity of that core [1]. The model's foundation is the assumption that magnetic fields in a material are both uniform and parallel to the cores axis [1]. Since  $A_c$  is included in the equation, it can be deduced that (Eqn 6) is proportional to core cross-sectional area. Thus, one does not expect a core loss per unit volume to be independent of core cross-sectional area if indeed this is a correct model of the loss behavior.

A derivation for Classical Eddy Current Loss,  $P_{cl}$ , follows. This derivation was conducted by Dr. David Perreault and the author using a cylindrical rod of homogenous permeability. It was also assumed that eddy currents flow tangential to that rod. The derivation is provided for the interested readers. Reference [13], [15], [16], [17] and [18] provides  $P_{cl}$  equations for several varying core shapes.

The assumptions for the derivation of Classical Eddy Current Loss are:

1. Homogenous Permeability
2. Flux Density,  $\hat{B}_{pk}$ , flows into a circular cross section cylinder
3. The magnetic fields in a material are uniform.

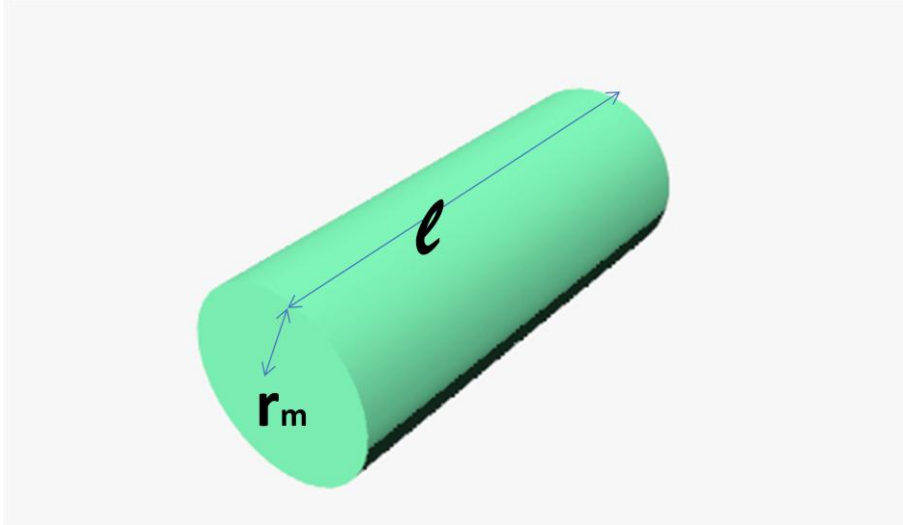


Figure 3: 3D Cylinder for  $P_c$  derivation

If the radius of a loop in the cylinder,  $r$ , varies between zero and the outer radius,  $r_m$ , and the cylinders enclosed flux,  $\Phi$ , is given by the equation  $\Phi = \pi r \hat{B}_{pk}$ , the loop voltage,  $V_{pk}$ , can be written as

$$V_{pk} = \pi r^2 \omega \hat{B}_{pk} \quad \text{Eqn 13}$$

Cylinder Resistance,  $R$ , can be written as cross-section of the cylinder,  $A_c$ , over the conductivity of the material times the length of the cylinder.  $R = 2\pi r / \sigma l$ .  $l$  is the length of the cylinder.

If magnetic field is constant over the cores cylindrical cross section, the Average Power Dissipated with respect to  $r$  is given by (Eqn 14).

$$P_{av}(r) = \frac{(V_{pk})^2}{2R} = \frac{(\pi \omega r^2 \hat{B}_{pk})^2 \sigma l dr}{4 \pi r} \quad \text{Eqn 14}$$

Total Power,  $P_{tot}$ , then becomes

$$P_{tot} = \int_0^{r_m} \frac{\pi \omega^2 r^3 \hat{B}_{pk}^2 \sigma l dr}{4 r} \quad \text{Eqn 15}$$

Integrating (Eqn 15) over the width of the cylinder results in (Eqn 16).

$$P_{tot} = \frac{\pi \omega^2 r_m^4 \hat{B}_{pk}^2 \sigma l}{16} \quad \text{Eqn 16}$$

To get power per unit volume, (Eqn 18), (Eqn 16) is divided by the volume of the cylinder.

$$P_{cl} = \frac{P_{tot}}{\pi r_m^2 l} \quad \text{Eqn 17}$$

$$P_{cl} = \frac{\omega^2 r_m^2 \hat{B}_{pk}^2 \sigma}{16} \quad \text{Eqn 18}$$

Angular frequency,  $\omega$ , is converted to  $2\pi f$  in (Eqn 19).

$$P_{cl} = \frac{\pi^2 f^2 r_m^2 \hat{B}_{pk}^2 \sigma}{4} \quad \text{Eqn 19}$$

With cylinder area,  $A_c$ , equal to the  $\pi r_m^2$ , (Eqn 19) can be written with respect to core cross-sectional area by (Eqn 20).

$$P_{cl} = \frac{\sigma \pi f^2 \hat{B}_{pk}^2 A_c}{4} \quad \text{Eqn 20}$$

The accuracies of the above equation are bounded by a cylindrical shaped core and the previous given assumption. The experimental portion of the thesis used a square toroid and not a cylindrical core, so a deviation from of the equation is required. This deviation is the result of a square toroid not having a uniform magnetic field in the core. For calculation, Bessel functions were required to obtain an estimate of the Core Loss.

Reference [18] provides the derivation for square cross-section toroid and is presented for the interest of the reader. The equation has been modified to allow a useful Classical Eddy Current equation to be used throughout this paper.

For  $d/2 \ll R_0$

$$P_{tot} = \frac{\omega \mu_o \mu_r I^2 N^2 2 \left(\frac{d}{2}\right)^3 \log\left(\frac{R_2}{R_1}\right)}{3 \pi \delta^2} \quad \text{Eqn 21}$$

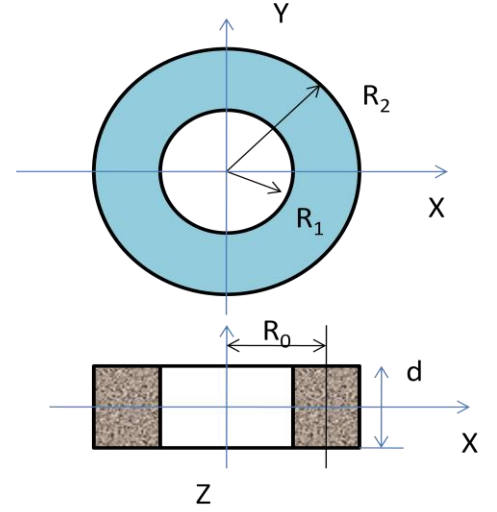


Figure 4: Rectangular toroidal Core Figure [40]

Where  $\omega=2\pi f$  the frequency,  $N$  is the number of turns,  $\mu_o$  and  $\mu_r$  are the permeability of free space and relative permeability respectively,  $I$  is the rms value of current,  $d$  is the height of the core,  $R_2$  and  $R_1$  are the outer and inner diameter of the core respectively, and  $\delta$  is the skin depth.

Given the following equations;

$$\delta = \sqrt{\frac{1}{\pi f \mu_o \mu_r \sigma}} \quad \text{Eqn 22}$$

$$I = \frac{\hat{I}}{\sqrt{2}} \quad \text{Eqn 23}$$

$$\hat{H} = \hat{I} N / l_e \quad \text{Eqn 24}$$

$$\hat{B}_{pk} = \mu_o \mu_r \hat{H} \quad \text{Eqn 25}$$

and the  $P_{tot}$  from above the following is the  $P_{tot}$  in terms of  $\hat{B}_{pk}$  and  $f$ .

$$P_{tot} = \frac{\sigma \pi f^2 \hat{B}_{pk}^2 d^3 l e^2 \log\left(\frac{R_2}{R_1}\right)}{12} \quad \text{Eqn 26}$$

$le$  is the core equivalent length,  $\sigma$  is the conductivity,  $d$  is the height of the toroid in the Z direction,  $R_1$  and  $R_2$  are the inner and outer dimensions of the toroid,  $B$  is the magnetic flux, and  $f$  is the frequency of the wave-form.

The volume of the square core is estimated by (Eqn 27).

$$V_c = le(R_2 - R_1)d \quad \text{Eqn 27}$$

To get the Classical Eddy Current Power per unit volume, (Eqn 29), (Eqn 26) is divided by the volume of the core, (Eqn 27).

$$P_{cl} = \frac{P_{tot}}{V_c} \quad \text{Eqn 28}$$

$$P_{cl} = \frac{\sigma \pi f^2 \hat{B}_{pk}^2 d^2 l e^2 \log\left(\frac{R_2}{R_1}\right)}{12(R_2 - R_1)} \quad \text{Eqn 29}$$

If (Eqn 29) is factored to approximate the core cross sectional area of the square toroid to be given by (Eqn 30), (Eqn 29) can be written as (Eqn 20).

$$A_{sq} = \frac{d^2 l e^2 \log\left(\frac{R_2}{R_1}\right)}{3(R_2 - R_1)} \quad \text{Eqn 30}$$

$$P_{cl} = \frac{\sigma \pi f^2 \hat{B}_{pk}^2 A_{sq}}{4} \quad \text{Eqn 31}$$

As demonstrated in (Eqn 20) and (Eqn 31), the  $P_{cl}$  equations for cylindrical and square toroids, Classical Eddy Current Loss is proportional to core cross sectional area. Section 3.3 provides actual CPL data with varying core cross sectional area as a factor.

### 1.7.3 Excess Eddy Current Loss

---

As explained in Section 1.7, Excess Eddy Current Loss, (Excess Loss), as is one of the CPL mechanism that is not covered by either the Hysteresis Loss or the Classical Eddy Current Loss equation. Actually, many Excess Loss models,  $P_{ex}$ , use total CPL data minus the

Hysteresis Loss and Classical Eddy Current Loss equations to get the Excess Loss component in the STPL equation.

$$P_{ex} = P_{tot} - P_h - P_{cl} \quad \text{Eqn 32}$$

It is interesting to note that Anomalous Loss and Excess Loss are used interchangeably in CPL literature. Overshott emphasizes that Anomalous Loss is technically an inaccurate description of the loss, since Excess Loss is not an anomaly, just not mathematically adequately defined [19].

The general difference between Classical Eddy Current Loss and Excess Losses is the understanding that Classical Eddy Current Loss is derived by assuming that the core is both homogenous and has only one core eddy current loop throughout the core. Unfortunately, imperfections in the core material result in more than one eddy current loop. To account for these additional eddy current loops, STPL models use this Excess Loss term [20]. One of the reasons that (Eqn 31) is typically used to obtain this Excess Loss term is that the varying intrinsic properties of the material make Excess Loss very difficult to model.

Reference [20] lists several of the theoretical explanation used to explain Excess Loss. They are listed below to give the reader an idea that the concepts of Excess Loss are dependent on many material properties.

1. Occurrence of domain walls, domain wall angles.
2. Non-sinusoidal, non-uniform and non-repetitive domain wall motion.
3. Lack of flux penetration and domain wall bowing.
4. Non-sinusoidal flux density and localized variation of flux density.
5. Interaction between grains, grain size, grain orientation, and specimen thickness effects.
6. Nucleation and annihilation of domain walls.

## Section 2 Experimental Data Collection Method and Design

### 2.0 Required Experiments to achieve thesis goals

---

As explained in Section 1.1, the three goals of this thesis are:

1. to explain and compare several empirical Core Power Loss (CPL) equations against actual CPL experimental data,
2. to substantiate the validity of the use of two independent variables, core area and conductivity, which are commonly found in many CPL empirical equations,
3. and to verify the accuracy of the low frequency use of the Hysteresis Loss equation.

Actual CPL and conductivity data was measured to accomplish the above goals. Section 2 provides the method and the design apparatuses required for above measurements. Section 2 also provides an accuracy section for each test fixture.

Only one apparatus was built to accomplish all the goals. This apparatus needed to allow the user to define inputs such as frequency, excitation waveform, magnetic flux, and temperature. This apparatus would be used in future non-sinusoidal experiments.

Several standard methods exist which allow the measurement of a material's CPL. The first step in choosing the method to use is to first determine which method is applicable to the designer's needs. The following is a listing of the accepted International Standard 62044-3 CPL collection methods [21].

1. Root-mean-square method
2. V-A-W meter method
3. Impedance analyzer method
4. Digitizing Method
5. Vector Spectrum method
6. Cross-power method
7. Reflection measurement method
8. Calorimetric measurement

For this thesis, the Digitizing Method was the chosen collection method. The following are a few of the reasons why the other methods were eliminated. The Root-mean-square method is only proportional to CPL and does not account for phase shifts in the core [21]. V-A-W meter and Impedance Analyzer only use sinusoidal input waveforms [21]. As stated above, a method that allowed non-sinusoidal waveforms was desired. Vector Spectrum method required a network analyzer and the Cross-power method required Fast Fourier Transforms for all measurements. Reflection measurement method is usually used for frequencies above the scope of this thesis [21]. The Calorimetric measurement method was eliminated due to the time consuming measurements involved in the method.

One benefit to the Digitizing Method was it only required an oscilloscope, probes and a signal generator. With only a slight alteration to the apparatus, this method also allowed for conductivity measurements. Section 2.3 has a list of the equipment used in this thesis. The

Digitizing Method used the oscilloscope to measure time discrete quantizes of core current and voltages. These quantizes when multiplied give CPL data.

## 2.1 Digitizing Method for Core Power Losses Calculations

Figure 5 is the designed CPL measuring apparatus. This apparatus was developed using the Digitizing Method as outlined by the International Standard IEC 62044-1, IEC 62044-3 and [22]. A discussion of why the components selected in the Digitizing Method follows. A list of the equipment used in this thesis is found at the end of Section 2.4.

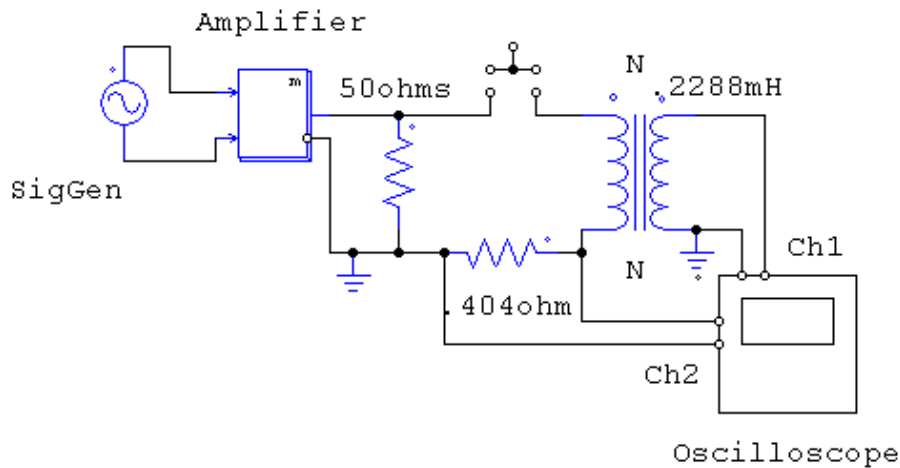


Figure 5: CPL Circuit Design

Two criteria were used in determining the both the material and shape of the magnetic core. The first criterion was to choose a core material and shape used commonly in power ferrite applications. The second was to choose a shape that simplified the CPL mathematical analysis calculation. The frequency range used in this experiment was 100 to 700 kHz and the material used was 3F3. 3F3 is a Manganese Zinc power ferrite manufactured by Ferroxcube. All the ungapped toroidal shaped CPL mathematical equations were found in International Standard IEC 62044-2. For simplicity reasons, this shape was chosen.

To measure 3F3 Core Power Losses, the 3F3 toroid core primary and secondary windings were wound with the same number of turns. International Standard IEC 62044-2 provided a base-line for the minimum number of core turns required for CPL data collection. As required by [21] the wire winding were wound as tight and as evenly around the core as possible. This ensured an even magnetic flux between the core and the windings. It also maximized the magnetic flux linkage coefficients [21]. To minimize phase shift between the two oscilloscope channels, reference [21] required component connections to the core to be as short as possible. A 50 ohm impedance matching resistor was placed in between and in parallel with the amplifier and the core. This resistor stabilized the inductive circuit.

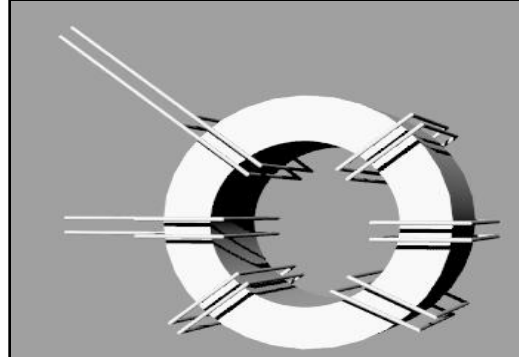


Figure 6: Ring Toroid

A sinusoidal waveform developed by the signal generator and magnified by the amplifier was applied to the primary of the 3F3 core. The resultant alternating magnetic field in the primary produced a voltage in the secondary. The average of the product of this current and voltage (over one cycle) is the Power Loss. Core Power Loss, CPL, is the average power loss per volume of the core as given in (Eqn 33).

$$P_v = \left\langle \frac{P}{V_{ec}} \right\rangle = \left\langle \frac{IV}{V_{ec}} \right\rangle = \frac{1}{V_{ec}T} \int_0^T I(t)V(t)dt \quad \text{Eqn 33}$$

The CPL, (Eqn 33) used the secondary transformer open circuit voltage (V) and the current through the primary (I) as inputs.  $V_{ec}$  is the effective volume of the core as determined by core data sheet. T is the period of one cycle of the waveform. Reference [22] explains that by measuring secondary open circuit voltage, the power loss due to both the secondary leakage inductance and winding resistance attributable to current flow are avoided in the measurements. A parasitic impedance path in parallel with the sense resistor was eliminated by connecting the secondary winding's ground to common ground [22]. This path could potentially have caused CPL measurement error. The value of the sense resistor resistance affected both the accuracy of the measuring circuit as outlined in reference [23] and the preconditioning circuit quality as described in Section 2.2. These two confines drove the sensing resistor to the smallest resistance feasible while still maintaining a suitable sense resistor component power rating.

The value of the inductance of the core, L, and number of transformer turns, N, were determined using the following equations:

$$L = \frac{N^2 \mu_c A_e}{l_e} \quad \text{Eqn 34}$$

$$N = \frac{2V_{pk}}{2\pi f B_{sat} A_e} \quad \text{Eqn 35}$$

$$i = \frac{B_{sat} l_e}{\mu_c N} \quad \text{Eqn 36}$$



$\mu_c$  is the core permeability determined using the manufacturer's data sheet.  $A_e$  and  $l_e$  are the effective core area and effective core length respectively.  $V_{pk}$  is the core's primary winding's peak voltage and  $B_{sat}$  is the material saturation induction value.  $i$  is the core material's current saturation value.

The three unknowns in the above equations are  $N$ ,  $V_{pk}$  and  $i$ . An optimization balance of the three was conducted to ensure both  $V_{pk}$  and  $i$  could be accurately measured by the oscilloscope. 40 volts was chosen as the peak primary voltage. Reference [23] required the number of turns be kept to a minimum for sinusoidal current excitation.

Since 12.33 is the number of turns required to reach  $B_{sat}$  for 700kHz sine-wave excitation in a TN23/14/7 core, the number was rounded to 13 turns. The HP 4192A LF Impedance Analyzer with a 16047A calibrated test fixture at 100kHz and 13 turns measured the TN23/14/7 core's inductance as 228.8  $\mu$ H. Several cores were used in this experiment although only the TN23/14/7 core is mentioned to prevent redundancy. The same method was used to figure out the turns ratio,  $V_{pk}$  and  $i$  for the other cores.

Two 500MHz 10 M $\Omega$  10x P6139A Voltage Probes were chosen to make the secondary winding and sense resistor voltage measurements. Reference [23] required all voltage measurements probes to have sufficiently high input impedance as to not affect the core output voltage. Both the probe's large input impedance and high frequency bandwidth features provided ideal probe characteristics for this experiment. The probes were calibrated using the same 500 kHz sine-wave input signal. See Section 2.3 for a list of the equipment used in the experiment.

In accordance with [22], the core was heated and maintained for 30 minutes to an experimental specified temperature. A heating plate, a cooling fan, and a large aluminum heat sink were used to the heating process. The 30 minute time length was used to ensure a temperature stable core. The Temp Fluke 52K/J Thermometer with a 1/10 decimal place accuracy was used for all temperature measurements. The Temp fluke was calibrated at 100°C. The Temp Fluke probe measured the top surface of the all the cores.

## 2.2 Preconditioning Circuit

---

Unfortunately, power ferrite materials are memory retaining materials. Memory is anytime a previous condition affects the state of the current condition. CPL values can vary based on the residual net magnetic fields obtained from exposures to previous magnetic fields. References [22] and [23] explain that magnetic core preconditioning is used to eliminate these core memory effects. One commonly employed preconditioning method is to build a decaying resonant tank circuit that swings magnetic field in the core to zero [23]. Reference [23] requires the decay of two consecutive current peaks to not be less than .78%. In addition, these decreasing consecutive peaks shall not cause an appreciable increase in core temperature. The initial field strength of the current peak must also take the core well above the saturation knee in the magnetization curve [23].

Figure 7 is the preconditioning circuit that was used during all CPL preconditioning measurements.

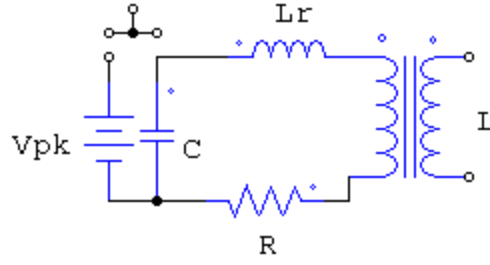


Figure 7: Preconditioning Circuit

To achieve a no more than .78% maximum decrease in consecutive current peaks means the tank circuit must have a quality factor of 13 or higher. Therefore, the following two equations were used to determine the preconditioning peak voltage,  $V_{pk}$ , and the preconditioning capacitor value,  $C$ .

$$\frac{1}{2} C V_{pk}^2 > \frac{1}{2} (L + L_r) i_{sat}^2 \quad \text{Eqn 37}$$

$$Q = \frac{\sqrt{\frac{L+L_r}{C}}}{R} \geq 13 \quad \text{Eqn 38}$$

$L$  is the value of the inductance of the 3F3 toroid core.  $L_r$  is a 246.2 micro-henry 3F3 gapped preconditioning inductor used to ensure that the saturation of the inductance  $L$  does not overly affect the decay waveform. A value close to the value of the 3F3 ferrite core was chosen.  $C$  is a 21 nano-farad mica charging capacitor. A mica capacitor was chosen due to the low parasitic resistance characteristics of this capacitor type.  $R$  is the value of the sensing resistor plus any parasitic resistance in the two inductors and the capacitor.  $Q$  is the quality factor of the tank circuit. Actual circuit values are given in Figure 6. Values were determined at 100 kHz using HP 4192A LF Impedance Analyzer with a 16047A calibrated test fixture. To ensure a quality above 13, 115 DC  $V_{pk}$  was used. Given the values of the design circuit, actual  $Q$  was determined to be approximately 38.

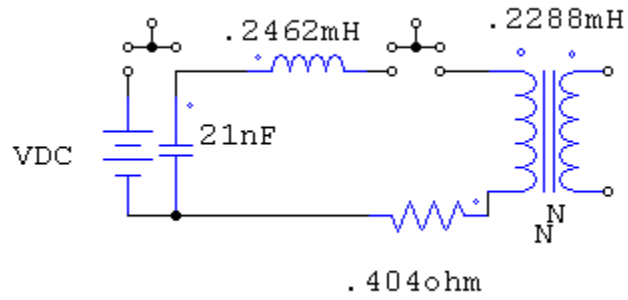


Figure 8: Preconditioning Circuit values

The resonant Frequency of the preconditioning circuit is 32.1 kilo-hertz as shown in Figure 7. Figure 7 was created using the PSIM program the above circuit values.

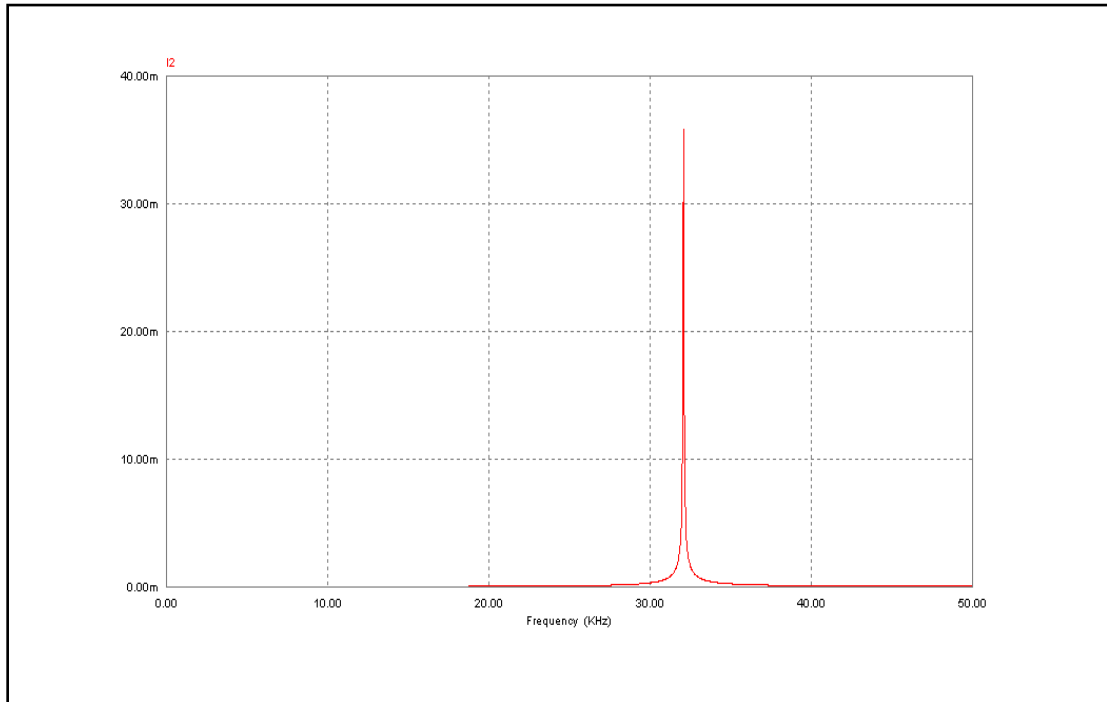


Figure 9: FFT of Current in Preconditioning Circuit

Figure 8 is the PSIM current decay result of charging the capacitor initially charged to 115 VDC. The decay of the tank circuit is well within the two consecutive current peaks requirement set forth in reference [23].

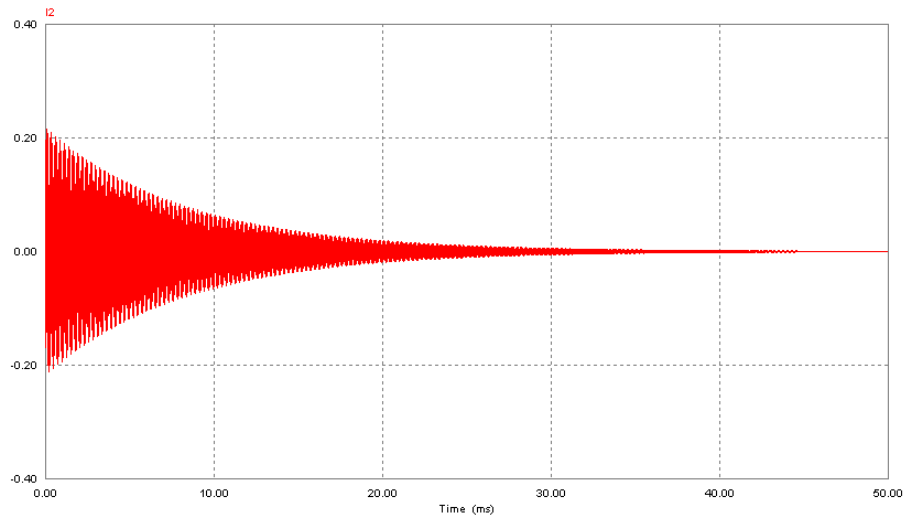


Figure 10: Current Decay of Preconditioning Circuit

$L_r$  and  $V_{pk}$  were adjusted to meet the .78% decay constant for every core using the same procedure.

As a side note, even though every CPL measurement was taken using the preconditioning circuit as outlined in reference [21],[22] and [23], the value of this step in this experimentation is questionable. As soon as the excitation signal is applied to the circuit and during the averaging process, the core obtains memory from the previous frequency cycle. Unfortunately, this memory is present during the following cycle measurement even with the preconditioning step.

### 2.3 Overall Circuit Design: Digitizing CPL and Preconditioning Circuit

---

Since high and low frequencies CPL measurements were required, two amplifiers were used. The HP 6827A amplifier was used for DC and 70-140 hertz measurements, while the Fluorocarbon Model 1040 Power Amplifier was used for 100-500 kHz power applications. The results of the measurements are in Section 3.1 and Sections 4.1-4.7.

Figure 11 is a schematic of the CPL Digitizing and Preconditioning circuit. Contact push switches were installed to integrate or disconnect either the Preconditioning or Digitizing circuit while the other circuit was in use. For every measurement, a charged preconditioning capacitor would discharge through the resonant preconditioning tank circuit which included the primary 3F3 core windings. The preconditioning circuit was then disconnected from the 3F3 toroid. The signal generator would be then turned on to produce a sinusoidal wave at a specified frequency and amplitude. This signal was then multiplied by the amplifier. The alternating signal from the amplifier was then fed through the primary winding of the core to a sense resistor. The oscilloscope measured the voltages of the sense resistor and the magnetic core's secondary winding. The oscilloscope digitally averaged these two waveforms 500 times. The averaging was done to eliminate circuit noise. The two signals were then saved and converted into an instantaneous power per volume value by MATLAB code. The MATLAB code used can be

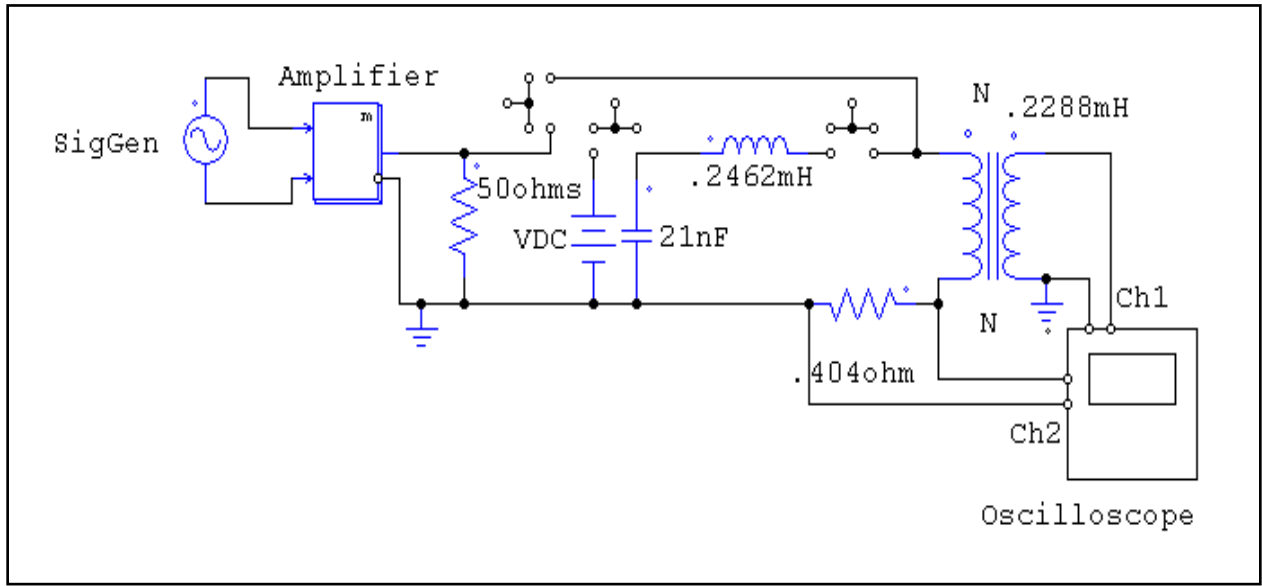


Figure 11: Overall Circuit Design: Digitizing CPL and Preconditioning Circuit

found in Appendix B. As stated in 2.1, temperature was measured and maintained at a specific specified value.

As stated also in Section 2.1, several varying sized cores were used using Digitizing CPL measurements. The core sizes were varied to determine the effect of core size on CPL. The results of the measurements are in Section 3.3.

The following is the parts inventory used in the apparatus.

1. Signal Generator: Stanford Research System Model DS345 30 MHz Synthesized Time Generator
2. HP 6827A Bipolar Power Supply/Amplifier
3. Amplifier: Fluorocarbon Model 1040 Power Amplifier 55db 10 kHz-500 kHz
4. HP 6827A Bipolar Power Supply/Amplifier
5. 50ohm: Vectronics Impedance 50ohms VSWR: 1:3:1 @ 150MHz Dissipation 300Watts
6. Oscilloscope: Tektronics TDS 3014B Four Channel Color Digital Oscilloscope
7. Probes: Channel 1 & 2: P6139A Voltage Probes 500Mhz 8.0 pF 10 MΩ 10x
8. Temperature Probe: Temp Fluke 52K/J Thermometer
9. .404 Ω 2 Watt Sense Resistor

## 2.4 Conductibility Apparatus and Measurement Procedure

The second goal of this thesis was to measure the validity of using conductivity as an independent variable in several commonly used CPL empirical equations. To achieve this goal a method and an apparatus to measure conductivity was required. A discussion of the method and apparatus used is presented in this section.

Conductivity,  $\sigma$ , with units Siemens per meter is a measure of a material's ability to conduct current. For power ferrite materials, conductivity is considered to be frequency and

temperature dependent [10] [24]. Since  $\sigma$  is a measure of a materials' ability to conduct current,  $\sigma$  is normally measured by first determining the material's resistance. Typically, a closed circuit known voltage is applied to the material and the resulting current through that material is measured.  $\sigma$  is proportional to the voltage over the current measurements, R.  $\sigma$  is given by Eqn 39 [24].

$$\sigma = \frac{l}{AR} \quad \text{Eqn 39}$$

$l$  is the length of the material,  $A$  is the cross sectional area of the material that the current flows through and  $R$  is the resistance of that material.

Three methods are typically used by engineers and scientist to determine  $\sigma$ . Since  $\sigma$  is dependent upon temperature and frequency, each method sets these dependent components to a predetermined value. The first method requires  $\sigma$  measurements to be taken at Direct Current (DC) values. The temperature of the material is heated to a specified temperature, either 25°C or the temperature of the power ferrite intended application. The second method is to measure  $\sigma$  at the same frequency and temperature used in the desired power ferrite application. This method requires complex mathematics which only the real portion of the resultant is used. The third method, which is the least accurate, is to use the manufactures' data sheet for the conductivity measurement. Typically, only DC  $\sigma$  values at 25°C are provided. An example of a manufacturer provided DC  $\sigma$  value is .5 S/m. This  $\sigma$  is the value provided 3F3 Ferroxcube data sheets for DC and 25°C and is the one used in this thesis [10].

Just recently, research into the conductivity of power ferrites was conducted in reference [24]. The result of this experiment demonstrated that power ferrites conductivity is also dependent upon AC electric field strength. Reference [24] concluded that the possible combination of high frequencies and high electric fields creates a phenomenon called tunneling. His conclusion was that the high AC electric fields cause neighboring ferrite grains separated by thin insulating films to charge tunnel. The effects of charge tunneling result in non-linear  $\sigma$  measurements [24].

To explore the results the experiment in reference [24], a test fixture based on the one used by [24] was built using a common power ferrite material, 3F3. Figure 12 is a schematic drawing of this apparatus.

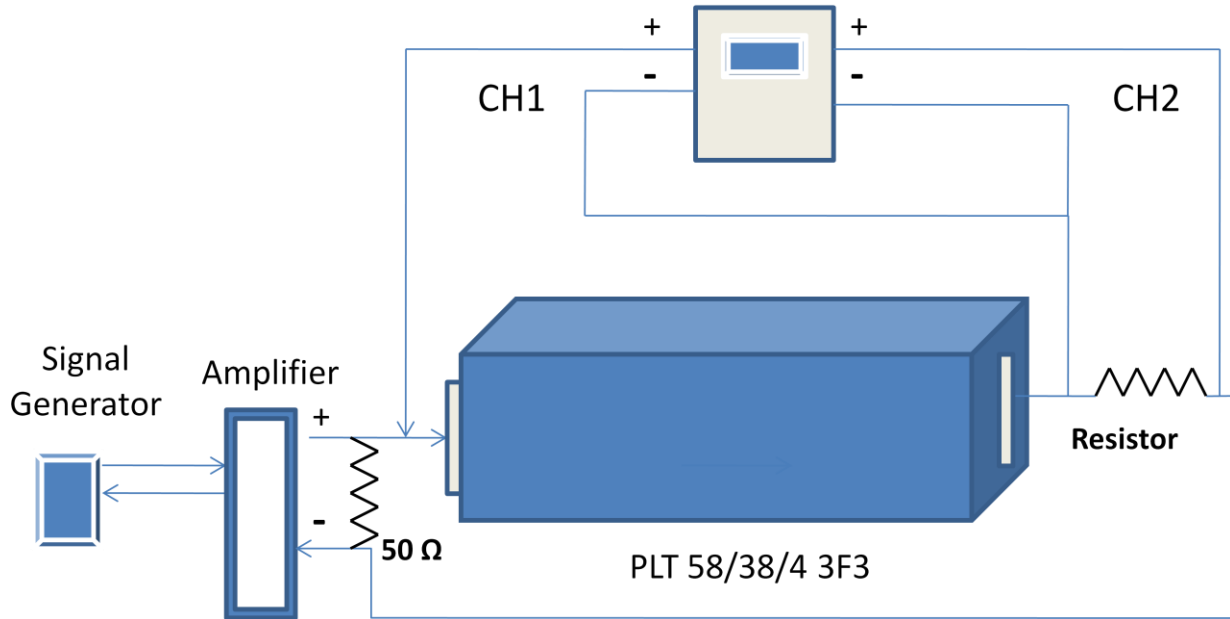


Figure 12: Conductivity Apparatus (Note: It was noted afterwards that there is the potential for dc grounding issues with this connection, but the RF measurements appeared reasonable.)

For AC signal generation the Stanford Research System Model DS345 was used. This produced a sinusoidal wave at a specified frequency and amplitude. This signal was then amplified using a Fluorcarbon Model 1040 Amplifier. The alternating signal is then fed through one end of a 3F3 PLT 58/38/4 material to a sense resistor. The 3F3 PLT 58/38/4 plate voltage and the voltage of the sense resistor are then measured by the oscilloscope. An oscilloscope common ground is obtained by connecting both oscilloscope probes to the same reference point. The current signal from the sense resistor is mathematically multiplied by negative one to compensate for probe arraignment. The oscilloscope averaged the two waveforms 500 times for noise elimination. The two signals are then converted into  $\sigma$  values by MATLAB code. This MATLAB code can be found in Appendix B. A 50 ohm impedance matching resistor was placed in parallel and in-between the 3F3 PLT 58/38/4 plate and the amplifier.

The conductivity apparatus has only a few slight modifications from the apparatus used in the CPL measurements. The modifications are the positions of the oscilloscope probes and the replacement of the 3F3 TN23/14/7 toroid with the 3F3 PLT 58/38/4 plate.

In accordance with the procedure used in the CPL measurements, the core was heated and maintained for 30 minutes to a specified temperature. A heating plate, a cooling fan, and a large aluminum heat sink were used achieve and maintain the specified temperature. The 30 minute time length was used to ensure a temperature stable material. The Temp Fluke 52K/J Thermometer with a 1/10 decimal place accuracy was used for all temperature measurements.

The Temp fluke was calibrated at 100°C. The Temp Fluke probe measured the top surface of the PLT 58/38/4. A thin layer of polyurethane tape was used to insulate the Temp Fluke probe from the 3F3 plate material. The tape eliminated erroneous temperature fluxuations noticed at 500 kHz by the Fluke. The Temp Fluke was used for both AC and DC  $\sigma$  measurements.

Two frequencies, 100 and 500 kHz, and two temperatures, 44°C and 64°C, were used in the  $\sigma$  experiment to validate the results of [24]. The results of the measurements are in Section 3.2. An oscilloscope was used to capture the phase and magnitude of the current and voltage through the 3F3 PLT 58/38/4. Figure 10 is an example of the two captured waveforms.

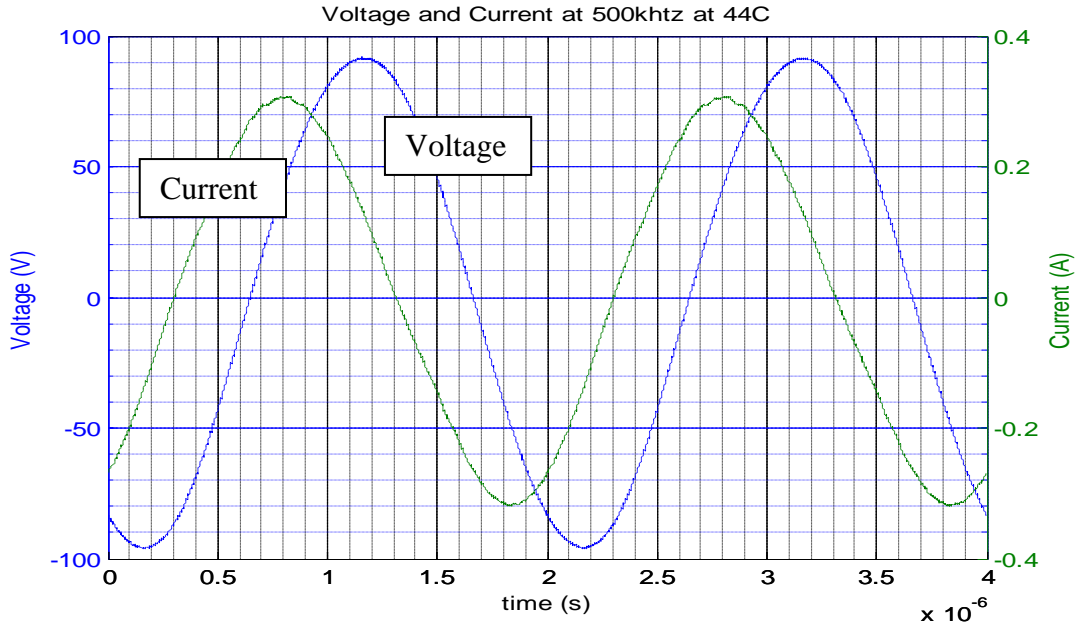


Figure 13: Current and Voltage of Conductivity of the plate

Since both the current and voltage signals have phase and magnitude, the complex conductivity was determined for each measured  $\sigma$  case. The mathematics below is the method used to determine the complex conductivity equation.

$$|V_o| < (\Phi_v) = |I_o| < (\Phi_I Z_o) \quad \text{Eqn 40}$$

The above equation is Amps Law in phasor mathematical form.  $|V_o|$  and  $|I_o|$  are absolute magnitudes of the voltage and current through the plate respectively.  $<$  is the phase angle bracket.  $\Phi_v$  and  $\Phi_I$  are the phase angle of the voltage and current signals. Figure 10 demonstrates that the plate acts capacitive with current leading voltage. So, if  $\Phi_I$  was assumed to equal 0,  $\Phi_v$  is then the phase shift time of between current and voltage,  $T_\phi$ , divided by 360° times the period of the current signal, T.

$$\Phi_v = -\frac{T_\phi}{T} 360^\circ \quad \text{Eqn 41}$$

If Eqn 40 is rearranged solving for Z, the impedance of the plate is given by Eqn 42.



$$Z = \left| \frac{V_o}{I_o} \right| < (\Phi_v) = R + jx \quad \text{Eqn 42}$$

R and jx are the real and imaginary component of plate Z, respectively.  $\sigma$  is shown below using both Eqn 39 and this determined R value [24].

$$\sigma = \frac{l}{AR}$$

A slight modification to  $\sigma$  apparatus used in the AC  $\sigma$  measurements was made to take DC  $\sigma$  measurements. The modification was the signal generator and Fluorcarbon Amplifier were replaced with the HP 6827A Bipolar Power Supply. The Bipolar Power Supply produced a DC voltage which was fed through one end of a 3F3 PLT 58/38/4 material to a sense resistor. Both the 3F3 PLT 58/38/4 plate voltage and the voltage of the sense resistor were measured by the oscilloscope. The two signals were then converted into  $\sigma$  values by MATLAB code. This MATLAB code can be found in Appendix B. A 50 ohm impedance matching resistor was placed in parallel and in-between the 3F3 PLT 58/38/4 plate and the amplifier. In accordance with the procedure used in the CPL measurements, the core was heated and maintained for 30 minutes to a specified temperature. A heating plate, a cooling fan, and a large aluminum heat sink were used to achieve and maintain the specified temperature. The 30 minute time length was used to ensure material temperature stability [23]. The Temp Fluke 52K/J Thermometer with a 1/10 decimal place accuracy was used for all temperature measurements. The Temp Fluke probe measured the top surface of the PLT 58/38/4. Three temperatures were measured, 44 °C, 55 °C, and 63 °C. The results of the measurements are in Section 3.2.

It should be noted that, the range of electric fields used in both the AC and DC  $\sigma$  experiments was limited. Values above those in Figure 25 and 26 caused large rapid local temperature increases with only slight Electric Field experiment increase above the values used. To maintain an even material temperature gradient these electric fields values were all together avoided.

A potential problem in the  $\sigma$  measurement design apparatus is obtaining an accurate power ferrite material temperature. Since  $\sigma$  is temperature dependent, the effects of  $\sigma$  by Electric Field strength could be masked by large material temperature gradients. For very thick materials, the value of surface temperature might not be indicative of the whole material. To minimize this potential path of  $\sigma$  measurement error, the plate used in this experiment was relatively thin. This ensured the local material temperature increases were measured at the surface and minimized the material temperature gradient.

The following is a list of the equipment used in the AC and DC  $\sigma$  experiments:

1. Signal Generator: Stanford Research System Model DS345 30Mhz Synthesized Time Generator
2. HP 6827A Bipolar Power Supply/Amplifier
3. Amplifier: Fluorcarbon Model 1040 Power Amplifier 55db 10khz-500kh
4. 50 $\Omega$  Sense Resistor: Vectronics Impedance 50ohms VSWR: 1:3:1 @ 150Mhz Dissipation 300Watts
5. Oscilloscope: Tektronics TDS 3014B Four Channel Color Digital Oscilloscope
6. Probes: Channel 1 & 2: P6139A Voltage Probes 500Mhz 8.0 pF 10Megaohm 10x
7. Temperature Probe: Temp Fluke 52K/J Thermometer

## 8. .404 $\Omega$ 2 Watt Sense Resistor

### 2.4 Capacitance and Conductivity vs Frequency using an Impedance Analyzer

---

A 4192A LF 5 Hz -13MHz Hewlett Packard Impedance Analyzer with a 16047A test fixture and the 3F3 PLT 58/38/4 plate was used to verify the effects of frequency in power ferrites. The Hewlett Packard open and short calibration instruction was used for each frequency measurement. Frequencies ranging from 100 Hz to 1MHz were used in this experiment. A 28°C 3F3 PLT 58/38/4 surface temperature was maintained for 30 minutes using heating plate, a cooling fan, and a large aluminum heat sink prior to the measurements. The Temp Fluke 52K/J Thermometer was used for the temperature measurements. Four parameters were analyzed with the impedance analyzer; capacitance (C), phase angle ( $\Phi$ ), real component of resistance (R), and impedance (Z). See Section 3.2 and Appendix B for the results of the measurements.

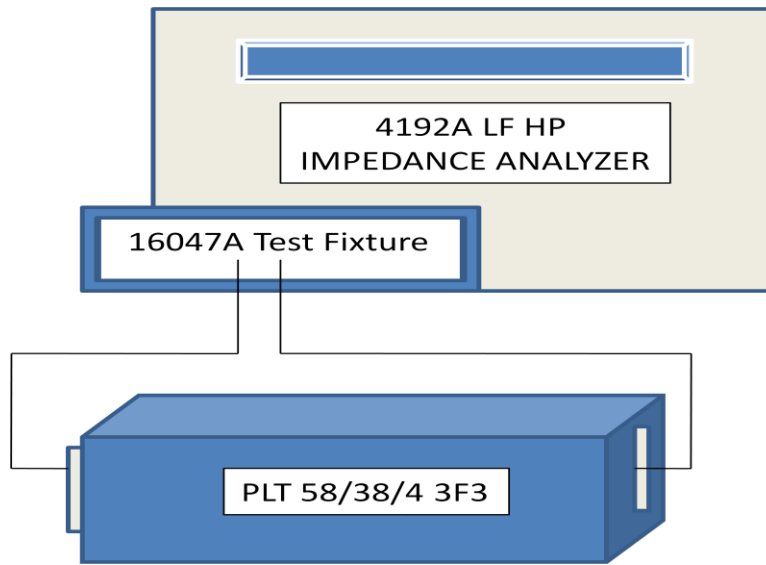


Figure 14: Impedance Analyzer Setup

### 2.5 Repetitive Digitizing Method for Primary Circuit Accuracy

---

The repeatability of the Digitizing Method and preconditioning circuit was measured by taking three data sets with the same frequency and magnetic field. The data sets were taken in the course of a 2 day period. Data Set 1 was taken in the morning; Data Set 2 was taken 6 hours later and Data Set 3 was taken the following morning. The experimental equipment was started and then shutdown for each data set. This was done to define the experiment's CPL variability. Figure 15 is the plot of the three TN23/14/7 core 100 kHz sinusoidal data sets. Each data set was measured with a TN23/14/7 core having a surface temperature of 50 °C. A 50°C plate temperature was maintained by a heating plate, a cooling fan, and a large aluminum heat sink for

30 minutes prior to measurements. The Temp Fluke 52K/J Thermometer was used for the temperature measurements.

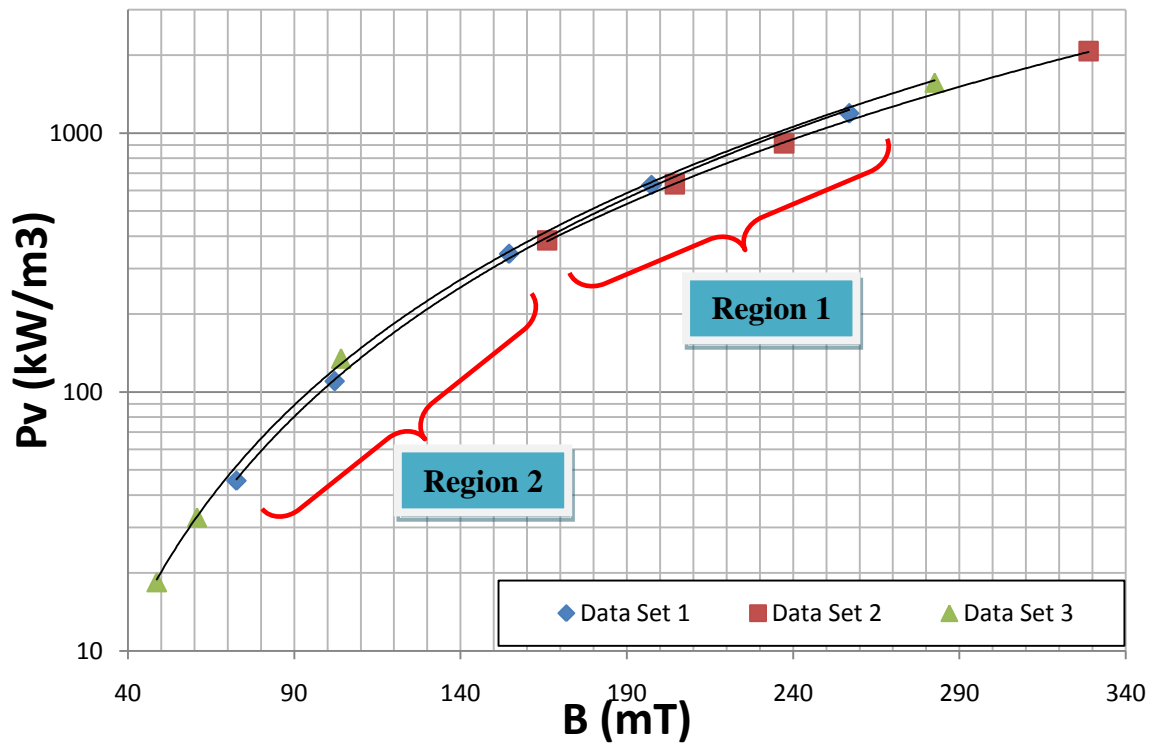


Figure 15: 3 Data Sets of 100 kHz Sinusoidal Signals for TN23/14/7 core

Figure 16 provides the graphical CPL results of Figure 15's Region 1. For the overlapping Region 1, the maximum error between the data sets was calculated to be 10.92% with a mean error of 6.54%.

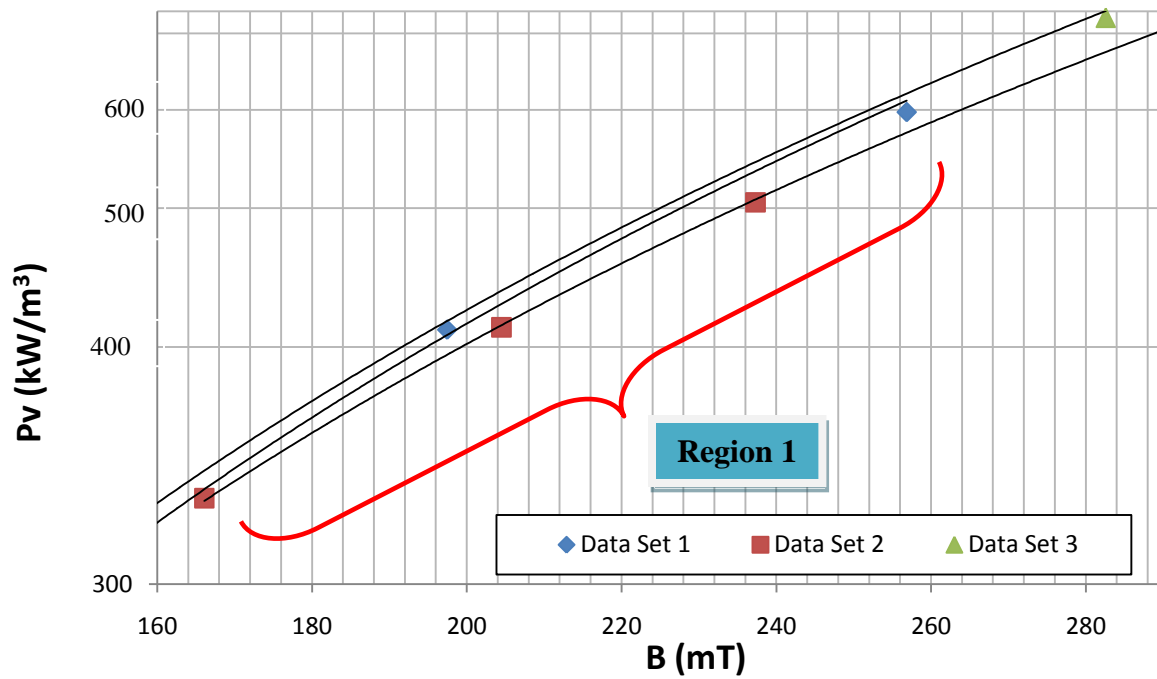


Figure 16: Region 1 of 3 Data Sets of 100 kHz Sinusoidal Signals for TN23/14/7 core

Figure 17 provides the graphical CPL results of Figure 15's Region 2. For the overlapping Region 2, the maximum error between the three data sets was 7.55% with a mean error of 5.8%.

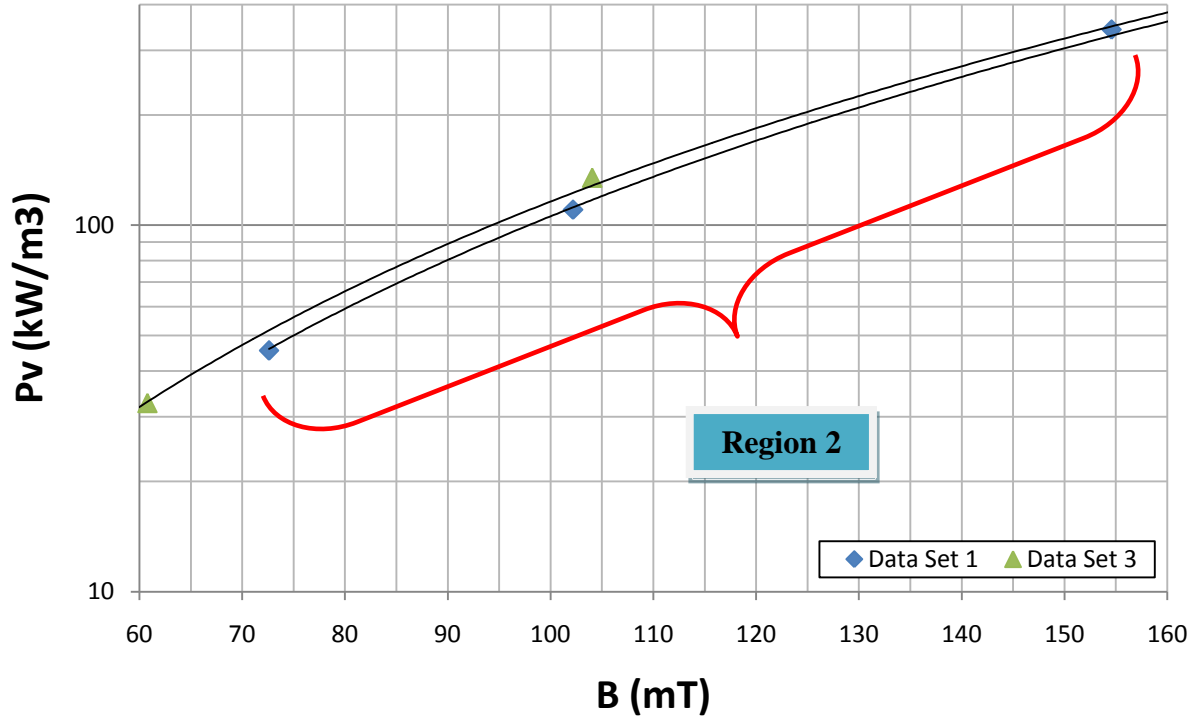


Figure 17: Region 2 of 3 Data Sets of 100 kHz Sinusoidal Signals for TN23/14/7 core

The results of only a 5-7% experimental average deviation between the three data sets demonstrates that the CPL measuring apparatus can be used for CPL measurements and CPL equation comparisons.

## 2.6 CPL Code Validation

For confirmation purposes, the accuracy of the MATLAB program was validated against a known solution. Reference [25] pg 437 provided a solution to an average power problem using a signal voltage of  $v(t) = 120 * \cos(377t + 45^\circ)$  and a signal current  $i(t) = 10 * \cos(377t - 10^\circ)$ . The answer to the analytical average power problem as provided by [25] was 344.15 Watts for one period. If the above inputs were fed into the CPL MATLAB code, the resulted average power was 344.18 Watts for one period. The comparison of the two answers validates the CPL MATLAB code. The slight difference between these values can be contributed to the inaccuracies of using the trapezoidal method of integration in the MATLAB code. The following figure is a graph of the two input signals. For the MATLAB code used in the analysis see appendix B.

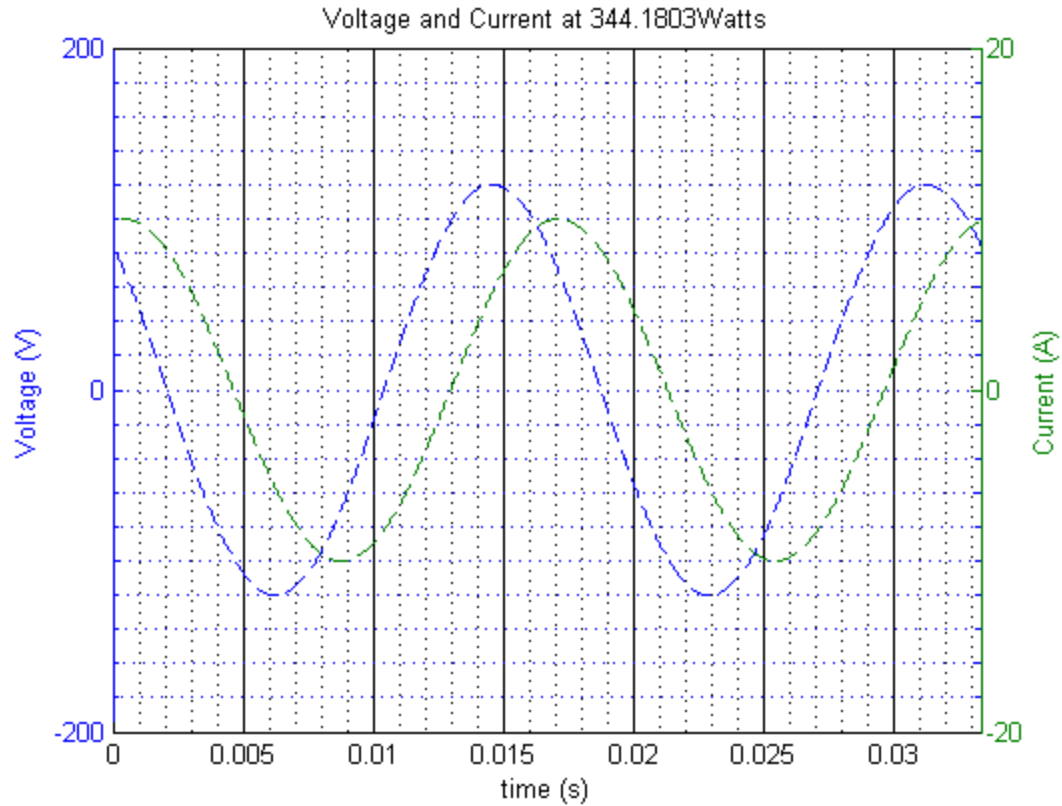


Figure 18: Validation of MATLAB Code Picture

The following was the additional MATLAB code required to validate the CPL MATLAB program.

```
w=377;
T=2*pi()/w;
tint=.0001;
t=linspace(0,2*T,1/tint);
V1=120*cos(377.*t+45*pi()/180);
I1=10*cos(377.*t-10*pi()/180);
```

## 2.7 Accuracy of Matrix and MATLAB Best Fit Method

Two Least Square Best Fit programs were written to provide curve fitted coefficients of several CPL equations found in Section 1.6 using actual measured CPL data. One Least Square Best Fit program uses matrix methods to find a linear least square best fit for  $\ln(A)$  and  $\ln(B)$  for which  $\alpha$  and  $\beta$  can be extracted. The other uses a MATLAB nonlinear fit subroutine (nlinfit) to directly find the best-fit parameters  $\alpha$  and  $\beta$  for the nonlinear model. To validate these program's accuracies, an equation with known coefficients was used to build a data set table which was fed into the two programs. The outputs of the programs were the programs best fitted coefficients to

that data set. A comparison of the output curve fitted coefficients to the known equation coefficients was used to provide program solution accuracy.

The Excess Loss equation, (Eqn 43), modeled off of Bertotti's model, (Eqn 9), was the equation used in the validation.

$$P_{ex} = C\sqrt{V_o}\hat{B}^\beta f^\alpha \quad \text{Eqn 43}$$

C has the value of .011579.  $V_o$  and  $\beta$  are curve fitted coefficients with values of 1 and 1.5 respectfully. Eqn 44 is Eqn 43 and the above known coefficient values.

$$P_{ex} = (.011579)\hat{B}^1 f^1 \quad \text{Eqn 44}$$

5 frequencies, 100-500 kHz, and magnetic fluxes ranging from 70 -140 mT were used in conjunction with Eqn 44 to establish a  $P_{ex}$  data set. Table 3 provides the data set used to determine the accuracy of the two methods.

Table 3: Matrix and MATLAB Validation Table

C	Vo	Beta
0.011579	1	1.5

Freq (Htz)	Bflux (mT)	$P_{ex}$ 3 (kW/m )
100000	70	6781.5838
100000	80	8285.5063
100000	90	9886.6199
100000	100	11579.347
100000	120	15221.447
100000	140	19181.216

200000	70	19181.216
200000	80	23434.951
200000	90	27963.584
200000	100	32751.34
200000	120	43052.754
300000	70	35238.143
300000	80	43052.754
300000	90	51372.384
300000	100	60168.053
300000	120	79092.959
300000	140	99668.52
500000	70	75820.412

Table 4: Results of the MATLAB and Matrix Method

	$R^2$	Unknowns	
		$V_o$	$\beta$
<b>Matrix</b>	.29997	0.998	1.5
<b>MATLAB</b>	0	1.00	1.5

The  $R^2$  value was obtained by the following equation, Eqn 45.

$$R^2 = \frac{(y_{data} - y_{fit})^2}{y_{data}} \quad \text{Eqn 45}$$

$R^2$  is the Least Square Best Fit Residuals value.  $y_{data}$  is the actual measured CPL data.  $y_{fit}$  is the Least Square Best Fit coefficients data.

Table 4 shows that both evaluation methods are good approximations of the data set, but the MATLAB non-linear program provided a higher accuracy. It is interesting that for an exact



input data set, both methods did not approximate the same coefficients. One reason the Matrix method might not have provided an exact solution to the data set is the Matrix method requires a linear equation. The original equation used to calculate the data set was not linear. The equation becomes linear when the log of both sides is taken and the power coefficients are multiplied by the log of B and f. As shown in Table 4, the MATLAB code provided the best solution. Unfortunately, the drawback to using the MATLAB nonlinear fit method exclusively is that the MATLAB method required initial coefficient input estimates for the nonlinear fit. To overcome this drawback, every MATLAB code fit included a Matrix fit to establish initial coefficient guesses.

The below is the Matrix Least Square Best Fit mathematics used in the above analysis. The MATLAB nonlinear fit program can be found in Appendix B.

Eqn 43 is divided by the C constant in Eqn 45. Eqn 45 is the log of Eqn 46. Eqn 46 is converted into Eqn 47, a linear equation. Eqn 48 is the matrix form of Eqn 47. Eqn 49 is the Least Square Best Fit equation for x. Eqn 50 is the matrix form of x.

$$P_{ex} = C\sqrt{Vo}\hat{B}^{\beta}f^{\beta}$$

$$y = P_{ex}/C = \sqrt{Vo}\hat{B}^{\beta}f^{\beta} \quad \text{Eqn 46}$$

$$\log(y) = \log(\sqrt{Vo}) + \beta \log(B) + \beta \log(f) \quad \text{Eqn 47}$$

$$A * x = b \quad \text{Eqn 48}$$

$$\begin{bmatrix} 1 & \log(f_1) & \log(B_1) \\ 1 & \log(f_2) & \log(B_2) \\ 1 & \log(f_3) & \log(B_3) \\ 1 & \cdot & \cdot \\ 1 & \log(f_n) & \log(B_n) \end{bmatrix} * \begin{bmatrix} \log(\sqrt{Vo}) \\ \beta \\ \beta \end{bmatrix} = \begin{bmatrix} \log(y_1) \\ \log(y_2) \\ \log(y_3) \\ \cdot \\ \log(y_n) \end{bmatrix} \quad \text{Eqn 49}$$

$$\bar{x} = (A^T A)^{-1} * A^T b \quad \text{Eqn 50}$$

$$\bar{x} = \begin{bmatrix} \log(\sqrt{Vo}) \\ \beta \\ \beta \end{bmatrix} \quad \text{Eqn 51}$$

## Section 3 Core Power Loss Equation Evaluation

### 3.0 Results of Empirical Equation Component Verification

---

Section 3 provides the results of several of the experiments explained in Section 2. These experiments were conducted to answer the following questions.

1. What is the validity of the Hysteresis Loss Equation for low frequencies?
2. Is CPL dependent upon core cross sectional area?
3. Is conductivity,  $\sigma$ , a constant value in a cross electrical field in ferrites and should it be included as such in power ferrite CPL empirical formulas?

Section 3 is broken into subsection accordingly. The reason these questions were investigated can be seen in Bertotti's model, an equation increasingly used in CPL estimates. Bertotti's model is divided into three component equations; a Hysteresis Loss equation (Eqn 5), a Classical Eddy Current Loss equation (Eqn 20) and an Excess Loss equation as given in the STPL equation (Eqn 12). Bertotti's model, (Eqn 9), is provided in its complete form by (Eqn 52).

$$P_v = P_h + P_{cl} + P_{ex}$$
$$P_v = k_h f \hat{B}^\beta + \frac{A_c \sigma \pi f^2 \hat{B}^2}{4} + 8\sqrt{(\sigma G A_c V_o)} \hat{B}^{1.5} f^{1.5} \quad \text{Eqn 52}$$

For the Hysteresis Loss Equation,  $(k_h f \hat{B}^\beta)$ ,  $k_h$  and  $\beta$  are the least square best fitted constants to actual data.  $f$  is frequency and  $\hat{B}$  is the peak induction value. This equation is typically used to model CPL at low frequencies and is discussed in Section 3.1. The next two component equations in the above model are Classical Eddy Current and Excess Eddy Current Loss,  $P_{cl}$  and  $P_{ex}$ . Two factors found in these equations were investigated; the area of the core,  $A_c$ , and conductivity,  $\sigma$ , terms.  $G$  is a unitless constant and  $V_o$  is another least square best fitted constant to actual CPL data and will be discussed in later sections.  $A_c$  and  $\sigma$  results are found in Section 3.2 and 3.3.

### 3.1 The Validity of the Hysteresis Loss Equation for Low Frequencies

---

The Hysteresis Loss equation, (Eqn 5),

$$P_h = k_h f \hat{B}^\beta$$

is the first term used in many STPL Equations. This equation has been tested and found valid for many materials, such as steel and iron, but the author was unable to find literature experimental evaluations of the Hysteresis Loss Equation for power ferrite materials. Therefore, a test fixture was built and a power ferrite 3F3 TN23/14/7 core was evaluated. The procedure and apparatus are outlined in reference [13] and Section 2.3. Figure 19 is a picture of the test apparatus used. For the given equation two unknowns exist,  $k_h$  and  $\beta$ . Both coefficients are

determined typically through CPL curve fitting [13]. [13] further explains that  $\beta$  is material dependent and usually ranges from 1.5 to 2 depending upon the material.

In the following section the Hysteresis Loss equation is going to be modified slightly to look like the PLE equation, Eqn 4.

$$P_v = k_h f \hat{B}^\beta \quad \text{Hysteresis Loss Equation}$$

$$P_v = k_h f^\alpha \hat{B}^\beta \quad \text{Power Law Equation}$$

The only difference between the two equations is  $\alpha$ , a curve fitted Least Square Best Fit (LSBF) constant.  $\alpha$  is constrained to be one in for the Hysteresis Loss Equation and unconstrained in the PLE. This change was done to demonstrate that if the CPL data set is curve fitted to the PLE equation, the Hysteresis Loss equation is obtained. So the following figures and calculations are given with  $\alpha$  even though it was set to one.

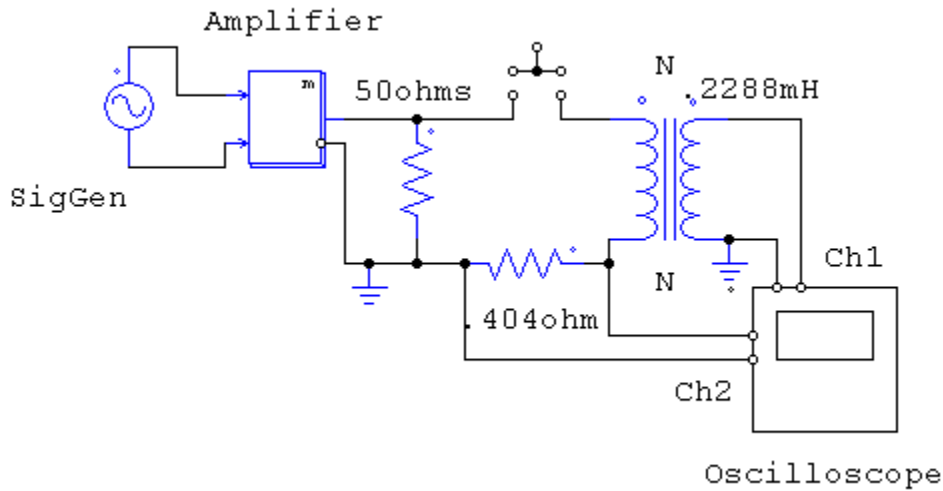


Figure 19: Core Power Loss Test Fixture used in Hysteresis Loss Equation

Reference [13] says that the area of the Hysteresis loop at very low frequencies is an accurate estimate for this STPL term, because for low frequencies, the power loss due to the other components in the STPL model is relatively zero. This makes Hysteresis losses dominant and measurable. The CPL due to Hysteresis Losses at low frequencies is then used to estimate the CPL at higher frequencies.

CPL data was measured using a 70 Hertz sinusoidal waveform. The data was then used to curve fit eqn 5 coefficients,  $k_h$  and  $\beta$ , using two Least Square Best Fit methods. 70 Hertz was used as the test frequency for convenience. It is low enough to provide a good CPL estimate and is sufficiently away from 60 Hertz power noise.

Reference [13] explains that only 2 points are required for the best fit, but, for the sake of accuracy and conformation, 4 points were used. Typically  $k_h$  and  $\beta$  solution are then applied to calculate the Hysteresis Component of STPL at higher frequencies for the ranges used in Power Ferrites [13]. Figure 20 is graph of the 70 Hertz data set.

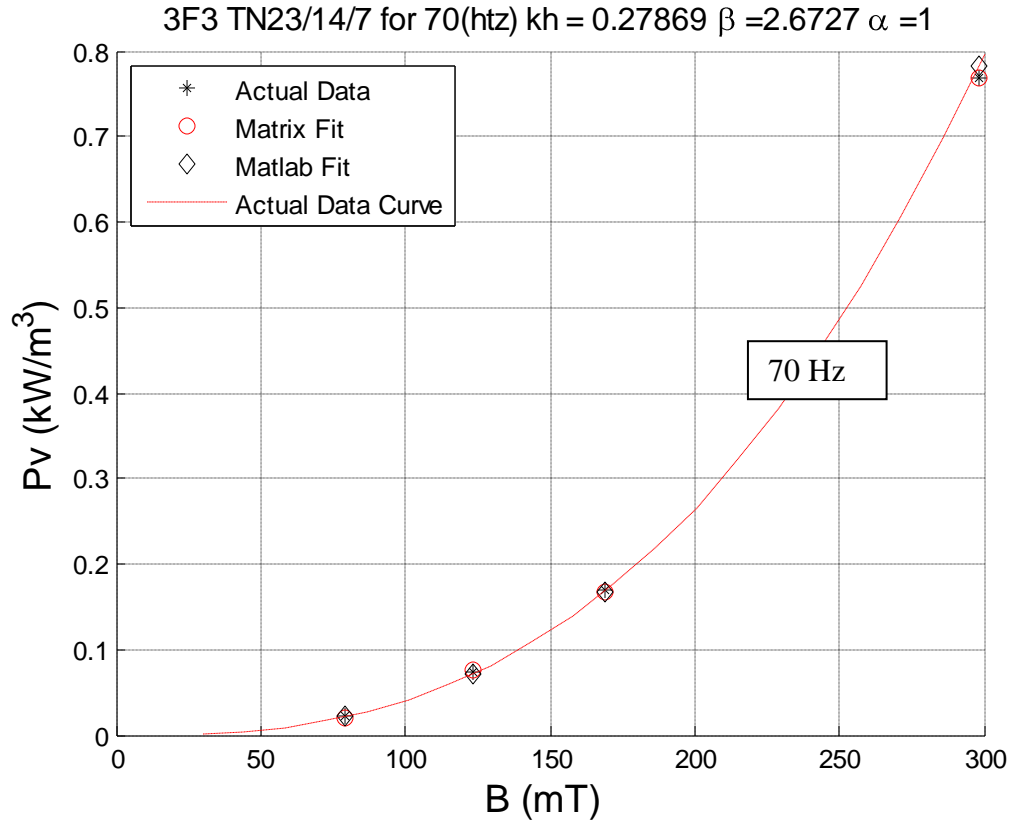


Figure 20: Hysteresis Loss at 70 Hertz

The best fit solutions to the 70 hertz data points for the MATLAB and Matrix method fits are given Table 5. The Best Fit Least Square residuals, Eqn 45, were lower for the MATLAB program so they were used in the plot of Figure 20. Usually this is all the data that is required for the Hysteresis Loss equation calculation in STPL equations, but a larger data set which included another frequency was collected to determine the accuracy of the statement.

Table 5: Residuals of Hysteresis Equation at 70 Hertz

Hysteresis Model ( $P_h$ )	$R^2$	$\alpha$	Unknowns	
			$k_h$	$\beta$
<b>MATLAB</b>	.00024	1	.2787	2.6727
<b>Matrix</b>	.00054	1	.2999	2.7126

To measure the accuracy of Eqn 5, a 140 Hertz CPL data set was also measured. By doubling the frequency, in the Eqn 5, the CPL should also double. The 140 hertz CPL data was compared to the CPL estimates obtained using Eqn 5 and the 70 hertz curve fit coefficients for MATLAB fit ( $k_h=.2787$ ,  $\alpha=1$  and  $\beta=2.6727$ ) and Matrix fit ( $k_h=.2999$ ,  $\alpha=1$  and  $\beta=2.7126$ ). Figure 21 is the results of the plot. The 70 and 140 actual CPL measured data is shown with the both estimated Least Square Best Fit (LSBF) CPL values.

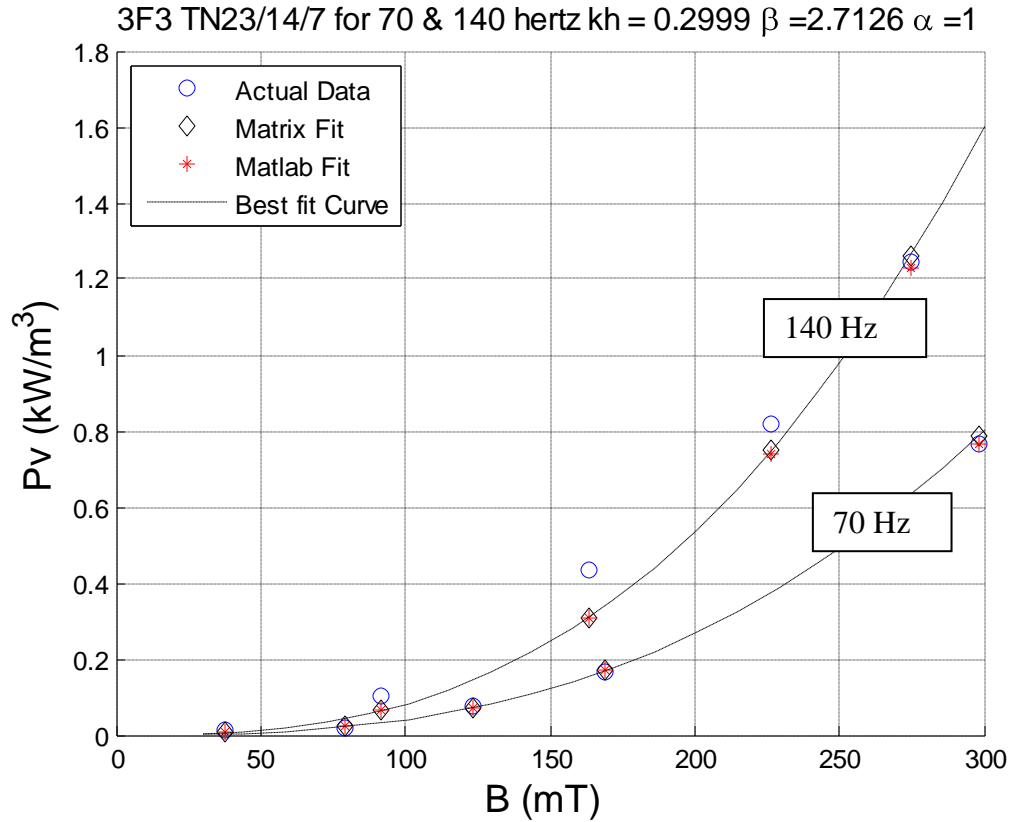


Figure 21: 70 & 140 Hertz graph using 70 Hertz Best Fit Coefficients

Table 6 is the BFLS results of the 70 and 140 hertz data using only the 70 hertz BFLS coefficients. It is interesting that the results of the BFLS lowest residuals were not the MATLAB BFLS coefficients found in Table 5. The Matrix fit provided a slightly smaller residual value, Eqn 45.

Table 6: Using the BFLS 70 hertz coefficients for 140 hertz estimates

Hysteresis Model ( $P_h$ )	$R^2$	$\alpha$	Unknowns	
			$k_h$	$\beta$
<b>MATLAB</b>	.0602	1	.2787	2.6727
<b>Matrix</b>	.0599	1	.2999	2.7126

To determine if using both the 70 and 140 hertz data provided a better fit then just the 70 hertz data, a BFLS was conducted on the data set. The fitted results are given in Table 7 and Figure 22. The BFLS residuals were lower for the 70 and 140 Hz data set then just for the 70 Hz data. However, this is not surprising. Typically, the greater the number of curve fitted data points used to fit data, the better the BFLS fit to that given data set. As demonstrated in Table 7, the Matrix method provided the best fit to the 70 and 140 hertz data using the Hysteresis Loss equation.

Table 7: BFSL 70 and 140 Hertz data for Hysteresis Loss Equation ( $\alpha=1$ )

Hysteresis Loss Equation ( $P_h$ )	$R^2$	$\alpha$	Unknowns	
			$k_h$	$\beta$
<b>MATLAB</b>	.0424	1	.1655	2.2535
<b>Matrix</b>	.0314	1	.2083	2.4438

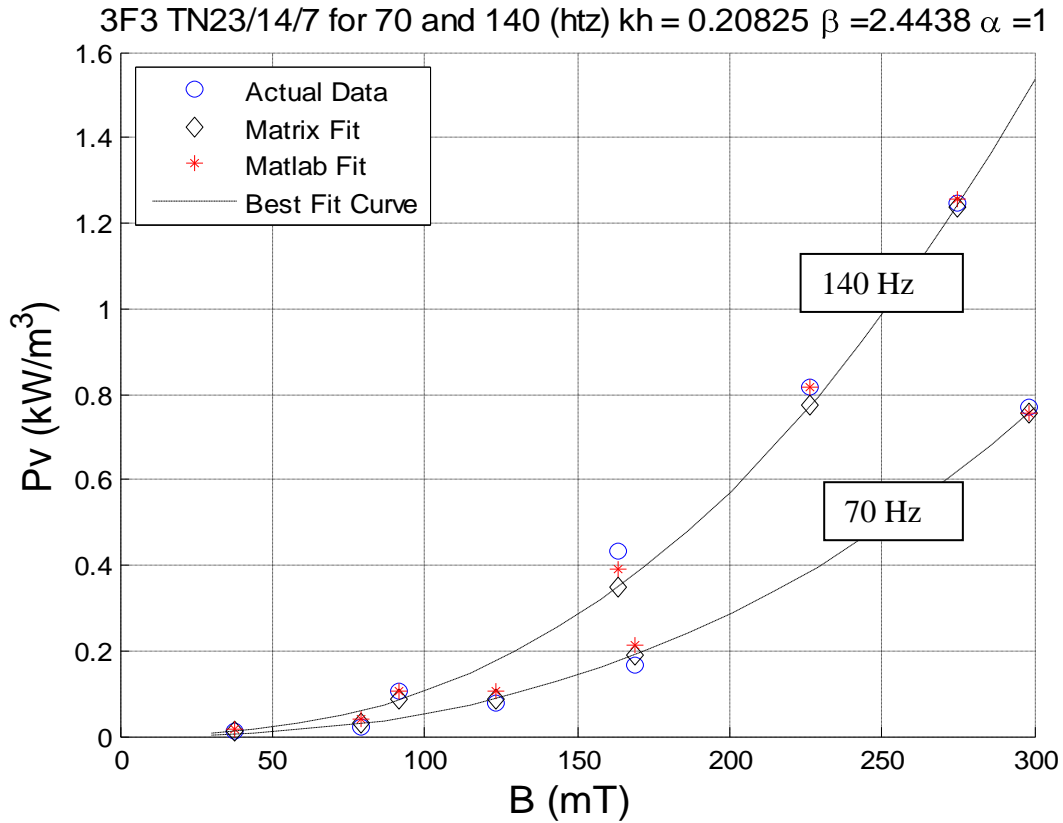


Figure 22: PLE for 70 and 140 Hertz with  $\alpha$  constrained to 1

Table 8 demonstrates the best fit PLE equation for the 70 and 140 hertz data has  $\alpha$  equal to 1.014. Figure 22 and 23 are the plots of the BFLS fits using the PLE equation with either  $\alpha$  constrained to 1 or  $\alpha$  as a free variable.  $k_h$  and  $\beta$  were both free variables in the analysis. With the accuracy of the given project, it can be assumed  $\alpha$  of 1.014 is approximately 1 and this analysis demonstrates that the Hysteresis Loss equation correlate wells to actual CPL 3F3 power ferrites data at low frequencies.

Table 8: BFSL 70 and 140 Hertz data for Hysteresis Loss Equation ( $\alpha$  unconstrained)

Hysteresis Model ( $P_h$ ) PLE Equation	$R^2$	Unknowns		
		kh	$\beta$	$\alpha$
MATLAB	.0397	1.556E-01	2.26	1.014
Matrix	.0537	3.244E-2	2.47	1.412

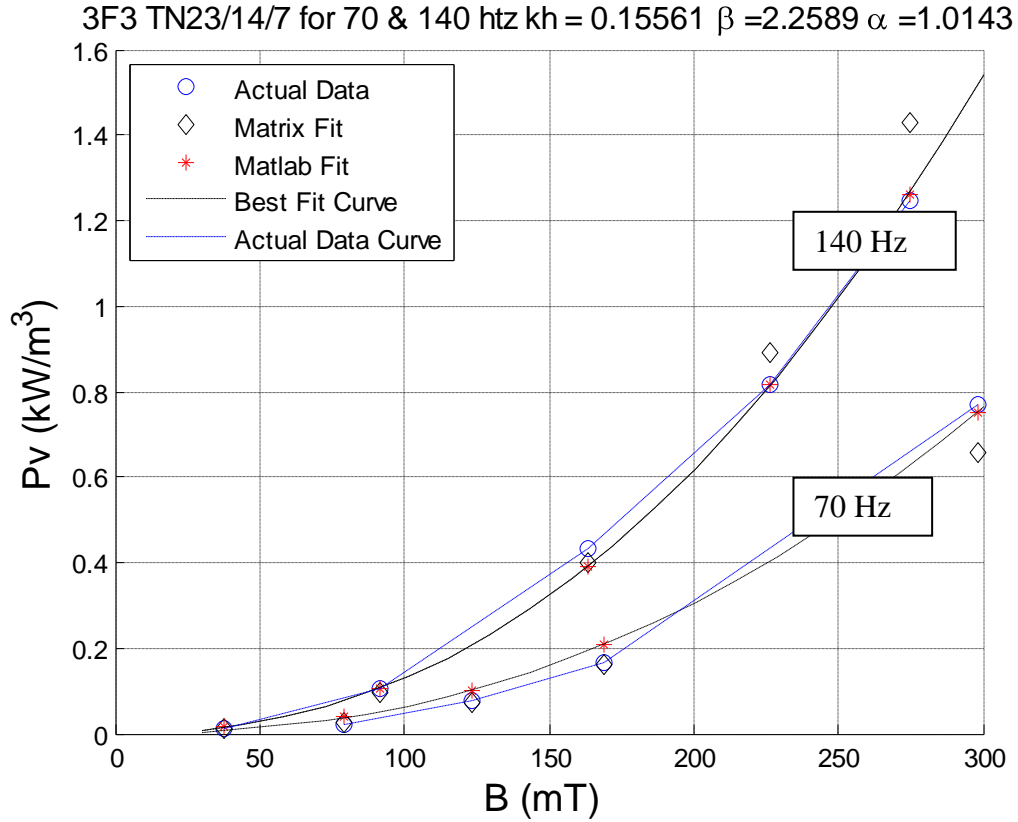


Figure 23: PLE for 70 and 140 Hertz with  $\alpha$  unconstrained

### 3.2 Conductivity in an Electrical Field

As explained in Section 2.4, conductivity,  $\sigma$ , performs an important role in many empirical equations and models. An example of this can be found in (Eqn 6), the Classical Eddy Current Equation (CECE), for cylindrical cores and sine-wave excitation.

$$P_{cl} = \frac{\sigma \pi f^2 \hat{B} d^2 A_c}{4}$$

Since many Separation of Total Power (STPL) models include the CECE, a good estimate of  $\sigma$  used in the CECE is important to get an accurate CPL estimate. A list of the terms in the CECE can be found in section 1.5. In several places in the literature ([5] and [26]),  $\sigma$  is said to be only temperature and frequency dependent, but an experiment conducted by reference [24] indicates that  $\sigma$  in power ferrites might also be electric field dependent. The His high electric field and frequency experimentations there produced very non-linear  $\sigma$  values. Reference [24] supposed that the possible combination of high frequencies and large electric fields produced a phenomenon called charge tunneling. See reference [24] for an in-depth explanation of this postulated charge tunneling phenomenon. His conclusion was that  $\sigma$  was AC electric field dependent.

To validate [24] results, a test fixture similar to [24] fixture was built. Figure 9 is a schematic drawing of this apparatus. A description of the apparatus and the mathematics involved in calculating  $\sigma$  are found in Section 2.5.

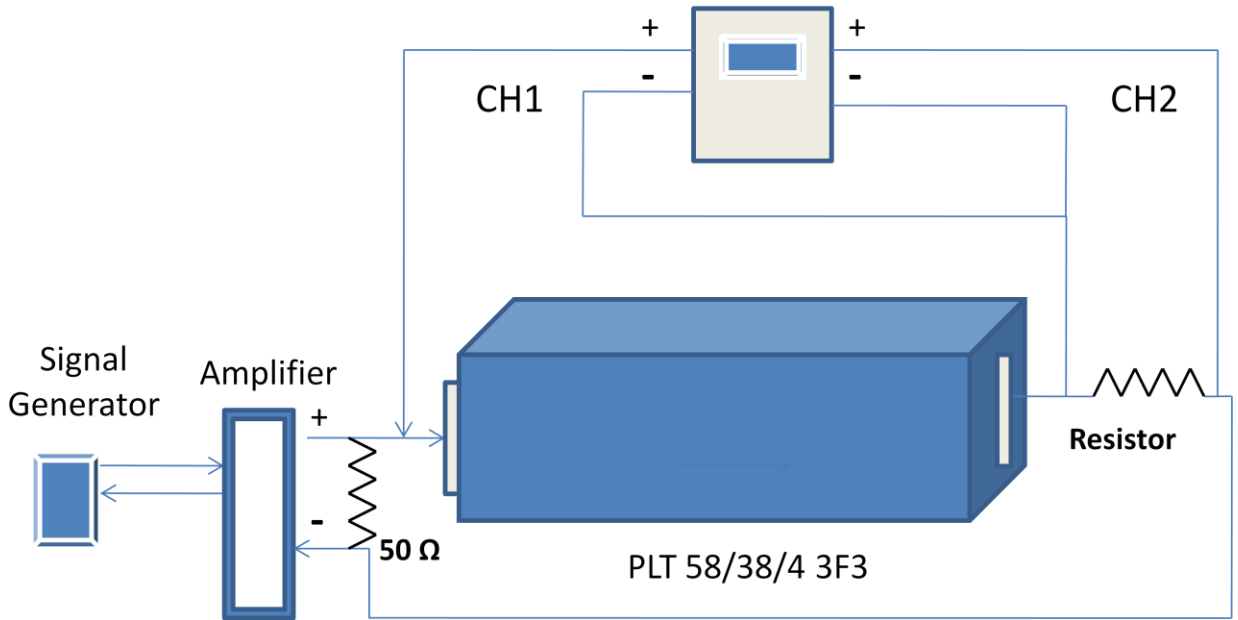


Figure 24: Conductivity Apparatus (Note: It was noted afterwards that there is the potential for dc grounding issues with this connection, but the RF measurements appeared reasonable.)



Varying 100 and 500 kHz sinusoidal voltages at two temperatures, 44°C and 64°C, were used in the experiment. Figure 25 is a plot of the results using  $\sigma$  and Electric Field as axes.  $\sigma$  is given by the following equation and Electric field is the voltage peak across the plate,  $V_o$ , divided by the length of the plate.

$$\sigma = \frac{l}{AR}$$

As explained in Section 2.4,  $l$  is the length of the material,  $A$  is the cross sectional area of the material that the current flows through and  $R$  is the resistance of the structure.

Figure 25 demonstrates that for a 3F3 Power Ferrite material and sine wave excitation, plate  $\sigma$  is clearly frequency dependent with a slight temperature dependency. This supported the above [5] and [26] assertions. Figure 25 also corroborates reference [24] conclusion that  $\sigma$  in power ferrite materials has electric field dependencies, since  $\sigma$  increased with rises in electric field strength. If  $\sigma$  was independent of electric field values,  $\sigma$  would have remained constant for increases in electric field strength.

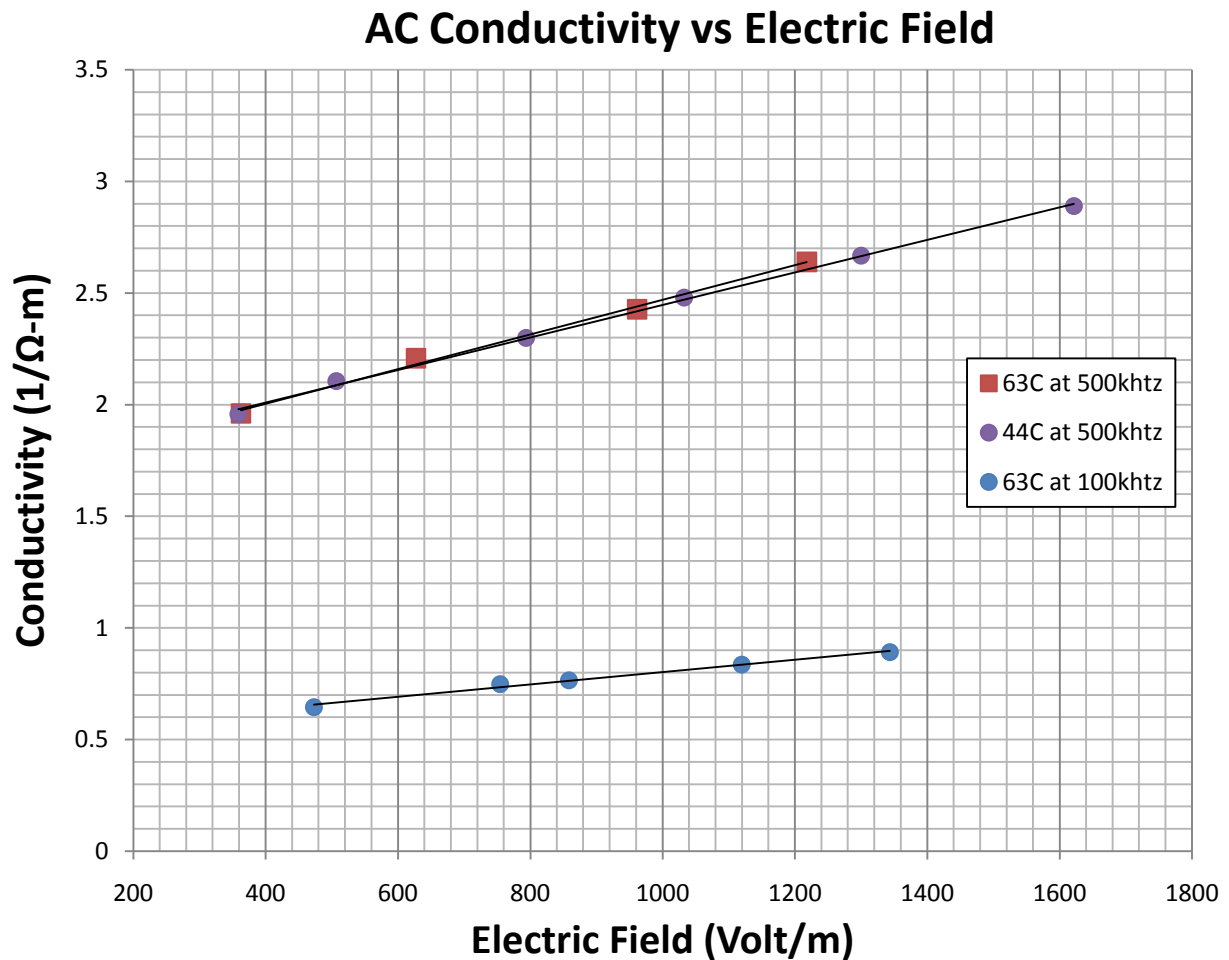


Figure 25: AC Conductivity vs varying AC Electric Field

If  $\sigma$  changes with changes in peak electric field strength as demonstrated by Figure 25, one can easily infer that  $\sigma$  also changes during the voltage fluctuations in every sine-wave half cycle. This would make CPL empirical equations models like CECE, which typically use constant DC  $\sigma$  values in their empirical estimation equations, both invalid and not accurate CPL estimation methods.

Reference [24] demonstrated that  $\sigma$  varied during a condition of both high AC frequencies and large electric fields. So, DC  $\sigma$  experiments were performed to see if similar  $\sigma$  variations would still be present. It was interesting to see that comparable results occurred.

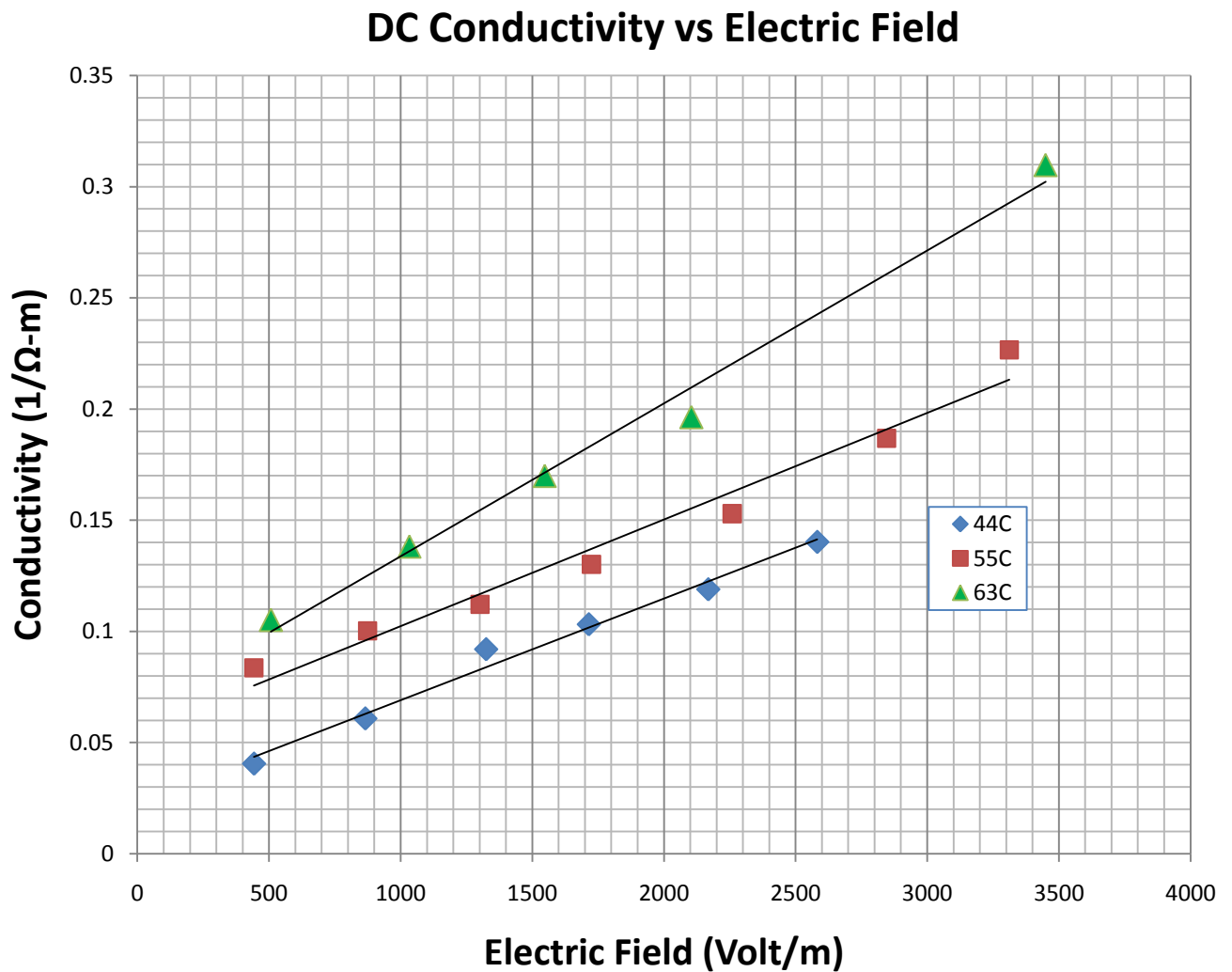


Figure 26: DC Conductivity vs Electric Field

The same apparatus was used, with the exception that the signal generator and amplifier were replaced with a DC amplifier. As seen in the AC  $\sigma$  experiment and in Figure 26, temperature affects complex  $\sigma$  values. It was also surprising that large DC electric fields also had variations of complex  $\sigma$ .

The results demonstrated in Figure 25 and 26 contradict several papers which explains that conductivity has a relatively constant value for varying electric fields. As the above figures show, the value of  $\sigma$  can fluctuate more than double to triple its lowest  $\sigma$  value depending upon the value of the electric field. This means CPL empirical equations that use  $\sigma$ , similar to the CECE, could also fluctuate 2 to 3 times depending upon which DC  $\sigma$  value was used in that equation.

Section 2.4 gives three methods typically used to obtain the  $\sigma$  value used in many CPL empirical equations:

1. to measure DC  $\sigma$  at a specified temperature, either 25°C or the temperature of the power ferrite intended application,
2. to measure AC  $\sigma$  at the same frequency and temperature used in the desired power ferrite application, and
3. to use the manufacturer's provide DC  $\sigma$  value. This value is usually measured at 25°C.

The most likely accurate method to obtain  $\sigma$  is to find a method that determines  $\sigma$  with the most similar parameters as the one used in the power ferrite application. The further away from intended use parameters, the more likely error will be present in the estimation.

The last experiment conducted to measure  $\sigma$  was performed using 4192A LF 5 Hz - 13MHz Hewlett Packard Impedance Analyzer with a 16047A test fixture on the 3F3 plate material. This experiment was conducted to analyze a surprising result found making the AC  $\sigma$  measurement using the 3F3 PLT 58/38/4 material.

As noticeable in Figure 27, which is an oscilloscope snap shot of the voltage and current through the 3F3 PLT 58/38/4 plate, the plate has a large capacitive value. As Figure 27 demonstrates the current leads voltage. What makes this fascinating is that most Power Ferrites are used as inductors. A possible reason to account the plate have a capacitive value might be due to the fact the 3F3 plate is made of Manganese Zinc, (MnZn). MnZn has a crystalline structure which is insulated by an isolating layer that creates pockets of MnZn throughout the material [26]. Ferroxcube, the manufacturer of 3F3, gives the size of MnZn grain between 10um to 20um. [26] The boundary between the grains is estimated to about ½ that value. The small pockets of ferrite material act like small capacitive plates separated by electrolytic boundary layers.

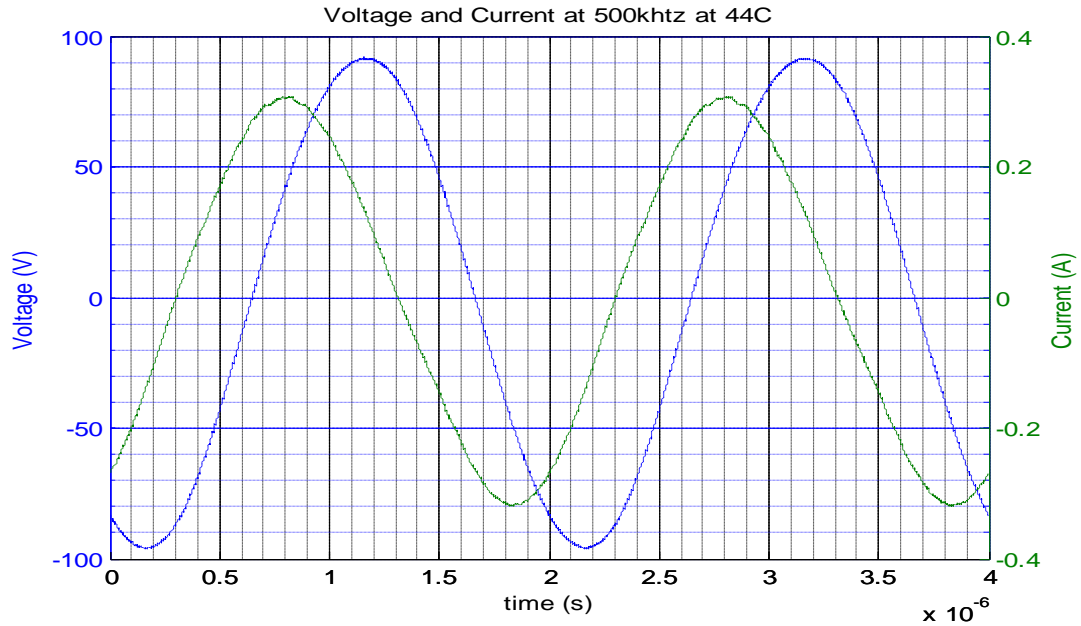


Figure 27: Voltage and Current of the 3F3 PLT 48/38/4  $\sigma$  measurements

The frequencies used in this experiment ranged from 100 Hz to 1 MHz. The Surface temperature of the 3F3 PLT 58/38/4 plate was maintained at 28°C. Four parameters were measured from the impedance analyzer; capacitance (C), phase angle ( $\Phi$ ), real component of resistance (R), and impedance (Z). See section 7 for a table of the results.

Figure 28 is a graph of capacitance versus frequency.

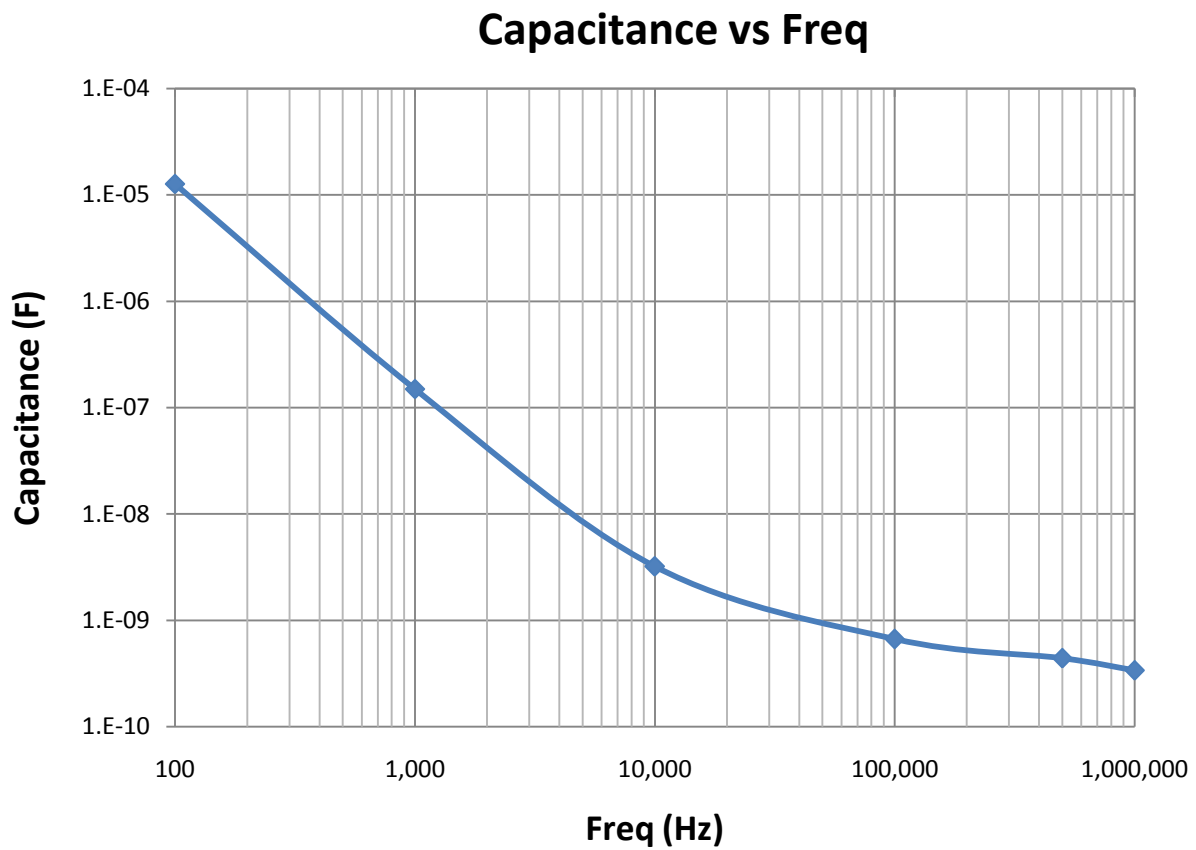


Figure 28: 3F3 Plate Capacitance vs Freq

Figure 29 is the phase versus frequency. At 100 hHz the measured phase angle between current and voltage for the 3F3 TN23/14/7 core was 57 °. This correlates well with the 62.4° impedance phase angle measured at 100 kHz by the impedance analyzer.

### Phase Angle Vs Freq

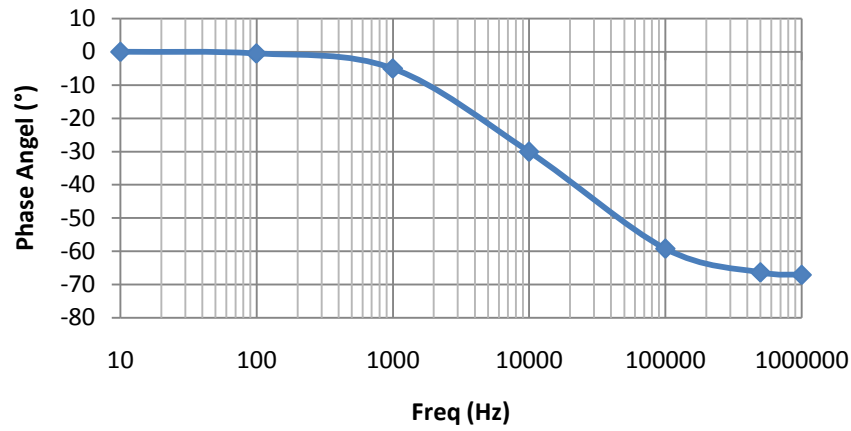


Figure 29: Phase Angle vs Freq

### Resistance Vs Freq

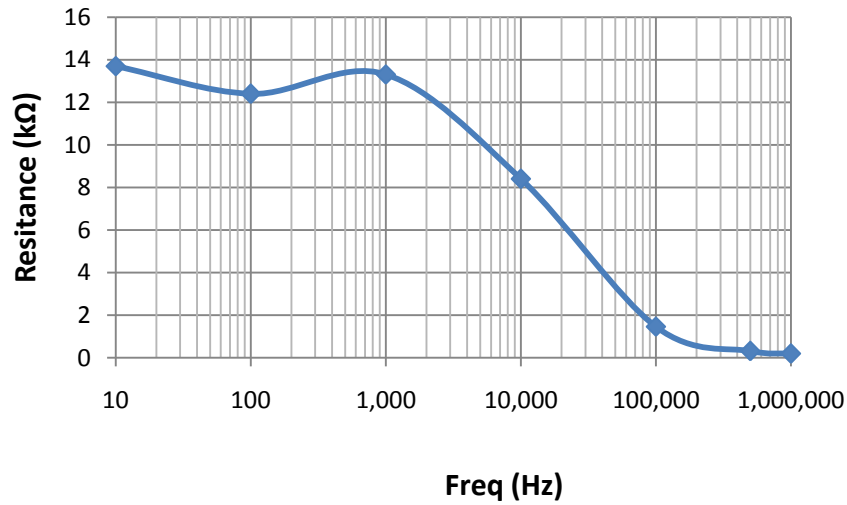


Figure 30: Resistance vs Freq for 3F3 Plate Measurement

## 3.3 Core Area as a factor in CPL per volume Equations

As emphasized in Section 2.0, there are many CPL empirical equations that use cross-sectional core area, ( $A_c$ ), as an empirical estimation equation factor. For example, Bertotti's model uses  $A_c$  for two of its component equations, the Classical Eddy Current Loss and Excess Power Loss equations, as demonstrated in Eqn 52.

$$P_v = k_h f \hat{B}^\beta + \frac{A_c \sigma \pi f^2 \hat{B}^2}{4} + \sqrt{A_c \sigma G V_o} f^{1.5} \hat{B}^{1.5}$$

One goal of this research thesis was to determine if CPL per volume is dependent upon core area for power ferrites. Numerous experimental literature exists on this topic for a wide range of materials, but very little was found using power ferrite materials.

In this experiment, six 3F3 toroid cores were analyzed with  $A_C$  ranging from 3 to 186  $\text{mm}^2$ . An in-depth explanation of the test procedure and the CPL test apparatus used for this experiment is located in Section 2.1.  $A_C$  for a perfect rectangular cross-section toroid would be the multiplication of the height of the core ( $h$ ) and width of the ferrite material ( $w$ ). Fig 5 is an example of the these dimensions used in  $A_C$  calculations.

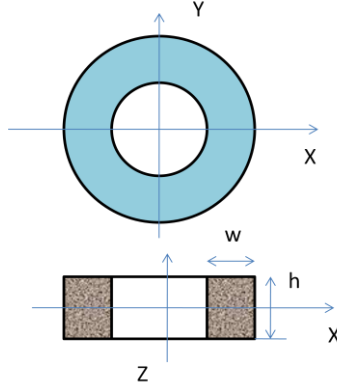


Figure 31: Rectangular Toroid Figure

Unfortunately, the cores used in the experiment were not perfect rectangular toroids. The manufacturer rounds the edges of the core using a tumbler. To account for difference due to rounded edges, the effective area ( $A_e$ ) provided by Ferroxcube's data sheets were used to determine the given  $A_C$  (Ferroxcube is the manufacturer of the 3F3 cores).

As stated above,  $A_C$  varied more than 60 times the smallest to the largest core. This is demonstrated in Figure 32. Figure 32 is an approximate visual demonstration of size difference between the largest (TX 50/30/19) and smallest (TC 6.3/3.8/2.5) core. A list of the 6 3F3 core's and their respective  $A_C$  can be found in Table 9.

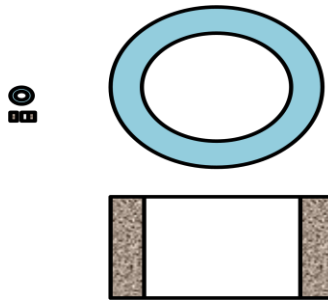


Figure 32: Core size visual difference

Table 9: Effective Core Area of Cores used

3F3 Core	Effective Area (mm <sup>2</sup> )
TC 6.3/3.8/2.5	3.06
TX 13/7.9/6.4	14.1
TN 23/14/7	30.9
TN 23/14/7	30.9
TX 36/23/15	97.5
TX 50/30/19	186

Several of the questions typically used establish the accuracy of CPL core size comparisons are:

1. Are the cores made from the same material?
2. Are the cores from the same manufacturer lot?
3. Were they measured using the same input parameters?
4. Were they measured using the same testing apparatus and by an identical process?

To satisfy these questions, 6 varying sized Ferroxcube 3F3 cores were obtained. They were made of the same material but were not known to be from the same lot. Same lot means that the cores were cut from the same bulk material. Regrettably, when a bulk material is manufactured, small intrinsic material variations occur that differentiates that that bulk material from the same type of material manufactured by the exact same process. These lot specific intrinsic variations can also vary the overall CPL results when compared to another lot. Usually, these CPL variations are eliminated in CPL core size comparison by using cores from the same lot or by just using one core that is machined smaller to make several smaller cores [8]. Unfortunately, these two options were not available for this experiment. 3F3 material is very brittle and did not machine well and it is very difficult to obtain several varying size same lot cores unless an expensive special manufacture order is conducted. Only two of the cores were from the same lot: the two TN23/14/7 cores.

The reason why two same lot same size cores were measured was to determine if that even same-lot same-sized cores had CPL variability. Figure 33 and Table 10 provides the results of this CPL variability experiment.



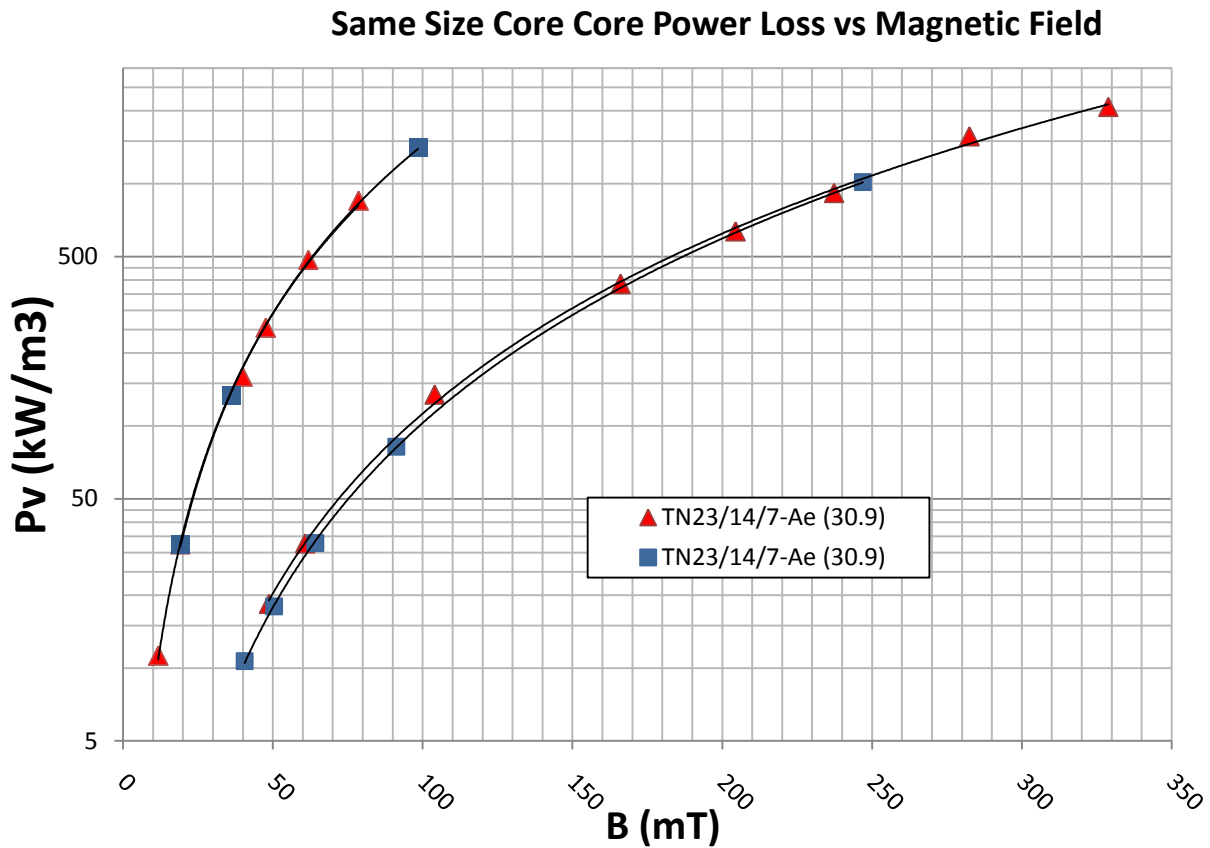


Figure 33: 3F3 TN 23/14/7 same size core lot Variability

Table 10 provides the average maximum error between the two same lot TN 23/14/7 cores for the same overlapping 100 and 500 kHz regions.

Table 10: Error for same lot same size cores

Frequency (kHz)	Average Error	Max Error
100	6.90%	13.40%
500	1.40%	3.78%

Since, the average error determined at 100 kHz between the same lot cores was 6.9% and the Section 2.5 average error between same size different lot core data sets was 6.54%, this experiment demonstrates the same lot cores might have greater variation than different lot cores.

As explained above, to minimize the potential errors that arise from comparing CPL from different lots, five different sized cores from unique lots cores were used. By using multiple lots and sizes, the overall chances of lot variability on one particular lot from affecting the general overall core size CPL trends is minimized.

Figure 34 is a plot of the 6 cores for both 100 and 500 kHz frequency data sets. The most interesting result of Figure 34 is there does not seem to be a clear trend in the data. The smallest core, TC6.3/3.8/2.5, actually had the highest loss. This is surprising if Bertotti's model (Eqn 52)

is correct. The expected lowest CPL core using Eqn 52 would be the core with the smallest area, since  $A_C$  is found twice in the equation with terms proportional to  $A_C$  and  $A_C^{1/2}$ .

## Pv at 100 and 500 kHz vs Magnetic Field

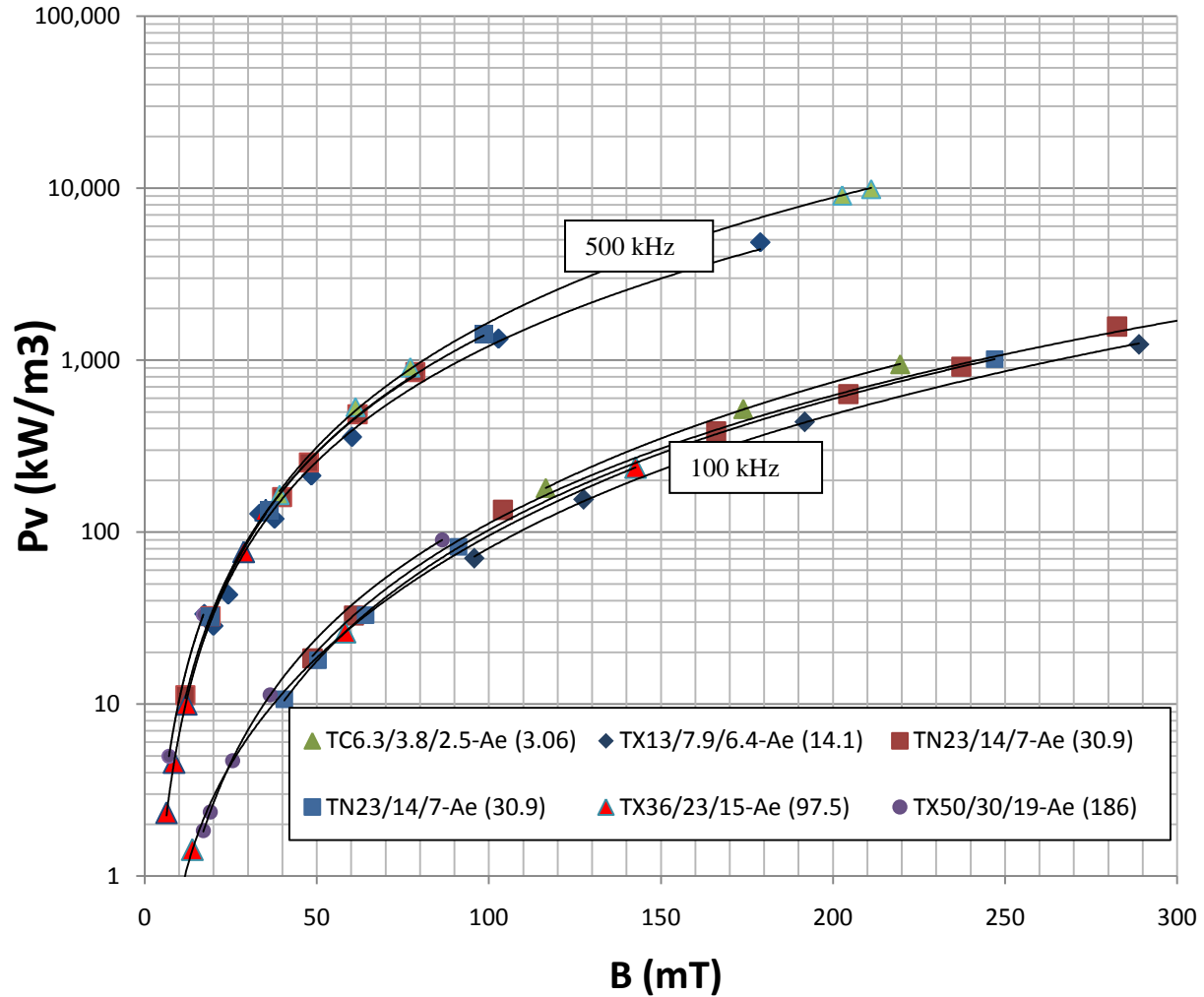


Figure 34: Core Area effects on Core Loss

Figure 35 provides the CPL loss data of Figure 34's for just 100 kHz. One of the TN23/14/7 cores was removed to provide a clearer picture of the trends. The removal of this core did not change the data trends. The graph was then is broken into overlapping curve regions. Only overlapping actual experimental data points were compared in the experiment to eliminate the potential error that experimental estimates could give.

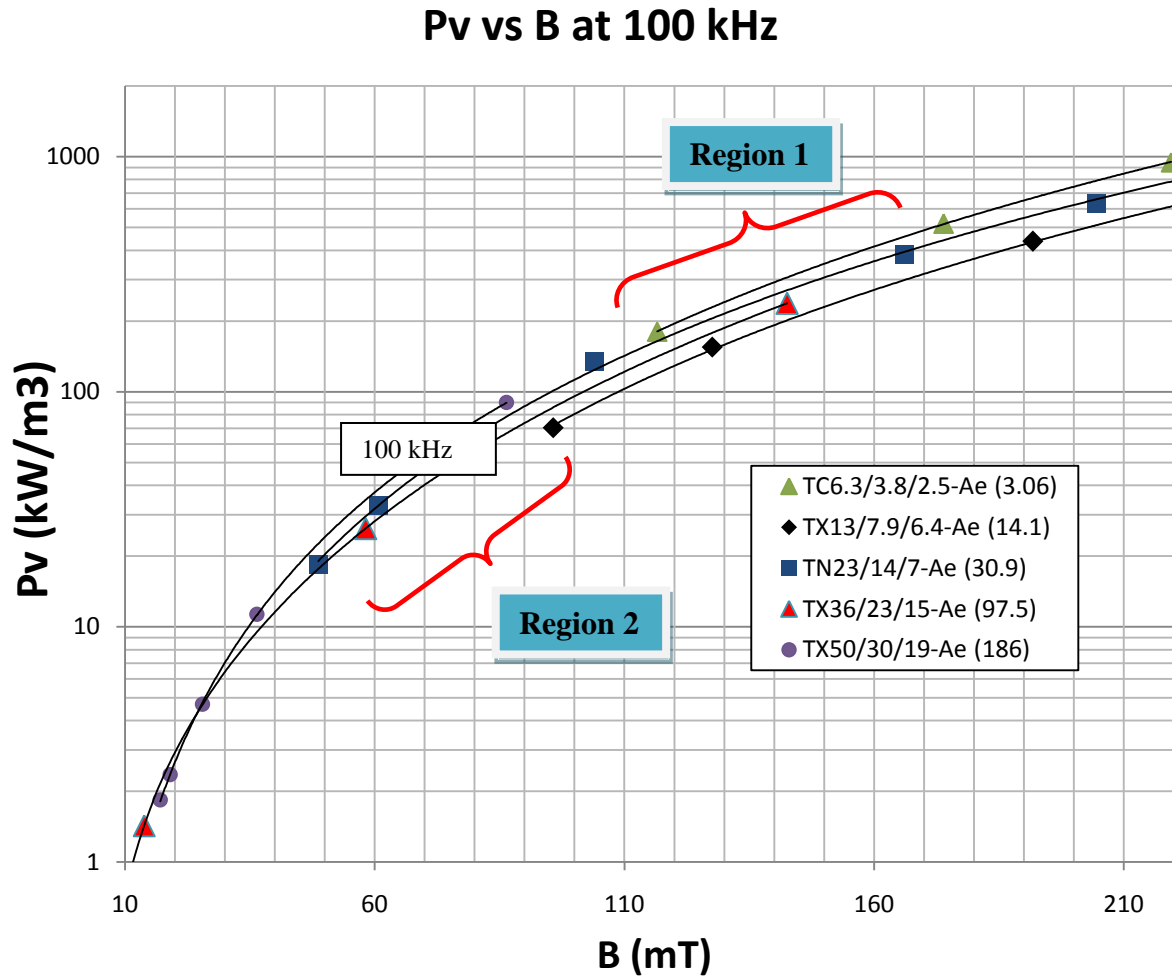


Figure 35: Core Area CPL Losses for 100 khz

Region 1 in Figure 35 envelopes 4 cores and Region 2 encases 3. Table 11 and 12 are the rankings of the cores in each region from smallest to largest  $A_C$  and their respective ranking of their Total CPL from lowest to highest (Ranking was ordered by figure trends, so the core with Lowest CPL trend had CPL rank of 1). Contrary to Classical Eddy Current Loss theory, for Region 1 the largest CPL loss was the smallest core and the second lowest loss core was the largest core. For Region 2 of Figure 35, the medium sized  $A_C$  had the lowest CPL.

Table 11: 100 kHz Region 1 Core Loss Core Comparison

100 (khz)	Core	$A_C$ (mm <sup>2</sup> )	Lowest CPL
Region 1	TC6.3/3.8/2.5	3.06	4
	TX13/7.9/6.4	14.1	1
	TN23/23/7	30.9	3
	TX36/23/15	97.5	2

Table 12: 100 kHz Region 2 Core Loss Core Comparison

100 (khz)	Core	Core Size (mm2)	Lowest CPL
Region 2	TN23/23/7	30.9	2
	TX36/23/15	97.5	1
	TX50/30/19	186	3

Figure 36 provides the results of Figure 34's CPL loss data for just 500 kHz. As in Figure 35, one of the TN23/14/7 cores was removed to provide a clearer picture of the trends. The removal of this core did not change the data trends. The graph is broken into overlapping curve regions. Only the overlapping experimental data points were compared in the experiment to eliminate the potential error that experimental estimates could give.

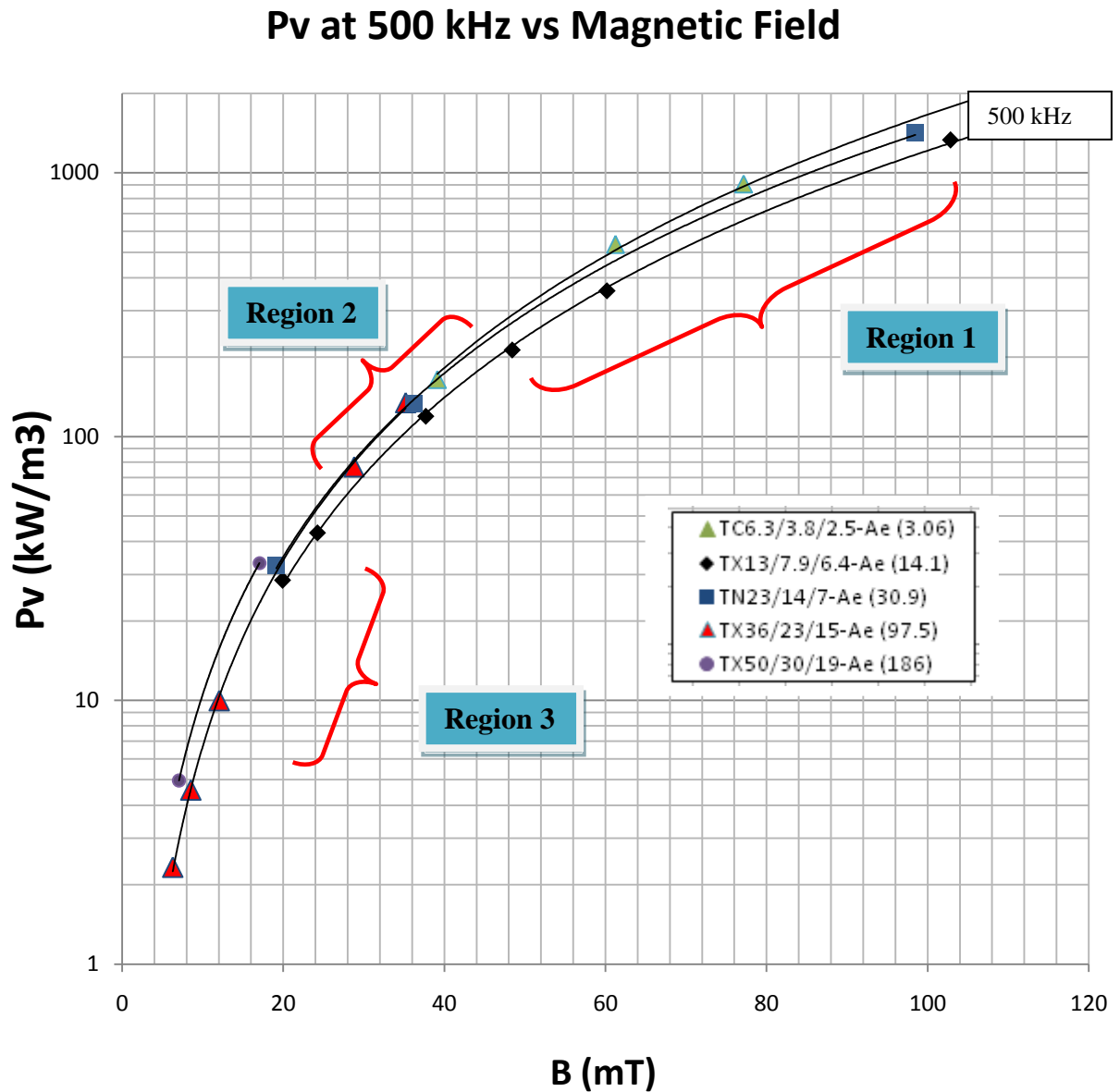


Figure 36: Core Area CPL Losses for 500 khz

Region 1 and 2 in Figure 35 envelops 3 cores and Region 3 only encases 2. Even at 500 kHz no apparent trend exists for the 6 core data set. Table 13, 14, 15 provides the different CPL overlapping regions for several different sized cores at 500 kHz. For Region 1, Table 9 demonstrates the smallest core had the largest loss and the second largest core had the lowest losses. Region 2 medium size core also had the largest loss. Only for Region 3 did the smallest sized core actually have the lowest CPL loss.

Table 13: 500 kHz Region 1 Core Loss Core Comparison

500 (khz)	Core	Core Size (mm2)	Lowest CPL
Region 1	TC6.3/3.8/2.5	3.06	3
	TX13/7.9/6.4	14.1	1
	TN23/23/7	30.9	2

Table 14: 500 kHz Region 2 Core Loss Core Comparison

500 (khz)	Core	Core Size (mm2)	Lowest CPL
Region 2	TX13/7.9/6.4	14.1	1
	TN23/23/7	30.9	3
	TX36/23/15	97.5	2

Table 15: 500 kHz Region 3 Core Loss Core Comparison

500 (khz)	Core	Core Size (mm2)	Lowest CPL
Region 3	TX36/23/15	97.5	1
	TX50/30/19	186	2

The conclusion that can be drawn from the data of figures 35 and 36 is that CPL is independent of  $A_C$ , or at least that  $A_C$  is not a dominant factor in CPL calculations for 3F3 power ferrite material. What needs to be emphasized is that if core area were a significant consideration then loss per volume would have varied greatly among the cores, since there is a factor of 60 area variation between the cores.

Three articles were found that discussed Power Ferrite core area versus CPL. Two of the references supported this author's claim that core area might not be a dominant CPL factor in Power Ferrites([5] and [8]), and one contradicted it [17].

The author of [5] explains that when a material is divided into small insulated electrical grain regions, the CPL per volume is more affected by the size of the grain and insulation layer around that grain than the overall dimension of the ferrite core. He further explains that for ferrite materials with high amplitude magnetic loss, the CPL per volume is independent of ferrite core dimension [5].

The above statement, about independence of loss per volume from core size, was experimentally verified by the authors of [8]. Their experiment systematically decreased the size of two MnZn ferrite cores through machining. The difference between the two cores was the amount of insulator in the cores. The first core, with little insulator, had low resistivity and a high value of permeability. Both properties are not typically found in high frequency applications [8]. In contrast, the second core, with more insulator, had ideal high frequency properties: high resistivity and low permeability. The experiment was conducted at two frequencies, 100 and 200 kHz. Table 16 provides these values. The experimental results demonstrated that CPL of the core

with little insulator was dependent upon core dimension, while the CPL of the more insulator core was not. This result supports that insulation layer thickness has an effect on CPL values.

The authors of [17] conducted CPL measurements using two different sized, but same MnZn material, power ferrite cores. The lot of the cores was not mentioned. Their core intrinsic material of choice also had a high resistivity and a low permeability, both ideal power ferrite application materials [8]. Table 16 provides these values. The cores were measured using 10 to 1000 kHz. Their conclusion did not agree with those of [8]. For their data set, there seemed to be a correlation of core size and CPL for cores with the same characteristics of the second core used in [8]. Their conclusion is that a portion of Power Ferrites CPL is due to the displacement of current distributions in the core. Different shaped and size cores would change this distribution [17].

Table 16 demonstrates that the cores chosen in this thesis resemble both the second core used in [8] and both cores used in [27]. The results of this thesis did not show a trend in core size to CPL, which was supported by [5] and [8]. The difference in the testing of the cores, might be a factor in the differing results of the between this thesis, [8] and [17].

Table 16: Core Resistivity and Permeability values

Core used in experiment		$\rho$ @DC ( $\Omega\text{m}$ )	$\mu_r$
[8]	MnZn First Core (Little insulator)	0.15	10000
[8]	MnZn Second Core (More insulator)	6.5	2300
[Thesis]	MnZn 3F3 Ferrite Core	8	3000
[17]	MnZn Both Cores	10	3080

## Section 4 CPL Data Fitting and Statistics Analysis

Section 4 provides the Least Square Best Fit (LSBF) statistical analysis for the CPL estimation equations listed in Section 1.6. As stated in Section 2.7, two mathematic LSBF methods were used for this analysis, a matrix and a MATLAB non-linear fit. Section 4 is broken into subsections, one for each equation. Each subsection includes the matrix math used to obtain both the LSBF curve fitted coefficients and the LSBF residuals value. The MATLAB code used to calculate the coefficients and LSBF residuals ( $R^2$ ) in each of the following subsections can be found in Appendix B. For each equation, the curve fitted coefficients of the lowest LSBF residual method were used in the plot of the equation. The method, the procedure and CPL measuring apparatus used to obtain the CPL data set used for the LSBF, is located in Section 2.3. The  $R^2$  were calculated using Eqn 45.

$$R^2 = \frac{(y_{data} - y_{fit})^2}{y_{data}}$$

As stated in Section 2.7,  $R^2$  is the Least Square Best Fit Residuals value.  $y_{data}$  is the actual measured CPL data.  $y_{fit}$  is results of using LSBF coefficient data.

### 4.1 Steinmetz Equation

Steinmetz proposed an equation in 1892 for the loss of energy due to hysteresis loss for machine steel. The equation had the form  $P_v = k\hat{B}^\beta$  [7].  $P_v$  is the power loss per unit volume,  $\hat{B}$  is the maximum peak flux amplitude,  $\beta$  and  $k$  are curve-fitted coefficients of actual experimental data. For Steinmetz's applications, this equation was a good solution for estimating CPL. Unfortunately, this equation is not robust enough to account for the CPL dependent frequency component. Power Ferrites are typically used frequencies in the range of 100 kHz to a few MHz, while Steinmetz experimentation used only low frequency sine wave data (50-200 hertz) for his  $k$  and  $\beta$  coefficients estimate [7].

To use Steinmetz Equation, the user has two options. The user can either find the  $k$  and  $\beta$  coefficients by obtaining them through the manufacturer's data sheet, if available, or measure these coefficients through actual experiment.

The accuracy of Steinmetz Equation is only as accurate as the data set used to obtain these coefficients. For example, the  $R^2$  are extremely low, i.e. accurate, for the LSBF curve fit to actual CPL data taken at 70 Hz or 140 Hz, but not when the combined data set of 70 and 140 Hz is used for the LSBF. Table 17 provides these  $R^2$  values.

Table 17: Steinmetz Equation

Steinmetz Equation	$R^2$	Unknowns	
		$k$	$\beta$
Low Freq (70 & 140) Matrix	.059	18.89	2.38
Low Freq (70) MATLAB	.00006	19.68	2.67
Low Freq (140) MATLAB	.00098	22.77	2.24



Figure 37 is a plot of actual 70 Hertz CPL data and the LSBF curve fitted solution to that data.

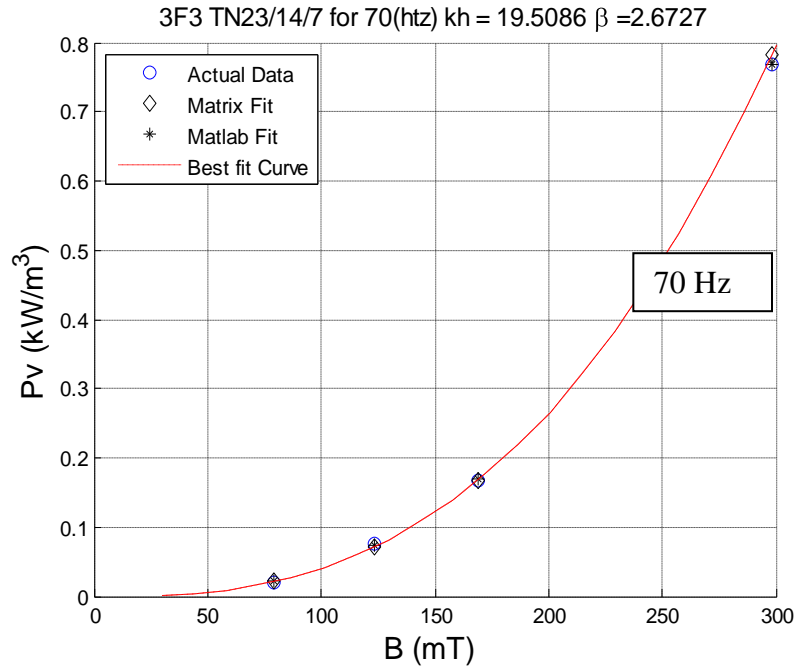


Figure 37: Hysteresis Loss Equation for 70 Hertz

The differences between  $R^2$  between the 70 Hz data and the 70 and 140 Hz combined data is due to Steinmetz equation (not accounting for the frequency dependency of CPL measurements). Figure 38 is a plot of the LSBF solution to the combined 70 and 140 Hz CPL data set.

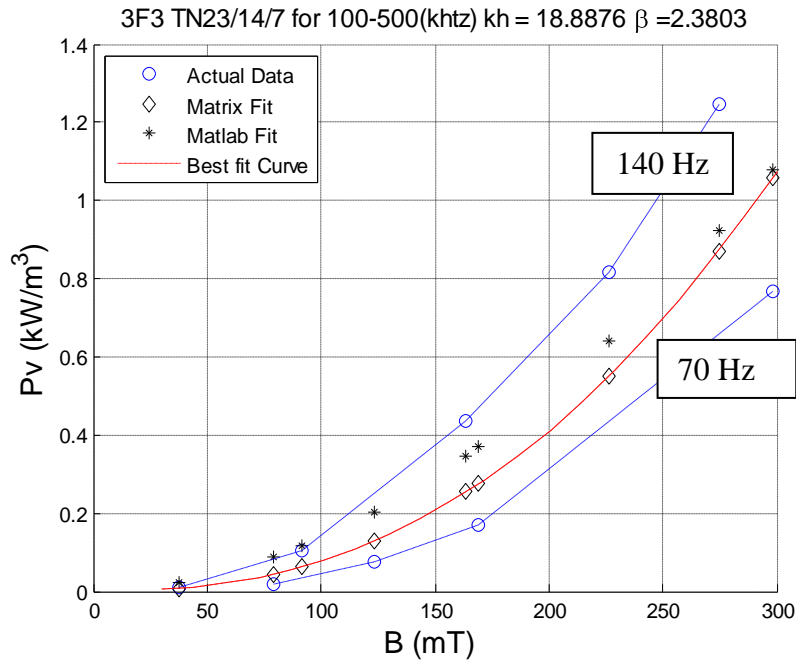


Figure 38: Low Frequency Core Power Loss for TN 23/14/7

The star dotted line is the LBFS solution to the actual CPL data at 70 and 140 hertz. Due to the input data sets having two different frequencies, the Steinmetz equation splits the difference between the two. As Table 17 demonstrates, the Steinmetz equation can only accurately approximate CPL if the frequency of the data set used to obtain the coefficients are the same as the frequency of the intended estimate.

Figure 39 is the Steinmetz Equation BFLS solution to the 3F3 TN23/17/4 100-500 kHz data set. As was shown in Figure 38, Steinmetz Equation still provided only a single line solution to the data set.

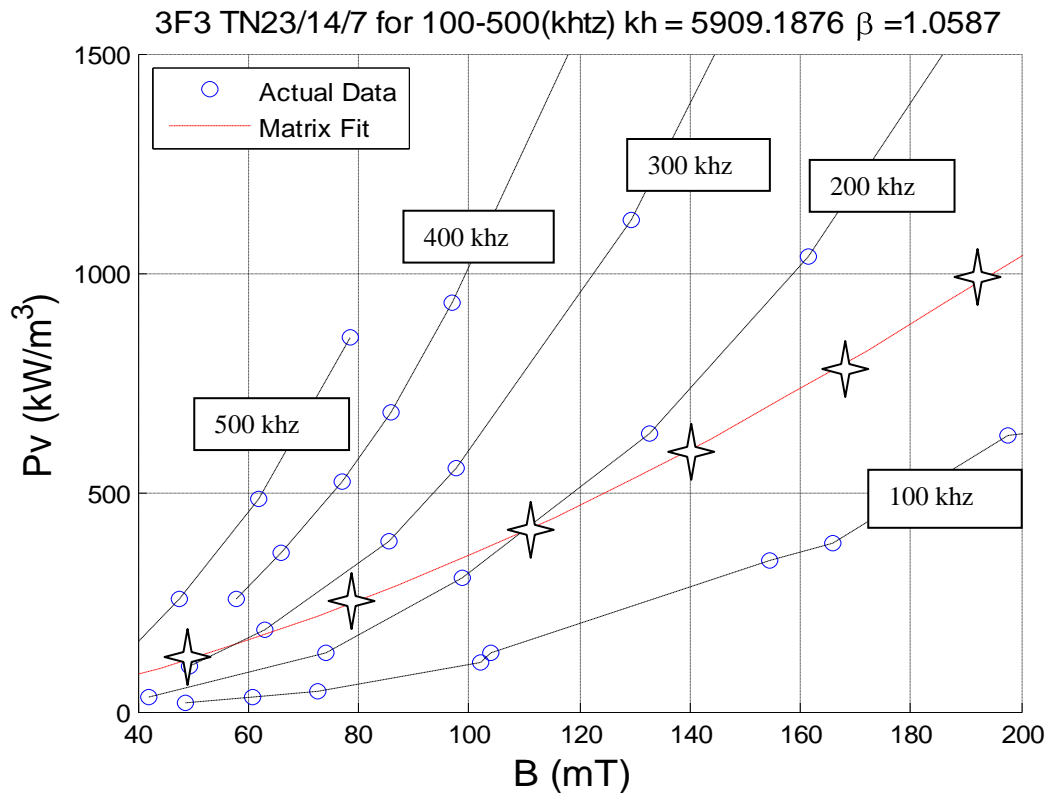


Figure 39: High Freq (100-500kHz) Steinmetz Equation

The LSBF  $R^2$  for the TN23/14/7 core for the 100 to 500 kHz data set is in Table 18.

Table 18:  $R^2$  and LSBF Steinmetz Equation coefficients at High Freq

Steinmetz Equation	$R^2$	Unknowns	
		k	$\beta$
High Freq (100- 500)	1956.5	5909.19	1.0587

The Matrix method was evaluated using the following equations. Using logarithms the Steinmetz Equation can be broken down into the form  $y= C+Dx$ . This is a linear equation, which

can be easily evaluated using LSBF matrix mathematics. The matrix math used in this CPL equation can found in reference [27].

$$\log(Pv) = \beta \log(B) + \log(k_1)$$

The matrix equivalent form of the above equation follows.

$$A * x = b$$

$$\begin{bmatrix} 1 & \log(B_1) \\ 1 & \log(B_2) \\ 1 & \log(B_3) \\ \vdots & \vdots \\ 1 & \log(B_n) \end{bmatrix} * \begin{bmatrix} \log(k_1) \\ \beta \end{bmatrix} = \begin{bmatrix} \log(Pv_1) \\ \log(Pv_2) \\ \log(Pv_3) \\ \vdots \\ \log(Pv_n) \end{bmatrix}$$

$$\bar{x} = (A^T A)^{-1} * A^T b$$

$$\bar{x} = \begin{bmatrix} \log(k_1) \\ \beta \end{bmatrix}$$

See Appendix B for the program used to calculate the MATLAB non linear solution.

## 4.2 Power Law Equation (PLE)

---

As shown in Section 1.6 and 4.1, for an equation to accurately estimate Power Ferrite CPLs over a broad range, that equation needs to have both a frequency and magnetic field term. The Power Law Equation is one such equation. Currently, the Power Law Equation (PLE) is of standard equation used by manufacturers, scientist and engineers. The simplicity of this approach is the parameters required for the equation can be found in manufacturer's material data sheets. Unlike several of the other empirical equations, this equation does not require the user to collect experimental data. Note that this equation does not account for possible variations in loss density, with core cross-sectional area.

The PLE (Eqn 5) has the following form:

$$P_v = C_1 f^\alpha \hat{B}^\beta$$

$P_v$  is the power loss per unit volume,  $\hat{B}$  is the maximum peak flux amplitude,  $f$  is the frequency, and  $\alpha$ ,  $\beta$  and  $C_1$  are curve-fitted coefficients of actual experimental data.

The 3F3 TN23/14/7 100-500 kHz data set was used to determine the PLE accuracy when compared to actual CPL core data. Figure 40 provides the LSBF curve fitted coefficients,  $C_1$ ,  $\alpha$  and  $\beta$ , for the PLE.

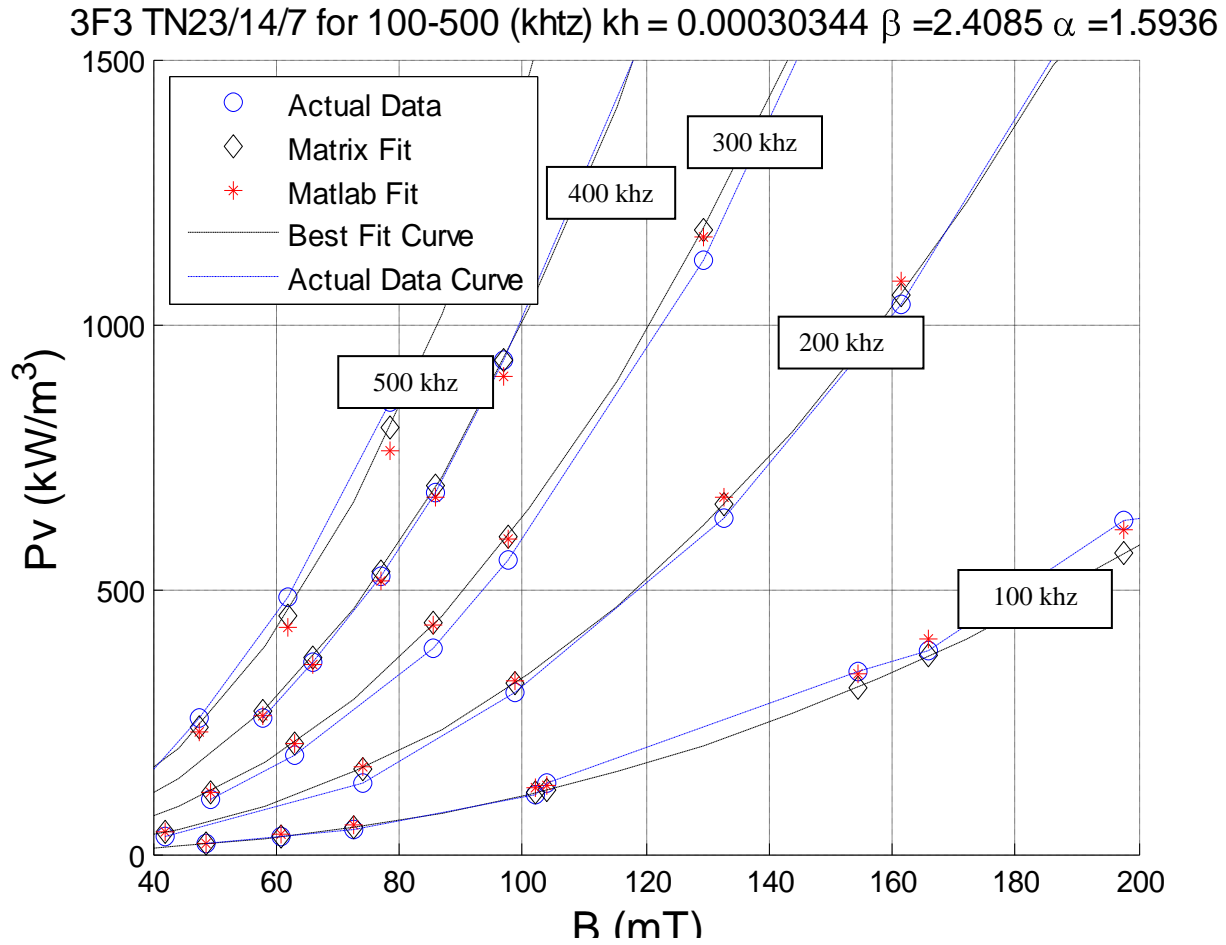


Figure 40: CPL graph using MATLAB Method

Table 19 gives the  $R^2$  for both Matrix and MATLAB method. For this equation, the MATLAB method provided the lowest LSBF  $R^2$  values.

Table 19: Residuals for High Freq using the Power Law Equation

PLE 100-500 (kHz)	$R^2$	Unknowns		
		$C_1$	$\alpha$	$\beta$
MATLAB	77.23	8.24E-04	1.51	2.41
Matrix	110.52	3.034E-4	1.593	2.409

Since Ferroxcube, the 3F3 manufacturer, provided the PLE curve fitted coefficients for three ranges: 100-300 kHz, 300-500 kHz, and 500-1000 kHz; the 100-500 kHz data set used in Figure 40 was broken into two smaller similar data sets: 100-300 kHz and 300-500 kHz. The LSBF curve fitted coefficients and the resulting  $R^2$  from these two data sets are located in Table 20 and 21. The lowest  $R^2$  curve fitted coefficients for the data sets were plotted in Figure 41 and 42.

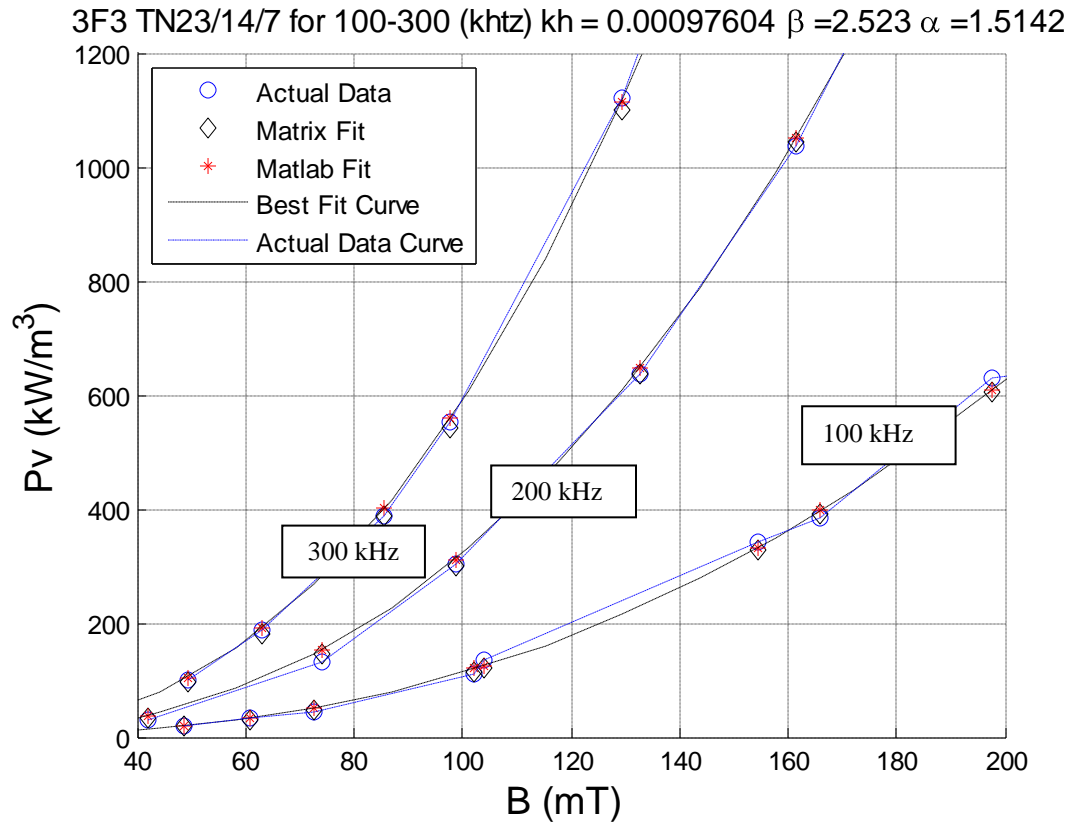


Figure 41: PLE LSBF for the 100-300 (kHz) data

Table 20: Residual data for 100-300 (kHz) PLE

PLE 100-300 (kHz)	$R^2$	Unknowns		
		$C$	$\alpha$	$\beta$
Matrix	20.83	9.76E-4	2.523	1.51
MATLAB	21.531	1.02E-3	2.467	1.50

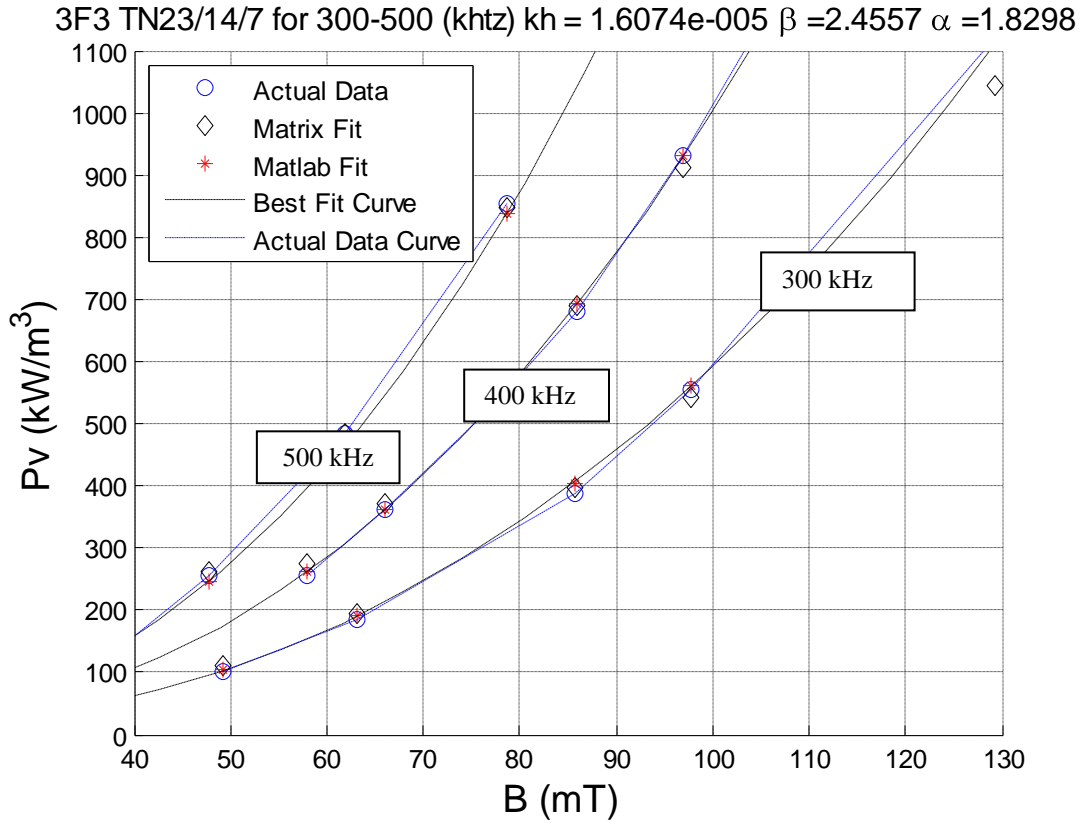


Figure 42: PLE LSBF for the 300-500 (kHz) data

Table 21: Residual data for 300-500 (kHz) PLE

PLE 300-500 (kHz)	$R^2$	Unknowns		
		$C$	$\alpha$	$\beta$
Matrix	27.02	7.3E-6	2.33	1.87
MATLAB	5.73	1.61E-5	2.46	1.83

Since the  $R^2$  found in Table 20 and 21 were lower than those for the complete 100-500 kHz data set in Table 19, one can postulate that the PLE equation provides a good but not perfect estimate of all the CPL loss mechanisms over a broad range.

The accuracy of Ferroxcube's provided PLE curve fitted coefficients found in [12] were evaluated against the coefficients determined in Table 20 and 21. The results are found in Table 22.

Table 22: Residuals of PLE for both Manufacturer Data and Estimated

Power Core Loss (Pv)		R <sup>2</sup>	Unknowns		
Frequency Range	Manufacturer Data		C	$\alpha$	$\beta$
	Matrix (Table 20)				
100-300 kHz	Ferroxcube (Table 1)	233.8	2.50E-04	1.63	2.45
	Matrix (Table 20)	20.83	9.76E-4	1.51	2.52
300-500 kHz	Ferroxcube (Table 1)	591.48	2.10E-05	1.8	2.5
	MATLAB (Table 21)	5.724	1.02E-5	2.46	1.86

The Ferroxcube's coefficients in Table 1 and 20 were collected by the manufacturer at a core temperature of 100 °C. Since CPL are temperature dependent, Ferroxcube provides a temperature correction factor for cores not at 100 °C in [12]. The Ferroxcube's PLE equation was adjusted to 50°C to allow the experimental results to accurately be compared to those of the manufacturer. Figure 43 and 44 is a plot of the Ferroxcube's estimate to actual CPL 3F3 TN23/14/7 data.

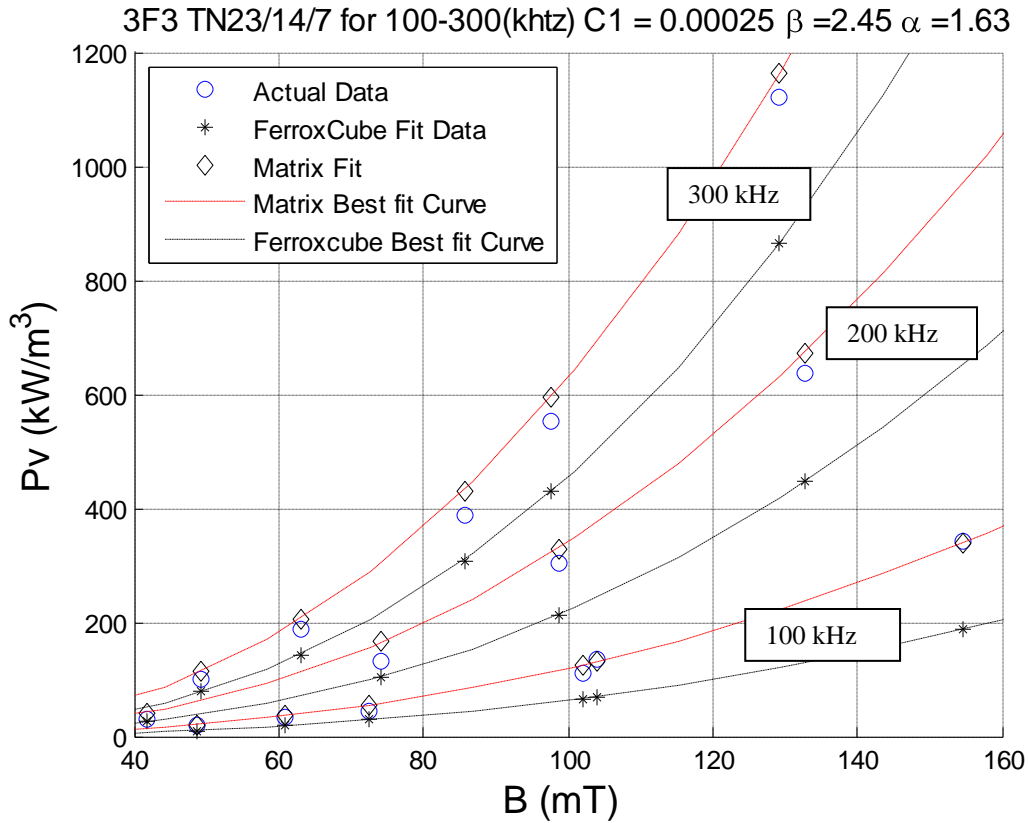


Figure 43: PLE 100-300 kHz Data for Ferroxcube Estimates and Best Fit Estimates

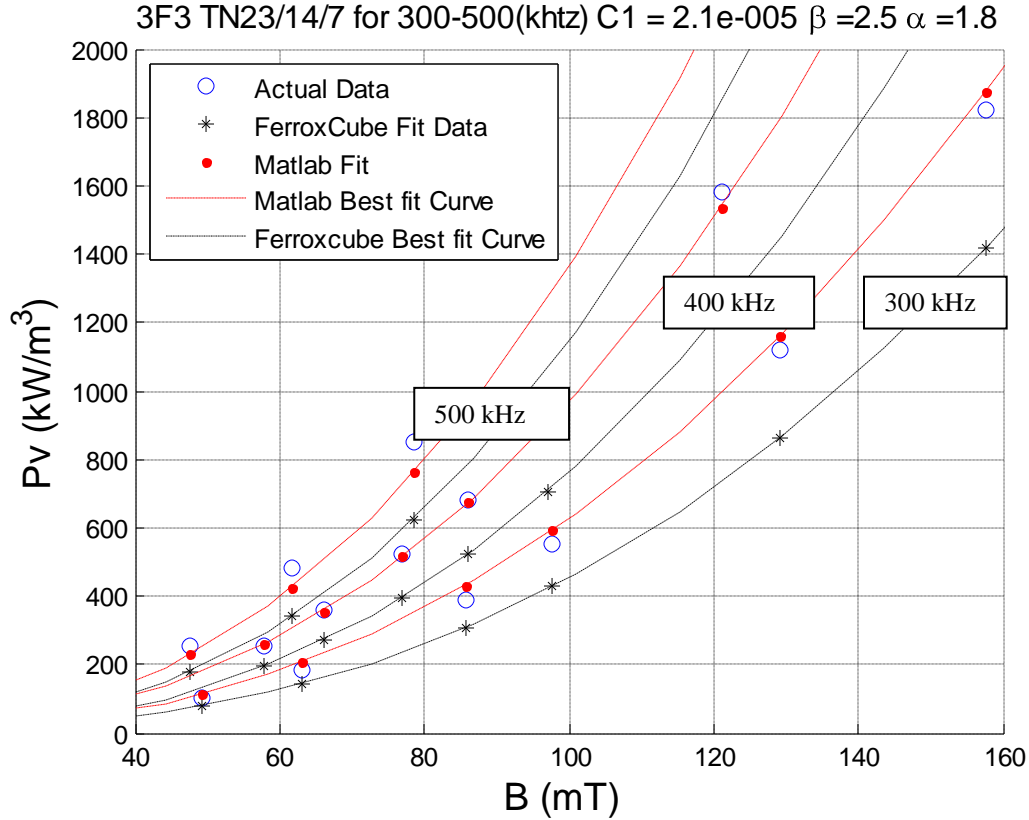


Figure 44: PLE 300-500 kHz Data for Ferroxcube Estimates and Best Fit Estimates

Table 22 and Figures 43 and 44 demonstrate that the PLE coefficients determined by experiment are a better fit to the actual measured data than the manufacturer provided coefficients. This is not a surprise since collected and then fitted data will always be more accurate to not fitted data. The differences between actual experimental data from this thesis and manufacturer data (while not large) could be due to different test apparatus and or methods for evaluation.

One of the difficulties in using the manufactured provided PLE coefficient equations is trying to understand which range or equation to use. For example, Table 2 provides two equations for PLE at 300 kHz. Normally, if the intended core application is above 300 kHz, the user would choose the 300-500 kHz range, and if below, the 100-300 kHz values would be used. The problem is deciding which equation to use if the application is at 300 kHz.

Figure 45 provides a plot of this situation. It shows that for 300 kHz data, the Ferroxcube LSBF coefficients for 100-300 kHz over estimates the actual 3F3 TN23/17/4 300 kHz CPL data while the Ferroxcube 300-500 kHz provided coefficient under estimates it.



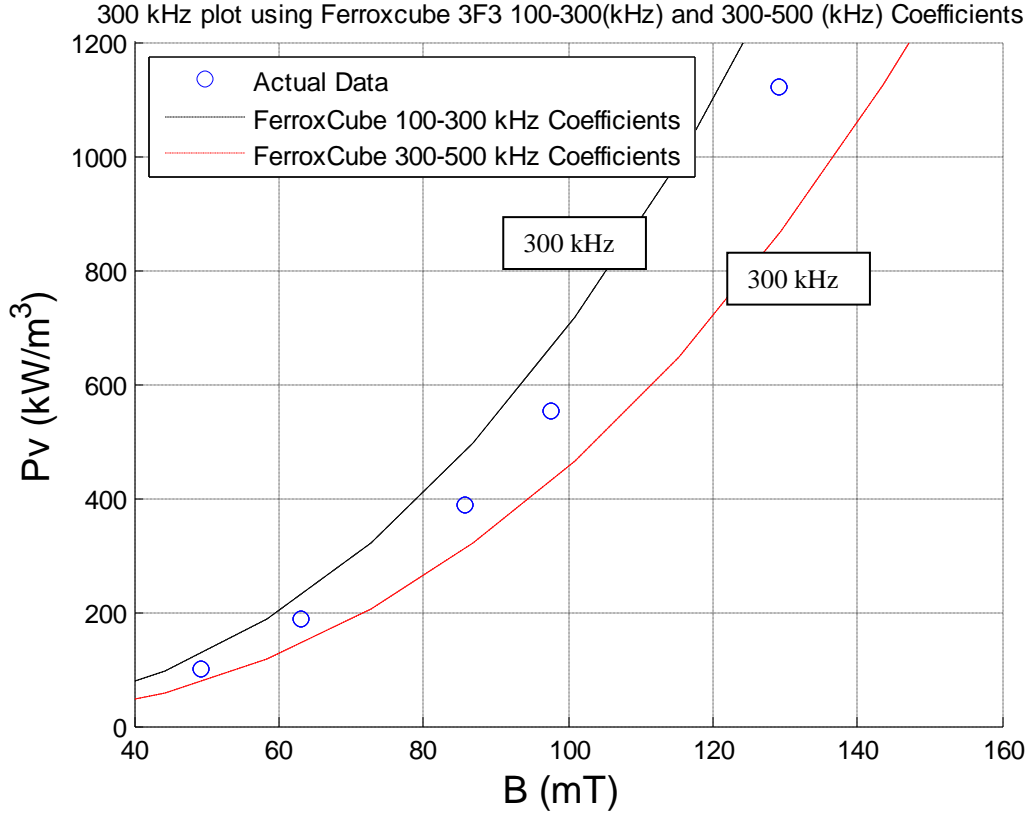


Figure 45: 100-300 and 300-500 kHz 3F3 Ferroxcube equations vs 300 kHz data

The Matrix method was evaluated using the following equations. PLE can be evaluated with logarithms in the form  $y = C + Dx + Ez$ . This is a linear equation, which can be easily evaluated using LSBF matrix mathematics. The matrix math used in this CPL equation can found in reference [27].

$$\log(Pv) = \alpha \log(f) + \beta \log(B) + \log(C_1)$$

The matrix equivalent form of the above equation follows.

$$A * x = b$$

$$\begin{bmatrix} 1 & \log(f_1) & \log(B_1) \\ 1 & \log(f_2) & \log(B_2) \\ 1 & \log(f_3) & \log(B_3) \\ 1 & \cdot & \cdot \\ 1 & \log(f_n) & \log(B_n) \end{bmatrix} * \begin{bmatrix} \log(C_1) \\ \alpha \\ \beta \end{bmatrix} = \begin{bmatrix} \log(Pv_1) \\ \log(Pv_2) \\ \log(Pv_3) \\ \cdot \\ \log(Pv_n) \end{bmatrix}$$

$$\bar{x} = (A^T A)^{-1} * A^T b$$

$$\bar{x} = \begin{bmatrix} \log(C_1) \\ \alpha \\ \beta \end{bmatrix}$$

See Appendix B for the program used to calculate the MATLAB non linear solution.

### 4.3 Hysteresis Loss Equation

The Hysteresis Loss Equation is given by Eqn 5,

$$P_h = k_h f \hat{B}^\beta$$

See Section 2.1 for a low frequency analysis of the given equation.

Figure 46 is a plot of the LSBF of the Hysteresis Loss equation for high frequency (100-500 kHz) data. Table 23 provides the LSBF curve fitted coefficients and the  $R^2$  for the Hysteresis Loss Equation at 100-500 kHz. Further, the 100-500 kHz data set is broken into 100-300 and 300-500 kHz data sets.

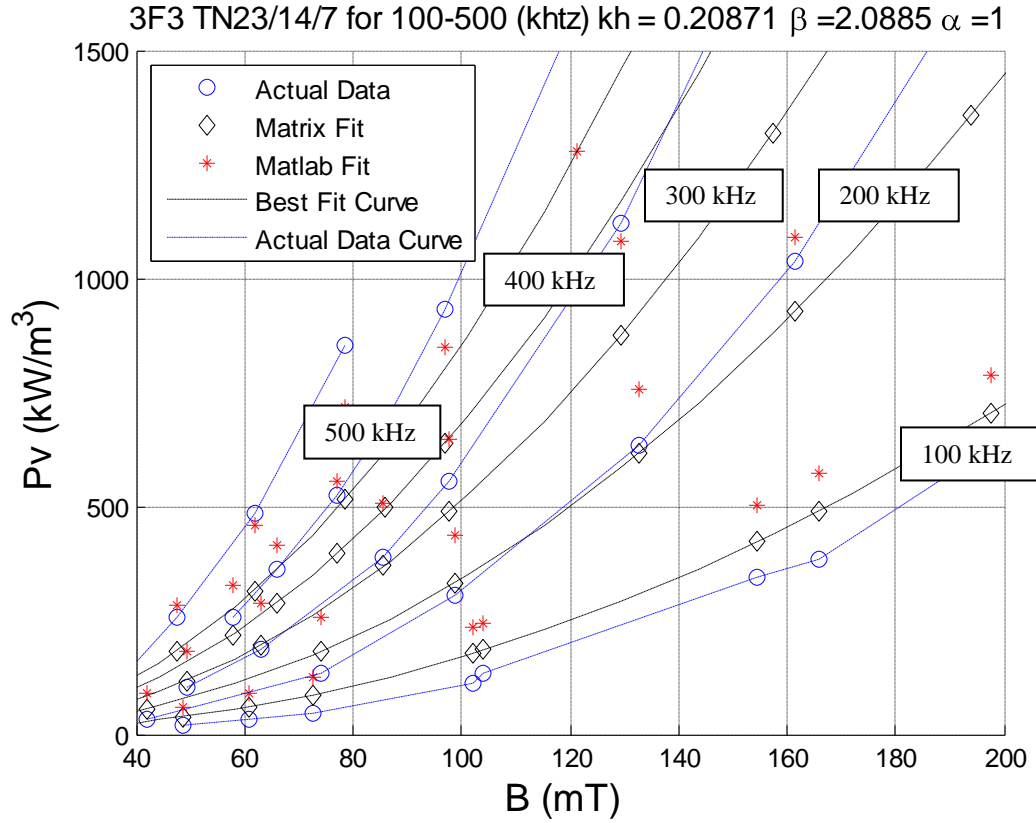


Figure 46: 100-500 BFLS for Hysteresis Loss Equation

Table 23: The Hysteresis Loss Equation LSBF for 100-300 kHz and 300-500 kHz

Hysteresis Loss Equation	$R^2$	$\alpha$	Unknowns	
			$k_h$	$\beta$
<b>MATLAB 100-500 kHz</b>	1549.9	1	.1588	1.85
<b>Matrix 100-500 kHz</b>	1175.1	1	.2087	2.09
<b>MATLAB 100-300 kHz</b>	917.1	1	.1801	1.94
<b>Matrix 100-300 kHz</b>	651.51	1	.3266	2.368
<b>MATLAB 300-500 kHz</b>	208.8	1	.3025	2.11
<b>Matrix 300-500 kHz</b>	184.8	1	.3291	2.17

The above analysis was LSBF fitting of  $k_h$  and  $\beta$  in the Hysteresis Loss Equation to the 100-500 kHz data set. Table 23 provides the  $R^2$  for these plots.  $R^2$  were calculated using the following equation.

$$R^2 = \frac{(y_{data} - y_{fit})^2}{y_{data}}$$

$R^2$  is the Least Square Best Fit Residuals value.  $y_{data}$  is the actual measured CPL data.  $y_{fit}$  is the Least Square Best Fit coefficients.

The following analysis used Table 7's Matrix LSBF Hysteresis Loss Equation coefficients determined by the best fit of the 70 and 140 Hz data for high frequencies, 100-500 kHz. This was done to test the accuracy of CPL models like Bertotti's Model, that use Hysteresis Loss coefficients obtained at low frequencies to extrapolate CPL estimates at high frequencies. Figure 47, 48, and 49 are plots of these Hysteresis Loss Equation coefficients for frequencies ranging from 100 to 500 kHz plotted against actual measured CPL data.

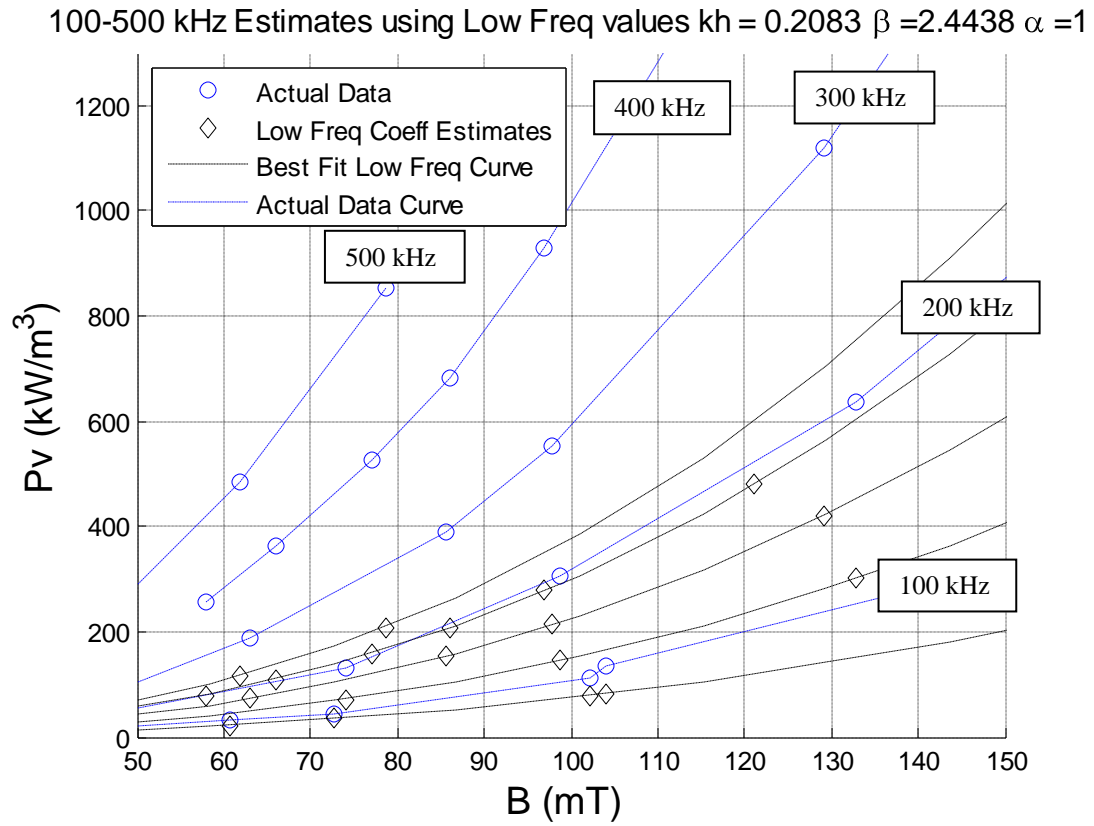


Figure 47: 100-500 kHz Using the Hysteresis Loss Equation Coefficients from 70 & 140 Hz data

100-300 kHz Estimates using Low Freq values  $kh = 0.2083$   $\beta = 2.4438$   $\alpha = 1$

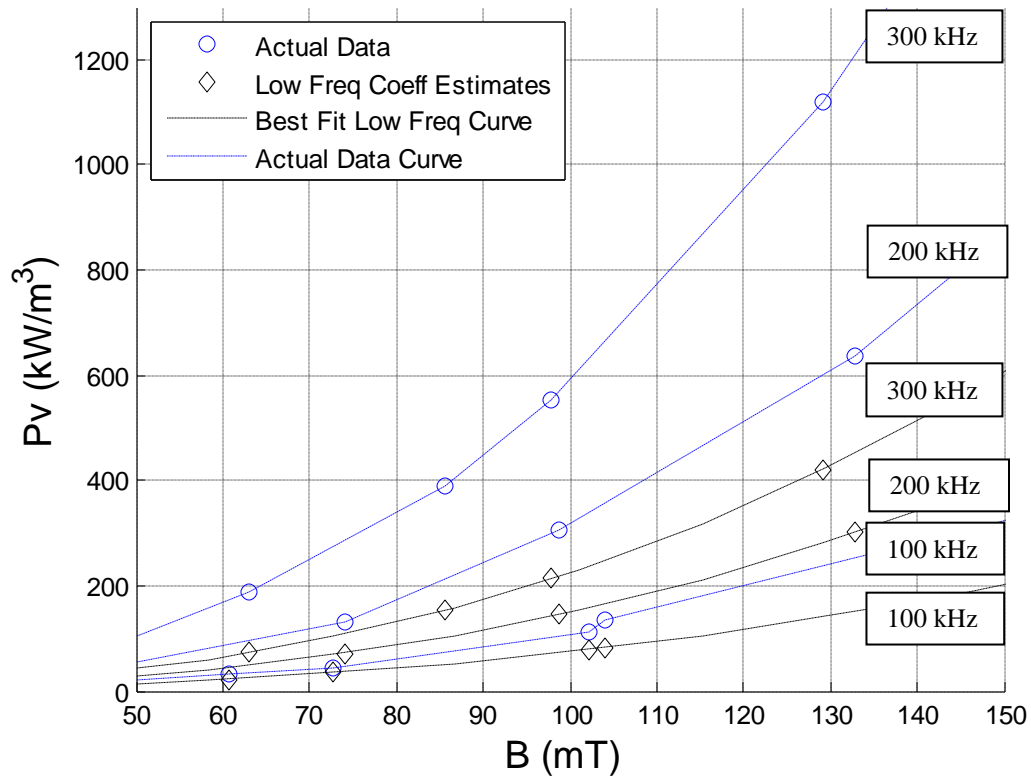


Figure 48: 100-300 kHz using the Hysteresis Loss Equation Coefficients from 70 & 140 Hz data

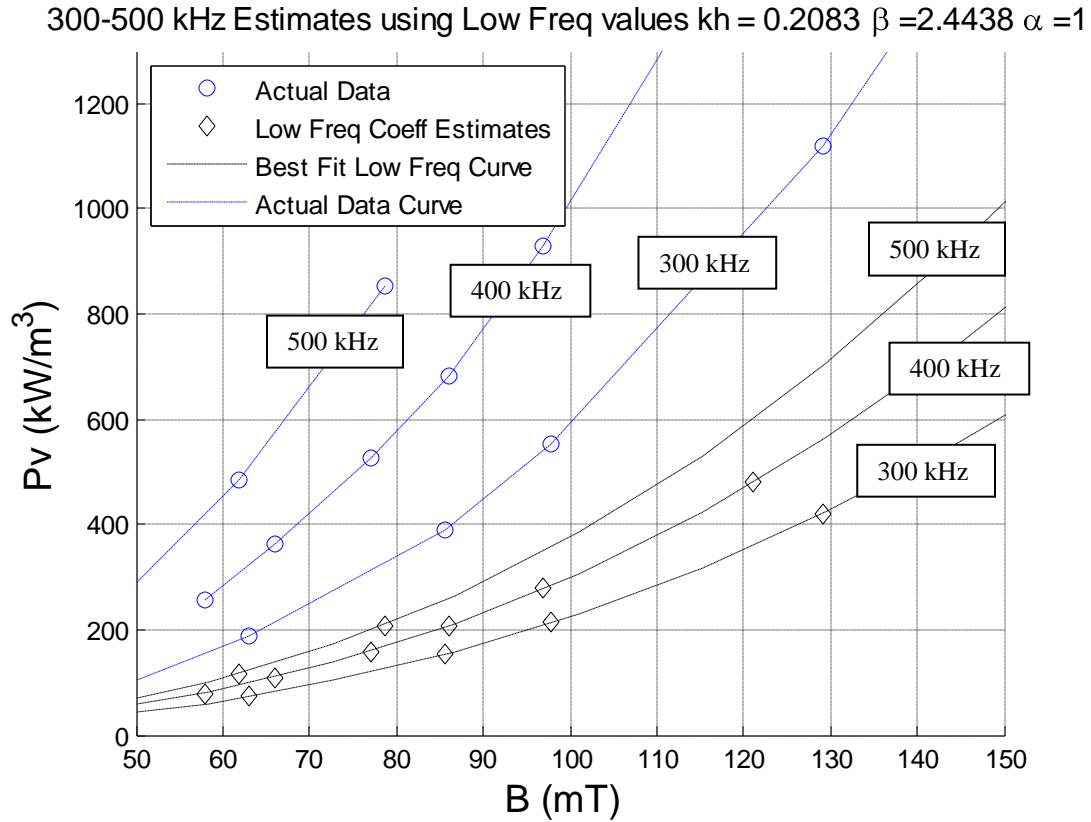


Figure 49: 300-500 kHz using the Hysteresis Loss Equation Coefficients from 70 & 140 Hz data

Table 24: LSBF of Low Freq Coefficients at 100-500 kHz

Hysteresis Loss Equation	$R^2$	$\alpha$	Unknowns	
			$k_h$	$\beta$
100-500 kHz	6842.9	1	.2083	2.4438
100-300 kHz	3699.4	1	.2083	2.4438
300-500 kHz	4749.2	1	.2083	2.4438

Table 24 provides the  $R^2$  for these plots. The  $R^2$  for 100-300 and the 300-500 kHz were determined by using these data sets separately. The  $R^2$  were calculated using the following equation.

$$R^2 = \frac{(y_{data} - y_{fit})^2}{y_{data}}$$

$R^2$  is the Least Square Best Fit Residuals value.  $y_{\text{data}}$  is the actual measured CPL data.  $y_{\text{fit}}$  is the LSBF coefficients found in Table 7 for the data fit of the 70 & 140 Hz data set.

The following is the Matrix method used in both Section 2.1 and this section.

$$\log(Pv/f) = \beta \log(B) + \log(C_1)$$

$$A * x = b$$

$$\begin{bmatrix} 1 & \log(B_1) \\ 1 & \log(B_2) \\ 1 & \log(B_3) \\ \vdots & \vdots \\ 1 & \log(B_n) \end{bmatrix} * \begin{bmatrix} \log(C_1) \\ \beta \end{bmatrix} = \begin{bmatrix} \log(Pv_1/f_1) \\ \log(Pv_2/f_2) \\ \log(Pv_3/f_3) \\ \vdots \\ \log(Pv_n/f_n) \end{bmatrix}$$

$$\bar{x} = (A^T A)^{-1} * A^T b$$

$$\bar{x} = \begin{bmatrix} \log(C_1) \\ \beta \end{bmatrix}$$

See Appendix B for the program used to calculate the MATLAB non linear solution.

#### 4.4 Classical Eddy Current Equation (CECE)

---

As described in Section 1.7.2, the Classical Eddy Current Loss Equation is derived using two assumptions; homogenous material is used and there is a uniform driving magnetic field across the core. The combination of these assumptions leads to a single eddy current loss in the material. As discussed in Section 1.7.2, this is an ideal material and not representative of actual power ferrite materials. Classical Eddy Current Loss Equation (Eqn 31) has the form:

$$P_{cl} = \frac{\sigma \pi f^2 \hat{B}_{pk}^2 A_c}{4}$$

For the square toroid, similar to those used in this thesis, the approximate equation for  $A_c$  is (Eqn 30).

$$A_c = \frac{d^2 l \log\left(\frac{R_2}{R_1}\right)}{3(R_2 - R_1)}$$

See Section 1.7.2 for a discussion of terms in the above Classical Eddy Current Loss Equation. To measure the accuracy of this equation, actual CPL data was measured using a 3F3 TN23/14/7 core and then compared to the above equation. The resultant  $R^2$  is found in Table 25. The  $R^2$  was calculated using the following equation.

$$R^2 = \frac{(y_{data} - y_{fit})^2}{y_{data}}$$

$R^2$  is the Least Square Best Fit Residuals value.  $y_{data}$  is the actual measured CPL data.  $y_{fit}$  is the value obtained by using Equation 31 for the TN 23/17/4 3F3 Core.

Figure 28 is actual PCL data plot alongside the Classical Eddy Current Loss equation for that data set.

Table 25: Residuals for Classical Eddy Current Equation

Eddy Current Loss Equation	$R^2$
MATLAB	5548.29

### 3F3 TN23/14/7 for 100-500(khtz) Classical Eddy Current Loss

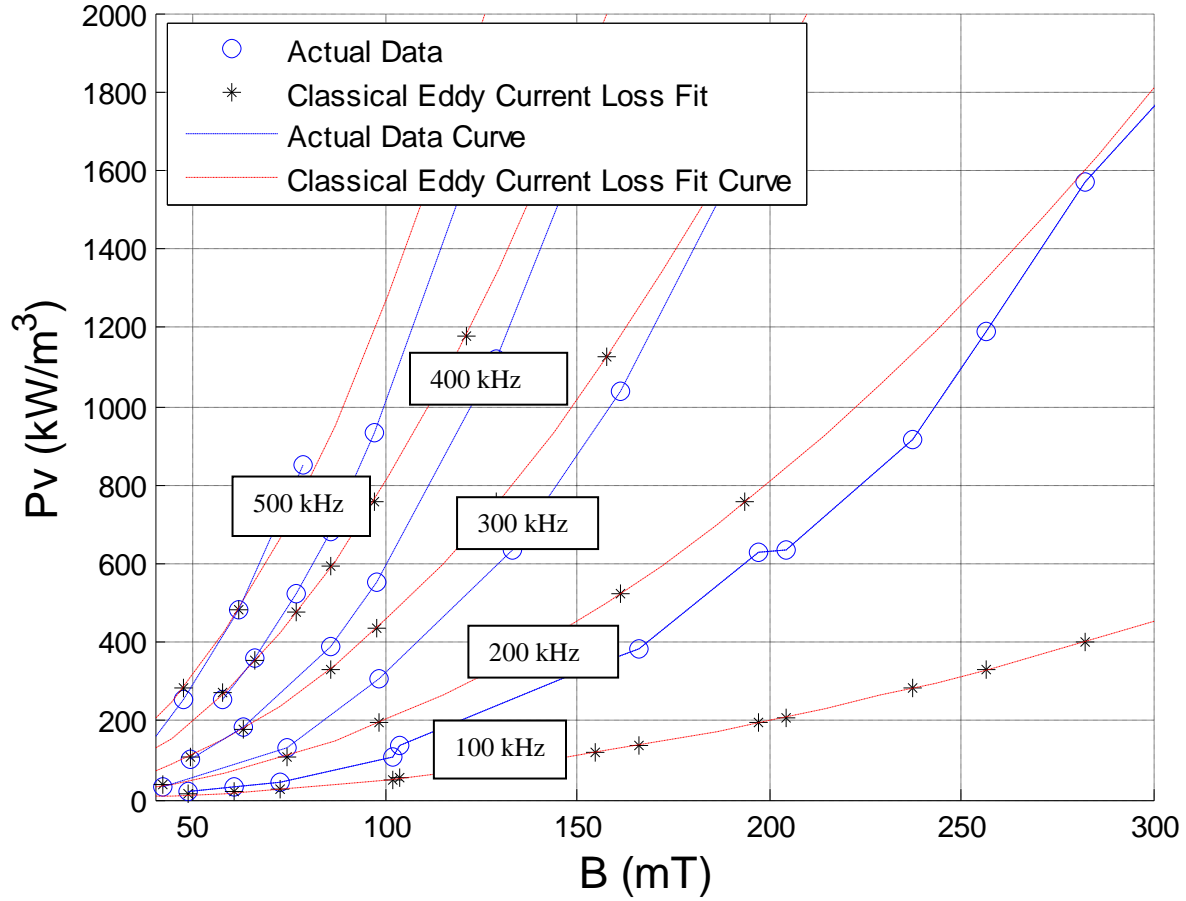


Figure 50: Classical Eddy Current Loss Equation for 100-500 kHz Data



## 4.5 Separation of Total Power Losses Models

---

The Separation of Total Power Losses (STPL) model is currently being used by several references as explained in Section 1.7. Several forms of this model exist, but the general form is (Eqn 12),  $P_v = P_h + P_{cl} + P_{ex}$ . See Section 1.7 for an explanation of this equation. The next several subsections will be using this or some form of this equation.

### 4.5.1 Bertotti's Model

---

The first STPL model to be analyzed is the Bertotti's Model (Eqn 9).

$$P_v = k_h \hat{B}^\beta f + \frac{A_c \sigma \pi f^2 \hat{B}^2}{4} + 8\sqrt{(\sigma G S V_o)} \hat{B}^{1.5} f^{1.5}$$

As it is easily shown, (Eqn 9) can be broken into (Eqn 12) subdivisions.

$$1. \quad P_h = k_h \hat{B}^\beta f \quad (\text{Eqn 5})$$

$$2. \quad P_{cl} = \frac{A_c \sigma \pi f^2 \hat{B}^2}{4} \quad (\text{Eqn 6})$$

Where  $A_c$  is (Eqn 30) for rectangular toroid given by

$$A_c = \frac{d^2 l \log \left( \frac{R_2}{R_1} \right)}{3(R_2 - R_1)} \quad (\text{Eqn 6})$$

$$3. \quad P_{ex} = 8\sqrt{(\sigma G S V_o)} \hat{B}^{1.5} f^{1.5} \quad \text{Eqn 53}$$

$P_h$  is the Hysteresis Loss Equation and a discussion of this equation can be found in both Sect 2.1 and 4.3. This equation is typically used to model CPL at low frequencies and is discussed in Section 3.1.  $P_{cl}$  is the Classical Eddy Current equation and is discussed in Sect 1.7.2 and 4.4.  $P_{ex}$  is the Excess Eddy Current Loss term discussed in Sect 1.7 and 1.7.3.  $\sigma$  is conductivity of the material.  $G$  is a unit-less constant with value of .1356.  $S$  is the cross-sectional area of the core.  $V_o$  is a curve fitted coefficient.

$P_h$  and  $P_{cl}$  have already been calculated and analyzed for 3F3 TN 23/17/4 in pervious sections and will not be discussed. However, these two STPL term losses will be used in conjunction with (Eqn 32) to determine  $P_{ex}$  in Sect 4.5.1.1.

In [9], Bertotti explains his Excess Eddy Current Loss (EECL) is given by (Eqn 53) and the  $V_o$  in that equation is a curve fitted coefficient using  $P_{ex}$  CPL data points determined by using (Eqn 54).

$$P_{ex} = P_v - k_h f \hat{B}^\beta - \frac{A_c \sigma \pi f^2 \hat{B}^2}{4} \quad \text{Eqn 54}$$

For Bertotti's Model to be used, only three experimental CPL points are required. Two low frequency points are essential for the  $k_h$  and  $\beta$  curve fit and one high frequency  $P_v$  points are needed to solve for  $V_o$  [9]. The  $k_h$  and  $\beta$  found in Sect 4.3 using the 70 and 140 Hz data and the the

Classical Eddy Current Equation determined in Section 4.4 were used. The 100 kHz 3F3 TN 23/14/7 data set was applied in (Eqn 54) to calculate  $P_{ex}$ .

Unfortunately, as discussed in Sect 3.2,  $\sigma$  is not constant for changes in magnetic field, temperature and frequency. Consequently, determining what value of  $\sigma$  to use in Eqn 54 was very difficult. Since many CPL model equations use  $\sigma$  determined at 25°C for DC conditions, Ferroxcube's provided 25°C DC  $\sigma$  value, (.5 S/m), was utilized.

Figure 51 is a plot of the  $P_v$ ,  $P_h$ ,  $P_{cl}$  and  $P_{ex}$  terms in the (Eqn 12) using (Eqn 54). It is interesting but not surprising that the  $P_{ex}$  is negative for portions of the graph. This demonstrates that either Bertotti's model is not completely accurate; the CPL  $P_v$  data obtained was not precise; or the choice of the  $\sigma$  value was incorrect. The results of Section 3.2 and 3.3 lean toward the  $A_c$  and  $\sigma$  values in the above equation being the possible root cause of the error. The  $P_{ex}$  negative value is accentuated when the 500 kHz data is used in Figure 52.

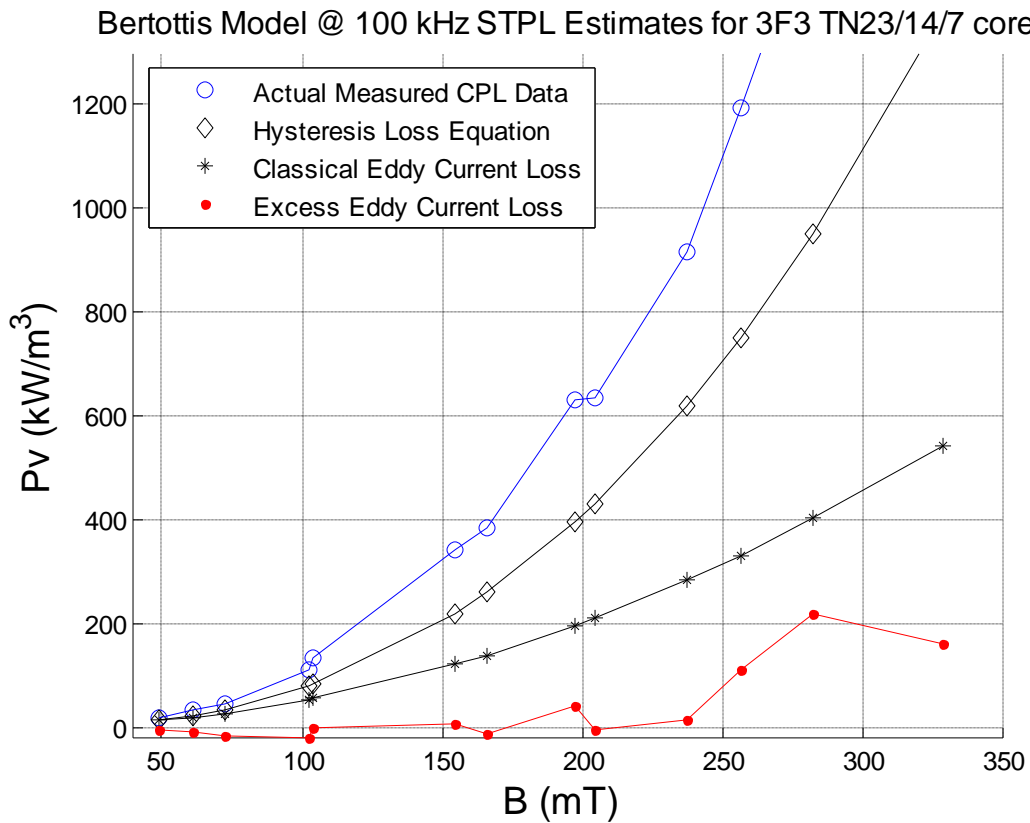


Figure 51: Bertotti's STPL Model Using 100 kHz Data

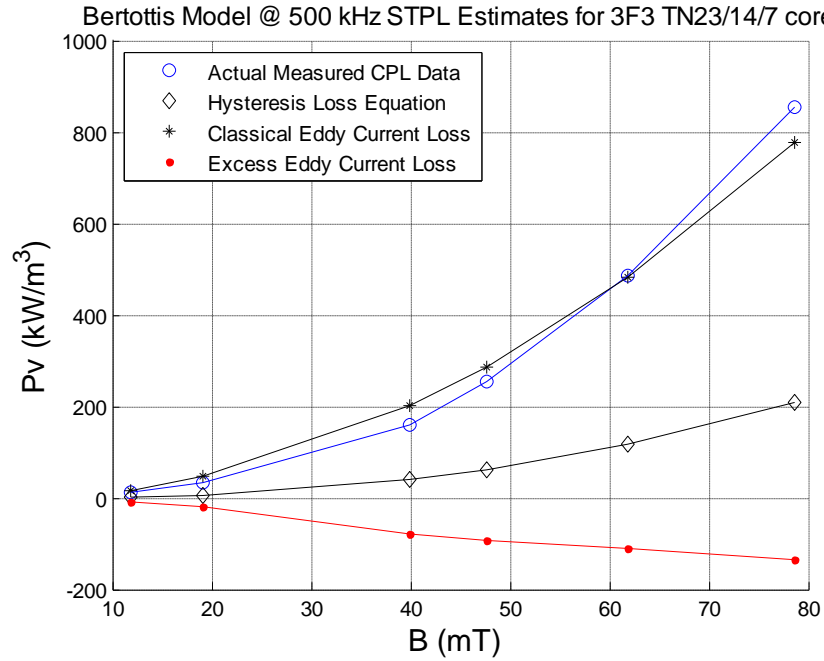
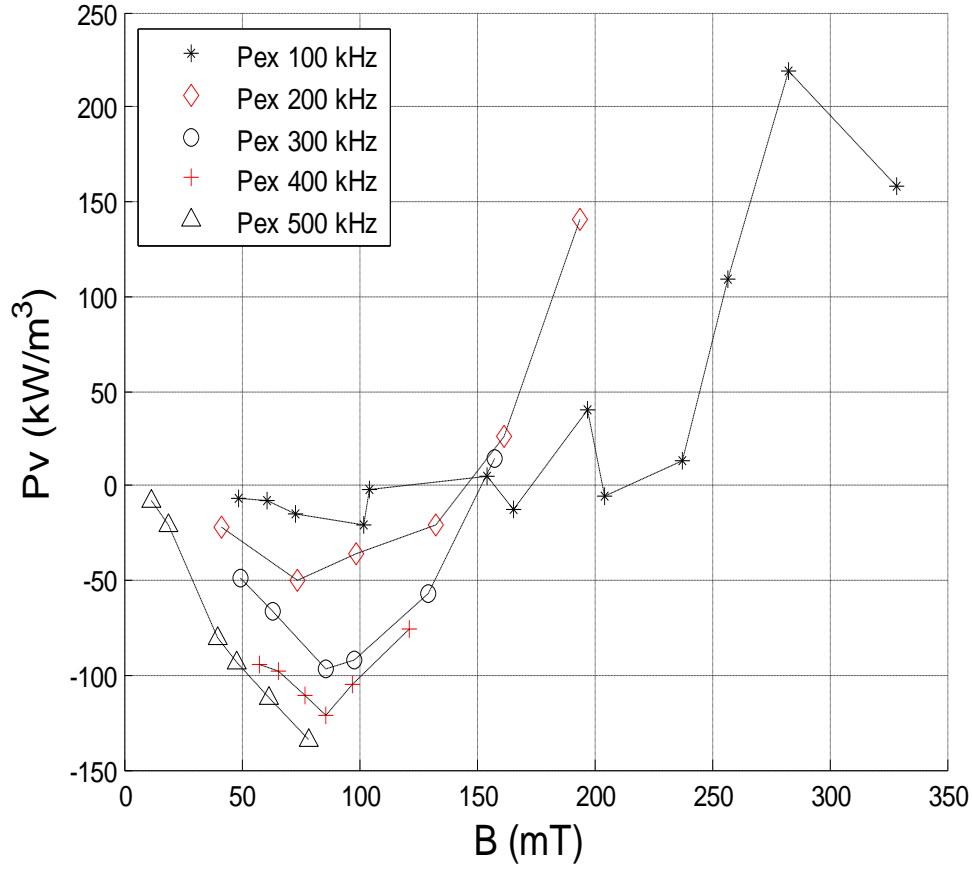


Figure 52: Bertotti's STPL Model Using 500 kHz Data

Figure 53 is a plot of the 100-500 kHz CPL  $P_{ex}$  values obtained using (Eqn 54), notice 4 of the 5  $P_{ex}$  plots in Figure 53 are below zero for more than half their plotted range, demonstrating Bertotti's  $P_{ex}$  model is a poor model at estimating CPL.

Figure 53: Pex using Bertotti's STPL Model for 10

Pex using STPL and Bertottis Model for 3F3 TN23/14/7 core



0-500 kHz data

As was stated above, only one high frequency data points is required for  $V_o$ , but for the sake of accuracy, all the 100 kHz data was used to determine the LSBF of  $V_o$ . Figure 54 provides a plot of the LSBF Pex results for finding  $V_o$ . Table 26 provides the value of  $V_o$  and the resultant  $R^2$  as determined by Figure 54.

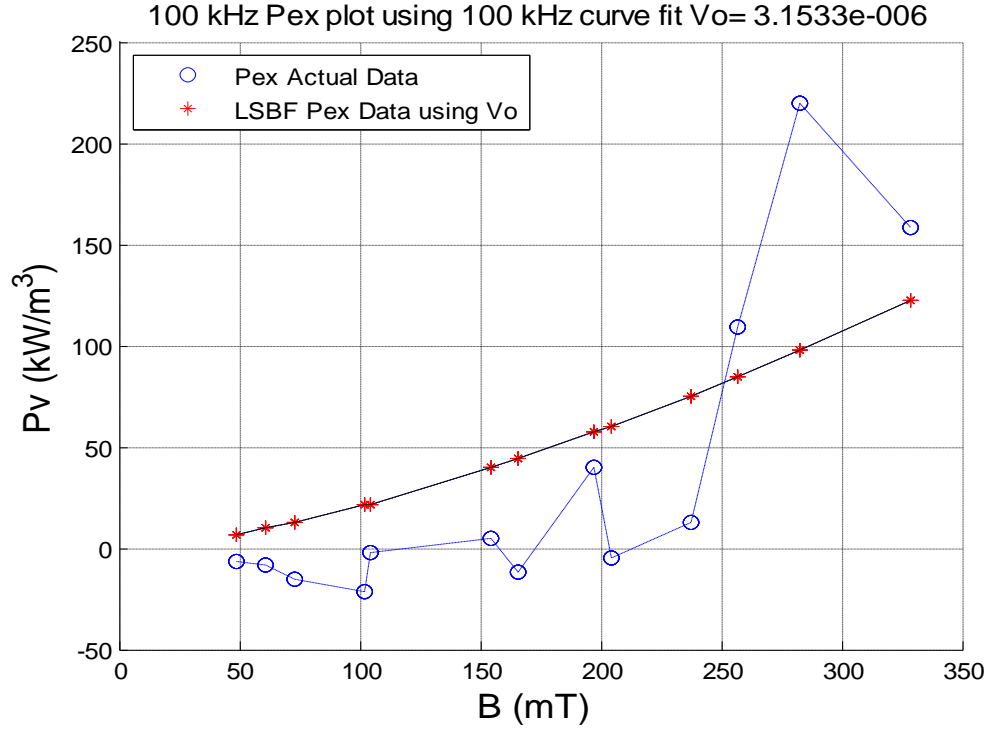


Figure 54: Bertotti's Excess Eddy Loss LSBF Vo term using 100 kHz data

The circle data points are the  $P_{ex}$  values obtained using (Eqn 54),

$$P_{ex} = P_v - k_h f \hat{B}^\beta - \frac{A_c \sigma \pi f^2 \hat{B}^2}{4}$$

and the star data points are the  $P_{ex}$  found using the LSBF Vo fit for (Eqn 53).

$$P_{ex} = 8\sqrt{(\sigma G S V_o)} \hat{B}^{1.5} f^{1.5}$$

Table 26: EECL LSBF Residuals in finding  $V_o$  by using 100 kHz data for the 100 kHz  $P_{ex}$

EECL (100 kHz LSBF)	$R^2$	$V_o$
Matrix	2191.4	3.153E-3

Figure 55 is a graph of the CPL determined by using (Eqn 52). Table 27 has the  $R^2$  for this LSBF using  $V_o$  as provided in Table 26 for 100-500kHz. The  $R^2$  for 100-300 and the 300-500 kHz were determined by using these data sets separately.

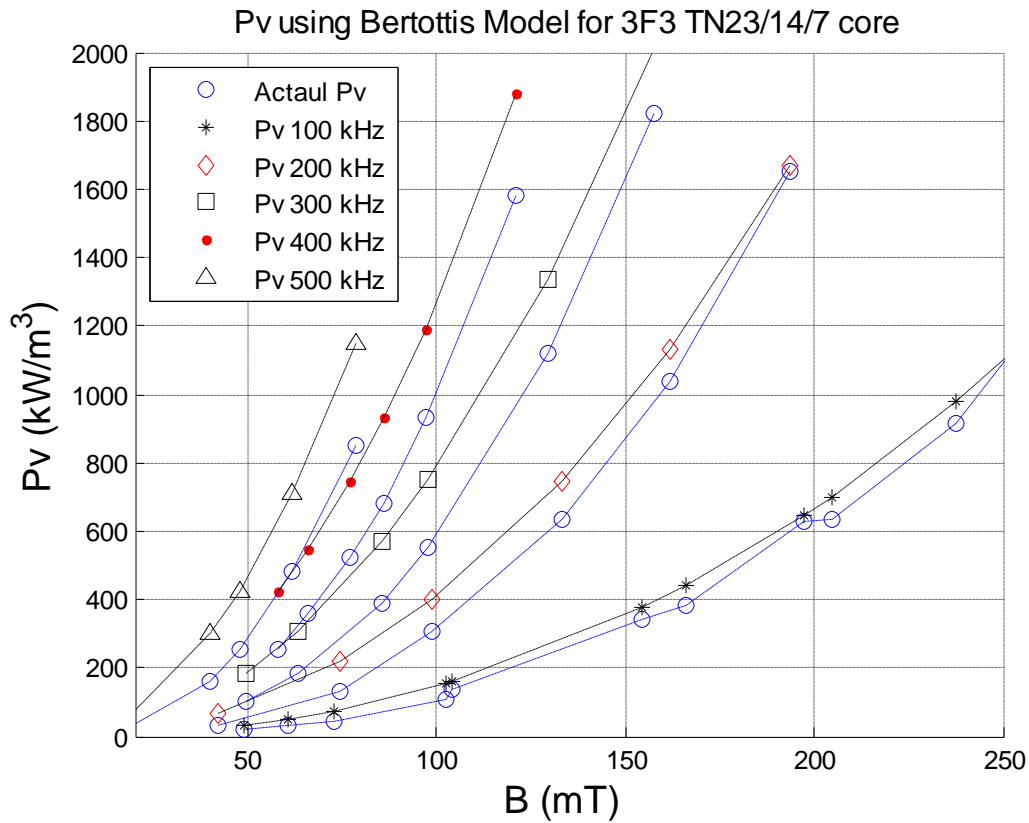


Figure 55: Bertotti's Model vs Actual data for 100-500 kHz

Bertottis Model	$R^2$	$k_h$	$\beta$	$V_o$
100-500 kHz	1649.2	.2083	2.4438	3.153E-3
100-300 kHz	616.2	.2083	2.4438	3.153E-3
300-500 kHz	1399.6	.2083	2.4438	3.153E-3

The Matrix method used to evaluate  $V_o$  has the following equations. The form of the  $P_{ex}$  can be broken down into the form  $y=C$ . This is a linear equation, which can be easily evaluated using LSBF matrix mathematics.

$$\left( P_{ex} / 8\sqrt{\sigma G S} f^{1.5} B^{1.5} \right) = \sqrt{V_o}$$

$$A * x = b$$

$$\begin{bmatrix} 1 \\ 1 \\ 1 \\ \vdots \\ 1 \end{bmatrix} * [\sqrt{Vo}] = \begin{bmatrix} (Pex_1/8\sqrt{\sigma GS}f_1^{1.5} B_1^{1.5}) \\ (Pex_2/8\sqrt{\sigma GS}f_2^{1.5} B_2^{1.5}) \\ (Pex_3/8\sqrt{\sigma GS}f_3^{1.5} B_3^{1.5}) \\ \vdots \\ (Pex_n/8\sqrt{\sigma GS}f_n^{1.5} B_n^{1.5}) \end{bmatrix}$$

$$\bar{x} = (A^T A)^{-1} * A^T b$$

$$\bar{x} = [\sqrt{Vo}]$$

#### 4.5.2 Hysteresis Loss Equation and Classical Eddy Current Equation (HLE & CECE)

The second STPL to be analyzed is (Eqn 10), the Hysteresis Loss Equation and the Classical Eddy Current Equation.

$$P_v = k_h f \hat{B}^\beta + k_c \sigma f^2 \hat{B}^2$$

Justification for this equation comes from the authors of [4], who say the Excess Loss term in many STPL models for Ferrites is small and negligible when compared to the other STPL terms for high induction levels and frequencies below 500 kHz. This statement was supported by the results of 4.5.1. The  $k_h$  and  $\beta$  determined in Sect 3.1 and given in Table 7 were used for the first STPL term in the above model. (Eqn 29) was used to provide the second term. The results of this analysis are provided in Table 27 and Figure 56. The analysis compared actual 3F3 TN23/17/4 CPL 100-500 kHz data to above STPL model.

Table 27:  $R^2$  for Bertotti's Model minus the Excess Loss Term

Bertotti's Model minus $P_{ex}$	$R^2$	$k_h$	$\beta$
100-500 kHz	473.1	.2083	2.4438
100-300 kHz	211.5	.2083	2.4438
300-500 kHz	351.8	.2083	2.4438

LSBF residuals ( $R^2$ ) were calculated using Eqn 45.

$$R^2 = \frac{(y_{data} - y_{fit})^2}{y_{data}}$$

$y_{data}$  is the actual measured CPL data.  $y_{fit}$  is results of using the Hysteresis Loss Equation and the Classical Eddy Current Equation results.

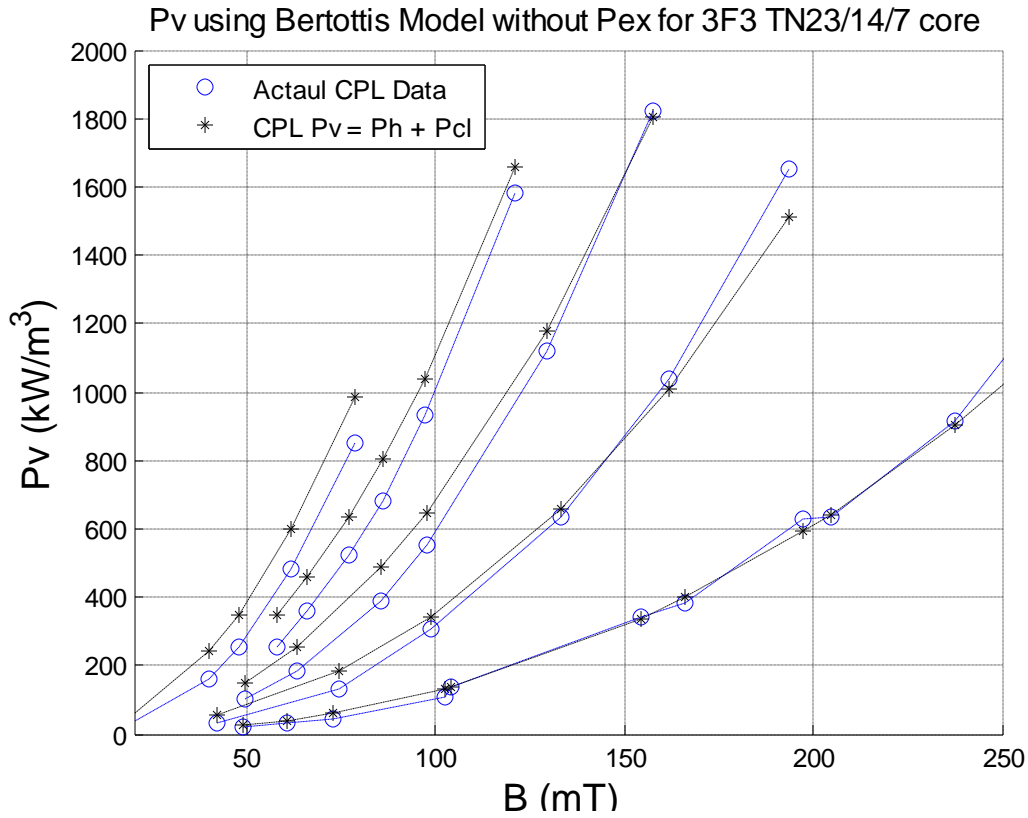


Figure 56: Plot of Bertotti's Model minus the Excess Loss Term

When the results of Sect 4.5.1 and 4.5.2 are compared, it is surprising to see, for at least the 3F3 100-500 kHz data, the lowest residuals were found without using the Excess Eddy Current Loss term.

See Appendix B for the program used to calculate the  $R^2$  values.

#### 4.5.3 Hysteresis Loss Equation and the PLE Equation Model (HLE & PLE)

The Hysteresis Loss Equation and the PLE Model, (Eqn 11), were analyzed to see if a good CPL estimation equation model could be achieved by combining these two equations.

$$P_v = k_h f \hat{B}^{\beta_1} + k_{ex} f^\alpha \hat{B}^{\beta_2}$$

The  $k_h$  and  $\beta$  determined in Sect 3.1 and given in Table 7 were used in for the Hysteresis Loss Equation coefficients.  $\alpha$  and  $\beta_2$  were determined by taking  $P_v$  actual data and subtracting the Hysteresis Loss Equation from it. The  $k_{ex}$ ,  $\alpha$  and  $\beta_2$  coefficients were then curve fitted to that resultant CPL values. Table 28 and Figure 57 provides the results of the LSBF of the model.



Table 28: HLE & PLE Model LSBF Results

HLE & PLE Method	$R^2$	$k_h$	$\theta_1$	$k_{ex}$	$\alpha$	$\theta_2$
Matrix 100-500 kHz	46.7	.2083	2.4438	1.51E-7	2.170	2.476
MATLAB 100-500 kHz	36.56	.2083	2.4438	8.54E-7	2.023	2.424
Matrix 100-300 kHz	21.44	.2083	2.4438	3.33E-7	2.132	2.640
MATLAB 100-300 kHz	21.93	.2083	2.4438	8.26E-7	2.035	2.493
Matrix 300-500 kHz	18.84	.2083	2.4438	2.19E-8	2.289	2.318
MATLAB 300-500 kHz	4.61	.2083	2.4438	6.40E-8	2.232	2.463

3F3 TN23/14/7 for 100-500 kHz  $k_c = 8.5442\text{e-}007$   $\beta = 2.4244$   $\alpha = 2.0232$

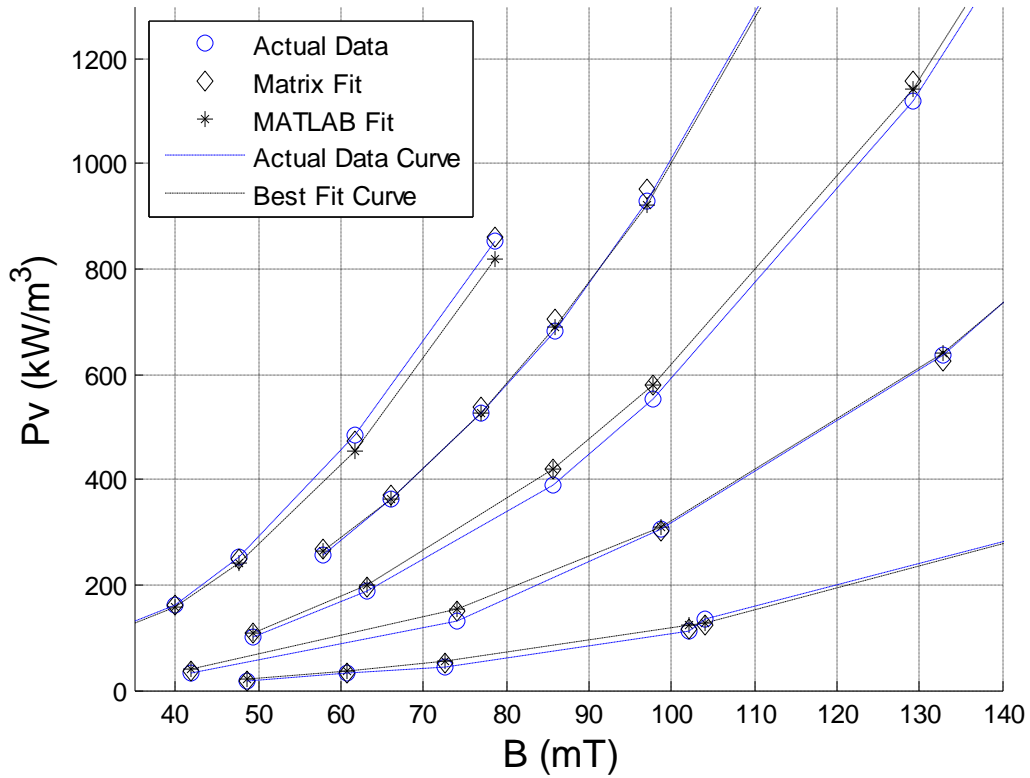


Figure 57: HLE & PLE Model Plot

LSBF residuals ( $R^2$ ) were calculated using Eqn 45.

$$R^2 = \frac{(y_{data} - y_{fit})^2}{y_{data}}$$

$y_{data}$  is the actual measured  $P_v$  CPL data.  $y_{fit}$  is the CPL mathematical result of combining the Hysteresis Loss Equation and the PLE.

The Matrix method used to evaluate  $k_{ex}$ ,  $\alpha$  and  $\beta$  coefficients used the following equations. The PLE can be broken down into the following linear form  $y = C + Dx + Ez$ . This is a linear equation, which can be easily evaluated using LSBF matrix mathematics.

$$\log(Pv) = \alpha \log(f) + \beta \log(B) + \log(k_{ex})$$

$$A * x = b$$

$$\begin{bmatrix} 1 & \log(f_1) & \log(B_1) \\ 1 & \log(f_2) & \log(B_2) \\ 1 & \log(f_3) & \log(B_3) \\ 1 & \cdot & \cdot \\ 1 & \log(f_n) & \log(B_n) \end{bmatrix} * \begin{bmatrix} \log(k_{ex}) \\ \alpha \\ \beta \end{bmatrix} = \begin{bmatrix} \log(Pv_1) \\ \log(Pv_2) \\ \log(Pv_3) \\ \cdot \\ \log(Pv_n) \end{bmatrix}$$

$$\bar{x} = (A^T A)^{-1} * A^T b$$

$$\bar{x} = \begin{bmatrix} \log(k_{ex}) \\ \alpha \\ \beta \end{bmatrix}$$

See Appendix B for the program used to calculate the MATLAB non linear solution.

## Chapter 5 Conclusions

### 5.0 Results

Four objectives were accomplished in this thesis. First, the Hysteresis Loss Equation was proven to be an accurate model for low frequency use in 3F3 power ferrites. Second, changes in 3F3 core cross sections do not seem to affect overall values of CPL. This suggests that core loss per volume in high resistance MnZn Ferrites in general will not be a function of core cross sectional area, unlike some other materials. Third, the accuracy of using a constant value of  $\sigma$  in CPL estimation equation was proven to be poor, since  $\sigma$  was shown to vary with varying electric field. The last, which are in Table 29 and 30, was a ranking of the loss models in order ascending Least Square Best Fit (LSBF) residuals for two frequency ranges (100-300 kHz and 300-500 kHz).

In Table 29, all the HLE models were fit to the low frequency coefficients in Table 7 unless noted in the table. Using the PLE equation on the data set provided the best model. Unfortunately, this model required actual user determined CPL experimental data to obtain the results. The second best model was the HLE & PLE Model. This model required the most actual CPL data. The only two models in this data range that required absolutely no user obtained CPL data were the Ferroxcube PLE coefficients and the CECE model. Unfortunately, the CECE provided the least  $R^2$ . All the HLE equations required at least two data points. The Ferroxcube 3F3 provided PLE coefficients model was the best fit model with the least amount of user obtained CPL data collection. The second was the HLE & CECE model.

Table 29: LSBF  $R^2$  for all Models using only 100-300 kHz 3F3 TN23/17/4 data

<b>Model</b> <b><i>Freq (100-300 kHz)</i></b>	<b>Equation</b>	<b><math>R^2</math></b>
PLE	$P_v = k_h f^\alpha \hat{B}^\beta$	20.83
HLE & PLE	$P_v = k_h f \hat{B}^{\beta_1} + k_{ex} f^\alpha \hat{B}^{\beta_2}$	21.44
HLE & CECE	$P_v = k_h f \hat{B}^\beta + k_c \sigma f^2 \hat{B}^2$	211.5
Ferroxcube PLE Coefficients	$P_v = k_h f^\alpha \hat{B}^\beta$	233.8
Bertotti's Model	$P_v = k_h f \hat{B}^\beta + k_c \sigma f^2 \hat{B}^2 + 8\sqrt{(\sigma GSV_o)} f^{1.5} \hat{B}^{1.5}$	616.2
HLE (Fit using 100-500 kHz data)	$P_h = k_h f \hat{B}^\beta$	651.51
HLE (Fit using 70&140 Hz data)	$P_h = k_h f \hat{B}^\beta$	3699.4
CECE	$P_{cl} = k_c \sigma f^2 \hat{B}^2$	5367.1

As above, all the HLE models in Table 30 were fit to the low frequency coefficients in Table 7 unless noted in the table. Using the HLE & PLE equation on the data set provided the best most accurate model, but required the most CPL data. The second best model was the PLE.

This equation also required a tremendous amount of actual data to obtain an accurate model. The only two models analyzed that required zero CPL data was the Ferroxcube PLE coefficients and the CECE. The Ferroxcube PLE coefficient model was slightly better than the CECE. All the HLE equations required at least two data points. So once again, the most accurate model for the least amount of user collected CPL data is the Ferroxcube 3F3 provided PLE coefficients model. The second was the HLE & CECE model.

Table 30: LSBF  $R^2$  for all Models using only 300-500 kHz 3F3 TN23/17/4 data

<b>Model Freq (300-500 kHz)</b>	<b>Equation</b>	<b><math>R^2</math></b>
<b>HLE &amp; PLE</b>	$P_v = k_h f \hat{B}^{\beta_1} + k_{ex} f^\alpha \hat{B}^{\beta_2}$	4.61
<b>PLE</b>	$P_v = k_h f^\alpha \hat{B}^\beta$	5.73
<b>HLE (Fit using 100-500 kHz data)</b>	$P_h = k_h f \hat{B}^\beta$	184.8
<b>HLE &amp; CECE</b>	$P_v = k_h f \hat{B}^\beta + k_c \sigma f^2 \hat{B}^2$	351.8
<b>Ferroxcube PLE Coefficients</b>	$P_v = k_h f^\alpha \hat{B}^\beta$	591.48
<b>CECE</b>	$P_{cl} = k_c \sigma f^2 \hat{B}^2$	651.51
<b>Bertotti's Model</b>	$P_v = k_h f \hat{B}^\beta + k_c \sigma f^2 \hat{B}^2 + 8\sqrt{(\sigma G S V_o)} f^{1.5} \hat{B}^{1.5}$	1399.6
<b>HLE (Fit using 70&amp;140 Hz data)</b>	$P_h = k_h f \hat{B}^\beta$	4749.2

## List of References

- [1] C. D. Graham, "Physical origin of losses in conducting ferromagnetic materials (invited)," J. Appl. Phys. 53(11), November 1982.
- [2] J. Reinert, A. Brockmeyer, R. W. De Doncker, "Calculation of losses in ferro-and ferromagnetic materials based on Modified Steinmetz Equation," in Proc. 1999 IEEE Ind.
- [3] J. Li, T. Abdallah, and C. Sullivan, "Improved Calculation of Core Loss with Nonsinusoidal Waveforms," IAS 2001.
- [4] J. Fan, F. Sale, "Analysis of Power Loss on Mn-Zn Ferrites Prepared by Different Processing Routes," IEEE Transactions On Magnetism, Vol. 32, NO. 5, Sept 1996.
- [5] E. Snelling, "Soft Ferrite: Properties and Applications," 2<sup>nd</sup> Edition, Butterworth, 1998 pg 35, 147.
- [6] P. Nakmahachalasit, K. Ngo, and L. Vu-Quoc, "A Static Hysteresis Model for Power Ferrites," IEEE Transactions on Power Electronics, VOL. 17, No. 4 July 2002.
- [7] C. Steinmetz, "On the law of hysteresis," AIEE Transactions, Vol 9, pp. 3-64, 1892.
- [8] Y. Sakai, T. Matsuoka, "Hysteresis Losses in Mn-Zn Ferrite Cores," IEEE Transactions On Magnetism, Vol. MAG-22, NO. 5, Sept 1986.
- [9] G. Bertotti, "General properties of power losses in soft ferromagnetic materials," IEEE Transactions On Magnetism, Vol. 24, pp. 621-630, Jan. 1988.
- [10] E. Snelling, A. Giles, "Ferrites for inductors and transformers," Research Studies Press LTD. Letchworth, Hertfordshire, England 1983.
- [11] A. Bossche, V. Valchez, D. Van de Sype, L. Vandenbossche, "Ferrite Losses of cores with square wave voltages and dc bias," Journal of Applied Physics 99, 08M908 (2006).
- [12] Ferroxcube A Yageo Company, "Design of Planar Power Transformers, Application Notes," Netherlands, February 2001.
- [13] S. Mulder, "Loss formulas for power ferrites and their use in transformer design," Philips Componets, 1994.
- [14] G. Bertotti, F. Fiorillo, G. P. Soardo, "Dependence of Power Losses on Peak Magnetization Frequency in Grain-Oriented and Non-Oriented 3% SiFe," IEEE Transactions on Magnetism, Vol. MAG-23, No. 5, September 1987.
- [15] J. Goodenough, "Summary of Losses in Magnetic Materials," IEEE Transactions on Magnetism, Vol. 38 Nov 5, September 2002.
- [16] R. Bozorth, "Ferromagnetism," IEEE Press, 2003.
- [17] H. Saotome, Y. Sakaji, "Iron Loss Analysis of Mn-Zn Ferrite Cores," IEEE Transactions on Magnetism, Vol. 33, No. 1, January 1997.
- [18] K. V. Namjoshi, J. D. Lavers, P. P. Biringer, "Eddy-Current Power Loss in Toroidal Cores with Rectangular Cross Section," IEEE Transactions on Magnetism, Vol. 34, NO. 3, MAY 1998.
- [19] K. J. Overshott, "The use of domain observations in understanding and improving the magnetic properties of transformer steels," IEEE Transactions on Magnetism, Vol. 12, pp840-845, 1976.
- [20] K. J. Overshott, "The Causes of the Anomalous Loss in Amorphous Ribbon Materials," IEEE Transactions on Magnetism, Vol. MAG-17, No. 6, November 1981.
- [21] International Standard IEC 62044-2 2005-03

- [22] A. Goldberg, "Development of Magnetic Components For 1-10 MHZ DC/DC Converters." Massachusetts Institute of Technology, September 1998 Phd Thesis.
- [23] International Standard IEC 62044-1 2002
- [24] W. Roshen, "Non-linear tunneling charge transport in soft ferrites," Journal of Magnetism and Magnetic Materials, Volume 312, Issue 2, May 2007, Pages 245-251
- [25] A. Sadiku, *Fundamentals of Electric Circuits*, Co 2000, McGraw Hill Publishing pg 437.
- [26] Ferroxcube A Yageo Company, "Soft Ferrite - Introduction." Netherlands, 01 September 2004
- [27] G. Strang, *Linear Algebra and Its Applications*, Second Edition, Co 1980 Academic Press, New York pg 118-119.

## Appendix A: MATLAB CODE

---

```
%*****
%The below is the MATLAB code used to determine the CPL of the different
cores
%This code was written by Colin Dunlop

clear all
%TC6.3/3.8/2.5
%   Resistor=.808; %Sensing Resistor
%   N=30;          %Number of Turns
%   le=15.2e-3;    %le effective length of Toriod (m
%   Ae=3.06e-6;    %Ae effective area of Toriod
%   Ve=46.5e-9;    %Ve effective volume core in (m^3)
%   Vecm=.0465;    %Ve in (cm^3)
%   mho=4*pi()*10^(-7);
%

% %TX13/7.9/6.4
%   Resistor=.808; %Sensing Resistor
%   N=13;          %Number of Turns
%   le=31.2e-3;    %le effective length of Toriod (m
%   Ae=14.1e-6;    %Ae effective area of Toriod
%   Ve=442e-9;     %Ve effective volume core in (m^3)
%   Vecm=.442;     %Ve in (cm^3)
%   mho=4*pi()*10^(-7);

%TN23/14/7
%   Resistor=.808; %Sensing Resistor
%   N=13;          %Number of Turns
%   le=55.8e-3;    %le effective length of Toriod (m
%   Ae=30.9e-6;    %Ae effective area of Toriod
%   Ve=1722e-9;    %Ve effective volume core in (m^3)
%   Vecm=1.722;    %Ve in (cm^3)
%   mho=4*pi()*10^(-7);

% %TX36/23/15
%   Resistor=.808; %Sensing Resistor
%   N=13;          %Number of Turns
%   le=89.7e-3;    %le effective length of Toriod (m
%   Ae=97.5e-6;    %Ae effective area of Toriod
%   Ve=8740e-9;    %Ve effective volume core in (m^3)
%   Vecm=8.75;     %Ve in (cm^3)
%   mho=4*pi()*10^(-7);

% %TX50/30/19
%   Resistor=.808; %Sensing Resistor
%   N=13;          %Number of Turns
%   le=120.4e-3;   %le effective length of Toriod (m
%   Ae=186e-6;     %Ae effective area of Toriod
%   Ve=22378e-9;   %Ve effective volume core in (m^3)
%   Vecm=22.378;   %Ve in (cm^3)
%   mho=4*pi()*10^(-7);
%
```

```

%%Reads files into

[V]=textread('V55.dat','%f');    %Reads in the Voltage Data
[I]=textread('I55.dat','%f');    %Reads in the Current Data

for j=5:(length(V))              % Seperates the Data into Usable form
    V1(j-4)=V(j);                %Found the offset
end

for j=5:(length(I))              % Seperates the Data into Usable form
    I1(j-4)=I(j)/Resistor;
end

tint=V(2);                       %Gives the indice of the time interval

%%%%%%%%%%%%%%%%%%%%%%%%%%%%%%%%%%%%%%%%%%%%%%%%%%%%%%%%%%%%%%%%%%%%%%%%%%%%%%For Hysterisis
%%%%%%%%%%%%%%%%%%%%%%%%%%%%%%%%%%%%%%%%%%%%%%%%%%%%%%%%%%%%%%%%%%%%%%%%%%%%%%test
% w=377;
% T=2*pi()/w;
% tint=.0001;
% t=linspace(0,2*T,1/tint);
% V1=120*cos(377.*t+45*pi()/180);
% I1=10*cos(377.*t-10*pi()/180);
%%%%%%%%%%%%%%%%%%%%%%%%%%%%%%%%%%%%%%%%%%%%%%%%%%%%%%%%%%%%%%%%%%%%%%%%%%%%%%

%%%%%%%%%%%%%%%%%%%%%%%%%%%%%%%%%%%%%%%%%%%%%%%%%%%%%%%%%%%%%%%%%%%%%%%%%% Put back in
t=linspace(0,length(V1)*tint,length(V1)); %Creates a time function for the
%%%%%%%%%%%%%%%%%%%%%%%%%%%%%%%%%%%%%%%%%%%%%%%%%%%%%%%%%%%%%%%%%%%%%%%%%%
V1=detrend(V1,'constant');

%gives the index of the Voltages to find what is a waveform
[Vzero, Zerot, Zerotact] = Zero(V1, t); %Shows the Zero pionts of the gragh

n=0;
while rem(length(Zerot)-1-n,2)==0 %used to give only a full cycle of Voltage
    n=n+1;                       %if odd number of zeros windows in
end
min1=1;                          %first zero crossing used later on
if length(Zerot)==3
    max1=2;
else
    %first zero crossing used later on
    max1=length(Zerot)-n-2;      %As n goes up the max value of zeros
    goes down
end                             %As n goes up the max value of zeros goes down

V1temp=V1(Zerot(min1):Zerot(max1+1));
vmean=mean(V1temp);

```



```

for i=1:length(V1)
    Vtemp(i)=V1(i)-vmean;
end

V1=Vtemp;
I1temp=I1(Zerot(1):Zerot(3));
Imean=mean(I1temp);
for i=1:length(V1)
    Itemp(i)=I1(i)-Imean;
end

I1=Itemp;
%Gives the Power of I1 and V1
for q=1:length(V1)
    P(q)=I1(q)*V1(q);
end
%gives the index of the Voltages to find what is a waveform
% [Vzero, Zerot, Zerotact] = Zero(V1, t); %Shows the Zero pionts of the
gragh
% n=0;
% while rem(length(Zerot)-1-n,2)==0 %used to give only a full cycle of
Voltage
%     n=n+1; %if odd number of zeros windows in
% end
% min1=1; %first zero crossing used later on
% max1=length(Zerot)-n %As n goes up the max value of zeros
goes down
z=1; %temp iterator
i=1;
y=1;
o=1;
while i~=(max1)/2+1 %uses a while loop, seemed to work better then for
loop do not know why
    for m=(Zerot(y):(Zerot(y+2))) %iterates over the range of one
voltage cycle
        Bflux(z)=tint*trapz(V1((Zerot(y)):m))/(N*Ae); %Starts at zero and
then gets Bflux
        if m~=Zerot(y+2) %for the cycle
            z=z+1;
        end
    end
    p=z; %sets the limit on one half cycle
    Bpeak(i)=(max(Bflux(o:p))-min(Bflux(o:p)))/2; %gives the Bpeak of
every cycle
    i=i+1; %iterates the while loop
    y=y+2; %iteratates the wave
    o=z; %sets the limit on one half cycle
end

if mean(Bflux)<=0 %% Ensures the B vs H leans to the right by flipping the
B values and making them positive
    Bflux=Bflux.*(-1);
end

```

```

Vtemp=V1(Zerot(min1):(Zerot(max1+1))); %Vtemp is used in the plot over the
range of Bflux
Btime=t(Zerot(min1):(Zerot(max1+1))); %Btime is used in the
plot of time the range of Bflux
Bpk=mean(Bpeak)*1000; %Gives the Bpeak
of the waveforms
Bmin=min(Bflux);
Bmax=max(Bflux);

%%%%%%%%%%%%%%%%%%%%%%%%%%%%%%%%%%%%%%%%%%%%%%%%%%%%%%%%%%%%%%%%%%%%%%%%
%%%%%%%%
%%Gives the H field using N,Reff, and I as input parameters
for q=1:length(I1)
    Hfield(q)=I1(q)*N/le;
end
y=1;
i=1; %Gives the Pk of the H
while i~=(max1)/2+1
    Hpeak(i)=(max(Hfield(Zerot(y):Zerot(y+2)))-
min(Hfield(Zerot(y):Zerot(y+2))))/2;
    i=i+1;
    y=y+2;
end
Hpk=mean(Hpeak);

Hused=Hfield(Zerot(1):Zerot(3));
Hlength=length(Hused);
Hmin=min(Hfield(Zerot(1):Zerot(3)));
Hmax=max(Hfield(Zerot(1):Zerot(3)));

%%%%%%%%%%%%%%%%%%%%%%%%%%%%%%%%%%%%%%%%%%%%%%%%%%%%%%%%%%%%%%%%%%%%%%%%
%Pvavg
z=1; %increments Paveout
i=1; %Breaks while loop
q=1; %Increments time average of P
y=1;
u=1;

%%%%%%%%%%%%%%%%%%%%%%%%%%%%%%%%%%%%%%%%%%%%%%%%%%%%%%%%%%%%%%%%%%%%%%%% for hysteresis
%%%%%%%%%%%%%%%%%%%%%%%%%%%%%%%%%%%%%%%%%%%%%%%%%%%%%%%%%%%%%%%%%%%%%%%% test
% Vecm=1
%Ve=Vecm/10^6
%%%%%%%%%%%%%%%%%%%%%%%%%%%%%%%%%%%%%%%%%%%%%%%%%%%%%%%%%%%%%%%%%%%%%%%%
while i~=(max1)/2+1
    for m=(Zerot(y):(Zerot(y+2)))
        if m-Zerot(y)==0
            Paveout(z)=0;
            z=z+1;
        else
            Paveout(z)=tint*trapz(P(Zerot(y):m))*(1000/Vecm)/(tint*(m-
Zerot(y)));
            if m~=Zerot(y+2)
                z=z+1;
            else

```

```

        Paveout1(q)=tint*trapz(P(Zerot(y):Zerot(y+2)))*(1e-
3/(Ve))/(tint*(Zerot(y+2)-Zerot(y))); % (Kw/m^3)
        q=q+1;
    end
end
end
i=i+1;
y=y+2;
end
% Paveout(z+1)=tint*trapz(P(Zerot(max1-
1):Zerot(max1+1)))*(1e+3/Vecm)/(tint*(m-Zerot(i)));
%%Figure plots
%%%%%%%%%%%%%%%%%%%%%%%%%%%%%%%%%%%%%%%%%%%%%%%%%%%%%%%%%%%%%%%%%%%%%%%%
%%%%%%%%%%%%%%%%%%%%%%%%%%%%%%%%%%%%%%%%%%%%%%%%%%%%%%%%%%%%%%%%%%%%%%%%
%
Paveout1=tint*trapz(P(Zerot(low):Zerot(high)))*(1e+3/Vecm)/(tint*(Zerot(high)
-Zerot(low))); % (mW/cm^3)
tave=t(Zerot(min1):Zerot(max1+1));
Pvave=P(Zerot(min1):Zerot(max1+1))*(1000/Vecm);
Paveout1=mean(Paveout1);

%%%%%%%%%%%%%%%%%%%%%%%%%%%%%%%%%%%%%%%%%%%%%%%%%%%%%%%%%%%%%%%%%%%%%%%%
%%%%%%%%%%%%%%%%%%%%%%%%%%%%%%%%%%%%%%%%%%%%%%%%%%%%%%%%%%%%%%%%%%%%%%%%
%GRAPHING
%7.4f

% mhospec=(Bmax/1000)/Hmax;
% mhorel=(Bmax/1000)/(Hmax*mho);
%
%
% fprintf('\n    Bpk        Paveout    Relative Perm    Specific Perm \n')
% fprintf('    %7.4f        %7.4f        %7.4f        %7.4f ', Bpk,Paveout1,
mhorel, mhospec )
% fprintf('\n')
%
% figure(1)
% plotVandI(t,V1,I1,tint,Bpk) %Plots the data of V and Current
% title('Voltage')
% figure(1)
% hold on
%
%plotBandH(Bflux(Zerot(min1):Zerot(min1+2)),Hfield(Zerot(min1):Zerot(min1+2))
,tint,Bpk)
% plotBandH(Bflux,Hused,tint,Bpk)
%
plotBandH(Bflux(Zerot(min1+2):Zerot(min1+4)),Hfield(Zerot(min1+2):Zerot(min1+
4)),tint,Bpk)
%
plotBandH(Bflux(Zerot(min1+4):Zerot(min1+6)),Hfield(Zerot(min1+4):Zerot(min1+
6)),tint,Bpk)
%
plotBandH(Bflux(Zerot(min1+6):Zerot(min1+8)),Hfield(Zerot(min1+6):Zerot(min1+
8)),tint,Bpk)
% figure(3)
% plot(tave,Pvave)
% grid on
% title(['Pv ',num2str(Bpk),' mT'])

```

```

% xlabel('time (s)')
% ylabel('Power (mW/cm^3)')
% figure(6)
% plotHandI(t,Hfield,I1,tint,Bpk) %Plots the data of H and Current
%
% figure(8)
% plotVvsIsingle(V1,I1,Bpk)
% figure(7)
% plotBandV(Btime,Bflux,Vtemp,tint,Bpk) %Plots the data of B and Voltage
%
% % r=1;
% % figure(9)
% % for i=Zerot(1):length(Zerot(1):Zerot(3))
% %     if i>=Zerot(2)
% %         Vtemp2(i)=-V1(i-length(Zerot))
% %         r=r+1;
% %     else
% %
% %
% %
% %
% figure(4)
% % plot(tave,Paveout)
% [AX,H1,H2]=plotyy(tave,Paveout,tave,Pvave);
% grid on
% title(['Pvavg ',num2str(Bpk),' mT'])
% [AX,H1,H2] = plotyy(t,V1,t,I1,'plot');
% set(get(AX(1),'Ylabel'),'String','<Pave> (mW/cm^3)');
% set(AX(1),'xlim',[t(1) t(length(t))]);
% set(AX(1),'XminorGrid','on');
% set(AX(1),'YminorGrid','on');
% set(AX(1),'YminorTick','on');
% set(AX(1),'YGrid','on');
% set(get(AX(2),'Ylabel'),'String','Pave (mW/cm^3)');
% set(AX(2),'xlim',[t(1) t(length(t))]);
% set(H1,'LineStyle','--');
% set(H2,'LineStyle','--');
% title(['Average Power and Power ',num2str(Bpk),' mT'])
% xlabel('time (s)')
% ylabel('Power (mW/cm^3)')
%
% [X,f,Pyy]=fftfunc(V1(Zerot(1):Zerot(3)),tint);

% windowSize=60;
% Hfilt=filtfilt(ones(1>windowSize)/windowSize,1,Hused);
% Bfilt=filtfilt(ones(1>windowSize)/windowSize,1,Bflux);
% figure(2)
% plotBandH(Bfilt,Hfilt,tint,Bpk)

% figure(3)
% grid on
% plotyy(Btime,Bflux,Btime,Hused)

```

```

for i=1:length(Hused)
    if abs(Hused(i)-Hmax)<=1e-7
        Hmax_in=i;
    end
    if abs(Hused(i)-Hmin)<=1e-7
        Hmin_in=i;
    end
end

Hused((Hlength+1):(2*Hlength))=Hused;
Bused=Bflux;
Bused((Hlength+1):(2*Hlength))=Bflux;

if Hmax_in < Hmin_in
    first_in=Hmax_in;
    sec_in=Hmin_in;
else
    first_in=Hmin_in;
    sec_in=Hmax_in;
end
Bused=detrend(Bused, 'constant');
third_in=first_in+Hlength;
sumtrap=-(trapz(Hused(first_in:sec_in),Bused(first_in:sec_in))+
trapz(Hused(sec_in:third_in),Bused(sec_in:third_in)));
Pvhys=(sumtrap/(tint*length(Zerot(1):Zerot(3))))*10^-3;
% figure(4)
% grid on
% hold on
% plot(Hused(first_in:sec_in),Bused(first_in:sec_in),'b')
% plot(Hused(sec_in:third_in),Bused(sec_in:third_in),'r')
Bmax=max(Bused)*1000;

% title(['Hysterisis ',num2str(Bmax),' mT'])
% xlabel('Hfield (A/m)')
% ylabel('Bflux (mT)')

% figure(5)
% plotVandI(t,Vl,I1,tint,Paveout1)

mhospec=(Bmax/1000)/Hmax;
mhorel=(Bmax/1000)/(Hmax*mho);

%fprintf('\n   Bpk       Paveout       Relative Perm       Specific Perm \n')
fprintf('\n%7.4f\n%7.4f\n%7.4f\n%7.7f', Bpk,Paveout1, mhorel, mhospec )
fprintf('\n')

```

```

%*****
%The below is the MATLAB code used to determine the Least Square Best Fit
%Residuals for the PLE equation and provide a plot of the data. All other
%models used this code with slight modifications. This program calls the
%LSQRmat file and a Pvddata dat file. Both codes will follow this program.
%This %code was written by Colin Dunlop

clc;
clear;

[X,y]=Pvddata();
name=@PLE_func;
[beta0,yfit]=LSQRmat; %The coefficient results are the matrix fit are fed
into
                        %fed into a array for plotting

yfitmatrix=feval(name,beta0,X);

options = statset('TolFun',1e-40,'TolX',1e-
40,'MaxIter',160000,'DerivStep',1e-10);
[beta,R,J]= nlinfit(X,y,name,beta0); %nlinfit is a built in Matlab function
ci = nlparci(beta,R,J); %which provides the non linear fit to
data
[Ypred, delta] = nlpredci(name,X,beta,R,J);
x=X(:,2);

%%%%%%%%%%%%%%%%%%%%%%%%%%%%%%%%%%%%%%%%%%%%%%%%%%%%%%%%%%%%%%%%%%%%%%%%
yfit=feval(name,beta,X);
for i=1:length(x)
    chi(i)=(((y(i)-yfit(i))).^2)/y(i);
end

RChiSquare = sum(chi);

% %%%%%%%%%%%%%%%%%%%%%%%%%%%%%%%%%%%%%%%%%%%%%%%%%%%%%%%%%%%%%%%%%%%%%%%%%
% %%% PLOTTING YOUR DATA AND FIT %%%
% %%%%%%%%%%%%%%%%%%%%%%%%%%%%%%%%%%%%%%%%%%%%%%%%%%%%%%%%%%%%%%%%%%%%%%%%%
%
figure(1); % opens figure 1 and makes it active
clf; % clears the active figure
hold on; % Makes matlab plot without clearing the graph

%plot(x,y,'k*')
%plot(x,y,'rx'); % Plots the fitted curve
hold on; % Makes matlab plot without clearing the graph

plot(x,y,'bo')
plot(x,yfitmatrix,'kd'); % Plots the fitted curve
plot(x,Ypred,'r. '); % Plots the fitted curve
array=(linspace(30,300,20))';
D=300000.*ones(length(array),1); %creates a ones array the length of the
number of B inputs

```

```

A=cat(2,D,array);
yfitcurve=feval(name,beta0,A);

%plot(array,yfitcurve,'r--');
%plot(x(1:13),yfitmatrix(1:13),'r--')
%plot(x(1:6),yfitmatrix(1:6),'r--')

%%%%%%%%%%%%%%%%%%%%%%%%%%%%%%%%%%%%%%%%%%%%%%%%%%%%%%%%%%%%%%%%%%%%%%%%Get rid of
name=@PLEMan_func;
yfitman=feval(name,beta,X);
%plot(x,yfitman,'k*')
%plot(x(1:13),yfitmatrix(1:13),'r--')

legend('Actual Data','Matrix Fit','Matlab Fit','Ferroxcube Fit','Best fit
Curve','Location','NorthWest ');
%

%plot(x(7:12),yfit(7:12),'r--')
%plot(x(13:18),yfit(13:18),'r--')
%plot(x(14:19),yfitmatrix(14:19),'r--')
%plot(x(20:25),yfitmatrix(20:25),'r--')
%plot(x(26:31),y(26:31),'k--')
%plot(x(32:37),y(32:37),'k--')

% array=(linspace(30,300,20))';
% D=300000.*ones(length(array),1); %creates a ones array the length of the
number of B inputs
%
% A=cat(2,D,array);
% yfitcurve=feval(name,beta,A);
%
% plot(array,yfitcurve,'r--');
%
% array=(linspace(30,300,20))';
% D=400000.*ones(length(array),1); %creates a ones array the length of the
number of B inputs
%
% A=cat(2,D,array);
% yfitcurve=feval(name,beta,A);
%
% plot(array,yfitcurve,'r--');
% array=(linspace(30,300,20))';
% D=500000.*ones(length(array),1); %creates a ones array the length of the
number of B inputs
%
% A=cat(2,D,array);
% yfitcurve=feval(name,beta,A);
%
% plot(array,yfitcurve,'r--');

x1=min(x);
x2=max(x);
grid on
% axis([40,340,0,2250]);

```

```

%axis([x1-1/16*x1,x2,min(y),max(y)]);
% sets visible range of the plot
% %
title(['3F3 TN23/14/7 for 100-300(khtz) kh = ',num2str(beta0(1,1)), ' \beta
=',num2str(beta0(2,1)), ' \alpha =',num2str(beta0(3,1))], 'fontsize',12);
% %
% Places the title on the graph
xlabel('B (mT)', 'fontsize',14, text(5,120,['\chi^2_{\nu-1} = ' str1]) ); %
Labels the 'x' axis
ylabel('Pv (kW/m^3)', 'fontsize',14); % Labels the 'y' axis
% %
str1=num2str(RChiSquare,2);
%text(170,.4,['\chi^2_{\nu-1} = ' str1]); % Plots the reduced chi-square
%text(170,.7,['\alpha = ' str1]); % Plots the reduced chi-square
%
%
xlabel('B (mT) ', 'fontsize',14 ); % Labels the 'x' axis
fprintf('      nlinfit kh      nlinfit beta  nlinfit alpha  nlinfit Rchi\n')
fprintf('      %7.7f      %7.7f      %7.7f      %7.7f \n', beta(1,1), beta(2,1),
beta(3,1),RChiSquare)
%%%%%%%%

%*****
%The below is the MATLAB code used to determine the matrix Least Square Best
%Fit: LSQRmat.m
%Residuals for the PLE equation matrix are provided
% All other models used this code with slight modifications. This program
calls %the Pvdata data file. This code follows this program.
%This code was written by Colin Dunlop

%%%%%%%%This code uses matrix mathematics to solve the simple formula
% y=kh*f*I^alpha Strang Linear Algebra and its Applications pg 118

function [beta1,yfit]=LSQRmat()
name=@PLE_func;
% clc; %clears the command window
% clear; %clears all variables

[X,y]=Pvdata(); %inputs the data

b=log(y); %gets the log of the formula set log(y/f)=alpha*log(I)+log(kh)
fm=log(X(:,1));

B=log(X(:,2)./1000);

Array=cat(2,B, fm);

D=ones(length(B),1); %creates a ones array the length of the number of B
inputs
A=cat(2,D,Array);

At=A';

```



```

x=inv (At*A) *At*b;

beta1 (1,1)=exp (x (1));
beta1 (2,1)=(x (2));
beta1 (3,1)=(x (3));

sig = sqrt (y);
yfit=feval (name,beta1,X);

for i=1:length(B)
    chi(i)=( (y(i)-yfit(i)).^2/y(i);
    % chi(i)=( (y(i)-yfit(i))./1).^2;
end

chisq=sum(chi);
RChiSquare = chisq;

fprintf('\n      Matrix C1      Matrix Beta      Matrix alpha      Matrix
Rchi\n')
fprintf('      %7.7f      %7.7f      %7.7f      %7.7f',beta1 (1,1),
beta1 (2,1),beta1 (3,1),RChiSquare)
fprintf('\n\n')

%*****
%The below is the MATLAB data file Pvdata. It provided the data for the above
two codes. This is for the TN23/14/7 3F3 toroid

function [X,y]=Pvdata()

X=[
70      78.99
70      123.55
70      169.27
70      298.07
140     37.74
140     91.90
140     163.63
140     226.49
140     274.43
100000  48.7365
100000  60.7911
100000  72.6238
100000  102.2023
100000  104.0705
100000  154.5854
100000  166.0821
100000  197.4659
100000  204.4652
100000  237.3057
100000  256.8447
100000  282.5612
100000  328.8517

```

200000	41.8692
200000	74.1496
200000	98.6685
200000	132.8864
200000	161.5689
200000	193.7655
300000	49.3198
300000	63.0888
300000	85.6389
300000	97.7819
300000	129.2605
300000	157.5516
400000	57.9333
400000	66.0335
400000	77.0299
400000	85.967
400000	97.0009
400000	121.1181
500000	11.8062
500000	19.1405
500000	39.9354
500000	47.6942
500000	61.8369
500000	78.6639

];

y=[  
0.0204  
0.0757  
0.1679  
0.7679

0.0113  
0.1037  
0.4344  
0.8166  
1.247

%  
18.4427  
32.7486  
45.4667  
110.2763  
134.794  
342.1314  
385.68  
631.2197  
635.5609  
915.6343  
1192.3756  
1570.1522  
2077.6729

```
31.3657
132.5157
305.0194
635.4071
1035.3813
1651.552
```

```
101.1267
186.263
388.6729
554.1156
1120.7266
1821.2589
```

```
254.9548
361.6122
524.7969
680.9328
930.8987
1583.1784
11.252
32.4611
159.8956
254.5507
484.7686
852.6831
```

```
];
```

```
x=X(:,2);
f=X(:,1);
```

## Appendix B: CPL Collected Data

---

The CPL data in Table 31 and 32 was used for all the CPL models for the TN23/14/7 core. Six frequencies and varying magnetic fluxes were used in the data set.

Table 31: TN23/14/7 Data 70 Hz, 140 Hz and 100 kHz data

Freq (Hz)	B (mT)	$P_v$ <sup>3</sup> (kW/m )
70	78.99	0.0204
70	123.55	0.0757
70	169.27	0.1679
70	298.07	0.7679
140	37.74	0.0113
140	91.90	0.1037
140	163.63	0.4344
140	226.49	0.8166
140	274.43	1.247
100000	48.7365	18.4427
100000	60.7911	32.7486
100000	72.6238	45.4667
100000	102.2023	110.2763
100000	104.0705	134.794
100000	154.5854	342.1314
100000	166.0821	385.68
100000	197.4659	631.2197
100000	204.4652	635.5609
100000	237.3057	915.6343
100000	256.8447	1192.376
100000	282.5612	1570.152
100000	328.8517	2077.673

Table 32 TN23/14/7 Data 200 - 500 kHz data

Freq (Hz)	B (mT)	$P_v^3$ (kW/m <sup>3</sup> )
200000	41.8692	31.3657
200000	74.1496	132.5157
200000	98.6685	305.0194
200000	132.8864	635.4071
200000	161.5689	1035.381
200000	193.7655	1651.552
300000	49.3198	101.1267
300000	63.0888	186.263
300000	85.6389	388.6729
300000	97.7819	554.1156
300000	129.2605	1120.727
300000	157.5516	1821.259
400000	57.9333	254.9548
400000	66.0335	361.6122
400000	77.0299	524.7969
400000	85.967	680.9328
400000	97.0009	930.8987
400000	121.1181	1583.178
500000	11.8062	11.252
500000	19.1405	32.4611
500000	39.9354	159.8956
500000	47.6942	254.5507
500000	61.8369	484.7686
500000	78.6639	852.6831

The data in Table 33 and 34 was collected using the apparatus described in Section 3.2 and the 3F3 PLT 58/38/4.

Table 33: Conductivity AC data for 3F3 Plata

Phase (°)	I pk	Vpk	Z		Conductivity	Freq	Temp (°C)	E/m
62.784	0.0207	27.4093	606.7098	-1179.7192	0.6445	100000	61.2	472.74
62.856	0.0382	43.731	522.2065	-1018.5513	0.7488	100000	61.7	754.24
62.784	0.0445	49.7621	511.0458	-993.7049	0.7651	100000	61.4	858.26
62.568	0.0639	64.929	468.2734	-902.1575	0.835	100000	62.3	1119.85
63.288	0.0798	77.8922	438.7402	-871.8829	0.8912	100000	62.3	1343.43
64.944	0.0447	21.0305	199.4334	-426.5972	1.9607	500000	62.8	362.72
63.864	0.0905	36.3687	177.0543	-360.8388	2.2085	500000	62.8	627.26
61.272	0.1664	55.7468	161.0563	-293.8343	2.4279	500000	62.8	961.48
61.2	0.2297	70.6188	148.1223	-269.4335	2.6399	500000	62.4	1217.99
67.176	0.0404	20.7961	199.7087	-474.5317	1.958	500000	43.6	358.68
66.312	0.0636	29.3915	185.7548	-423.4021	2.105	500000	43.3	506.92
65.304	0.113	46.0075	170.0527	-369.7891	2.2994	500000	43.4	793.51
64.584	0.163	59.8689	157.6757	-331.8251	2.4799	500000	43.6	1032.58
63.792	0.2272	75.3812	146.5576	-297.7394	2.668	500000	43.6	1300.12
63.144	0.3138	94.0156	135.3354	-267.2691	2.8893	500000	43.9	1621.52

Table 34: DC Conductivity for 3F3 Plate

Temp	E (V/m)	Voltage (V)	Current (mA)	$\sigma$
44.0	443.3	25.7	2.7	0.04
44.0	865.8	50.2	7.8	0.06
44.0	1324.6	76.8	18.1	0.09
44.0	1714.4	99.4	26.2	0.10
45.0	2168.0	125.7	38.2	0.12
45.0	2581.9	149.7	53.7	0.14
54.6	443.3	25.7	5.5	0.08
54.7	874.4	50.7	13.0	0.10
54.9	1302.2	75.5	21.7	0.11
55.2	1724.7	100.0	33.3	0.13
55.4	2259.4	131.0	51.2	0.15
55.9	2845.8	165.0	78.8	0.19
56.0	3311.5	192.0	111.3	0.23
62.7	507.1	29.4	7.9	0.11
62.9	1033.1	59.9	21.2	0.14
63.4	1547.1	89.7	39.0	0.17
64.0	2104.2	122.0	61.3	0.20
65.0	3449.5	200.0	158.4	0.31

Data in Table 35 was collected using the 4192A LF 5 Hz -13MHz Hewlett Packard Impedance Analyzer with a 16047A test fixture and the 3F3 PLT 58/38/4 plate explained in Section 2.4.

Table 35: Data using Impedance Analyzer

Temp (°C)	Z (kΩ)	Phase (°)	R (kΩ)	Freq (hz)	Capacitance (F)
27.4	14.1	0	13.7	10	0.000E+00
27.4	13.1	-0.5	12.4	100	1.270E-05
27.4	13.2	-5	13.31	1000	1.497E-07
27.4	9.8	-30.08	8.4	10000	3.217E-09
27.4	2.75	-59.18	1.459	100000	6.678E-10
27.4	0.8353	-66.34	0.3148	500000	4.400E-10
27.4	0.4391	-67.08	0.1941	1000000	3.388E-10

The CPL data in Table 36 and 37 was used for all the CPL models for the 6 cores.

Table 36: 6 Varying Core Sizes CPL Data 100 kHz

Core	Freq (Hz)	B (mT)	P <sub>v</sub> <sup>3</sup> (kW/m <sup>3</sup> )
TN23/14/7 Core 1	100000	166.0821	385.68
	100000	204.4652	635.5609
	100000	237.3057	915.6343
	100000	328.8517	2077.6729
TN23/14/7 Core 1	100000	48.7365	18.4427
	100000	60.7911	32.7486
	100000	104.0705	134.794
	100000	282.5612	1570.1522
TN23/14/7 Core 2	100000	40.571	10.6748
	100000	50.3946	17.9718
	100000	64.1714	32.795
	100000	91.2084	82.0175
	100000	246.9622	1015.5247
TC6.3/3.8/2.5	100000	116.595	180.4562
	100000	173.9523	519.6164
	100000	219.5139	947.4827
TX50/30/19	100000	17.0836	1.8337
	100000	19.0696	2.3511
	100000	25.5492	4.6827
	100000	36.4404	11.3051
	100000	86.389	90.0786
TX36/23/15	100000	8.946	0.546
	100000	13.8393	1.4257
	100000	58.221	26.2166
	100000	142.6036	237.9579
TX 13/7.9/6.4	100000	95.7404	70.4373
	100000	127.576	155.2404
	100000	191.7821	437.1653
	100000	288.918	1235.0865

Table 37: 6 Varying Core Sizes CPL Data 500 kHz

Core	Freq (Hz)	B (mT)	$P_v$ <sup>3</sup> (kW/m )
TX36/23/15	500000	6.2922	2.3313
	500000	8.5426	4.5691
	500000	12.0581	9.9721
	500000	28.7991	76.8474
	500000	35.2054	134.4838
TX 13/7.9/6.4	500000	19.9283	28.5248
	500000	24.2512	43.1979
TX 13/7.9/6.4	500000	37.695	119.5079
	500000	48.4352	212.8961
	500000	60.2097	357.1465
	500000	102.844	1330.979
	500000	178.938	4845.753
TN23/14/7 Core 1	500000	11.8062	11.252
	500000	19.1405	32.4611
	500000	39.9354	159.8956
	500000	47.6942	254.5507
	500000	61.8369	484.7686
	500000	78.6639	852.6831
TX51/32/19	500000	7.0594	4.9692
	500000	17.045	33.1908
TX 6.3/3.8/2.5	500000	39.1581	164.4293
	500000	61.2579	534.6423
	500000	77.1575	907.2635
	500000	202.696	9071.844
	500000	211.0727	9885.569
TN23/14/7 Core 2	500000	19.1405	32.4611
	500000	36.2616	133.1583
	500000	98.5013	1413.678